ISSN 1068-3755, Surface Engineering and Applied Electrochemistry, 2007, Vol. 43, No. 2, pp. 77–82. © Allerton Press, Inc., 2007.
Original Russian Text © E.T. Abdukarimov, A.Sh. Mirkarimov, A.A. Zaripov, 2007, published in Elektronnaya Obrabotka Materialov, 2007, No. 2, pp. 4–11.

ELECTRIC DIMENSIONAL TREATMENT OF MATERIALS

Electroerosion Treatment of Dielectric Materials

E. T. Abdukarimov, A. Sh. Mirkarimov, and A. A. Zaripov

Institute of Electronic Engineering of ASRU, F. Hodjaev St. 33, Tashkent, 700125 Republic of Uzbekistan

Received November 24, 2006

Abstract—The authors worked out a new method of combined electric-erosion and electric-chemical processing of dielectrics in an electrolytic medium. This article is dedicated to the study of the process of passing an electric current through an aqueous solution of an electrolyte. With the help of measurements of the volt–ampere characteristics of the current passing through the electrolytes under study, the total character of the electrolytes' dependence, which has 4 transition regimes, was determined. The characteristics of the transition regimes depend on both the electric regimes and the types of electrolytes and their concentration and don't depend on the distance between the electrodes. It's characteristic of the third phase that a plasma envelope appears that is accompanied by distraction of the dielectric. It's shown that the tension and corresponding current density at which the plasma envelope occurs exist for every type of electrolyte when the material of the cathode is not changed. The correlation between these parameters and the coefficient of the surface-tension of the studied electrolytes is determined. The results of the study include the dependence of the speed of the volumetric broaching upon such technological parameters as the electric power, the frequency of the revolution of the electrode device, the frequency of the relaxation of the generator, and the concentration of the electrolyte. The problem of the mechanisms of the influence of the electric discharge in the electrolyte upon dielectric is discussed.

DOI: 10.3103/S1068375507020019

INTRODUCTION

An analysis of the scientific and technical information on the treatment of nontraditional materials shows that progression of both the methods of fabrication and the types of materials obtained continues [1–3]. The procedures for treatment of such materials are also evolving.

In parallel with the improvement of the known techniques (abrasive, laser, ultrasonic, etc.), there is an attempt to widen the possibilities of these methods by combining them with chemical means and utilization of alkaline and acid electrolytic media. For instance, in works [4, 5], it is shown that the rate of treatment of composite materials grows if it is carried out in a KON working medium and laser and electroerosion methods different in their nature are used.

In this connection, we have enlarged the range of liquids serving as a working medium for use at electroerosion machining. In addition to NaCl aqueous solutions [6], NaOH and KOH alkaline solutions were chosen. The electric and time characteristics of pulse discharges in proximity to the electrode device were studied in the mentioned electrolyte solutions.

Measurements of the current–voltage characteristics (CVC) of the current passage reveal the general nature of the dependence, which had four transient stages. The transient stage performance depends on both the electric regimes, the electrolyte type, and the concentration and doesn't depend on the interelectrode spacing. The third stage is characterized by the appearance of a plasma sheath in the cathode region due to the voltage redistribution in the electrolyte circuit and the concentration of the whole applied electric field in this region. For each electrolyte (with the cathode material being the same), there exists voltage and respective current densities when the plasma sheath appears. The correlation between these parameters and the measured values of the surface tension coefficient of the studied electrolytes has been established.

Expressions permitting one to perform the calculation of the voltage drop and choose the regimes beneficial for working of dielectric materials (glass and ceramics) have been obtained from an analysis of the potential distribution in the electrolytic circuit.

1. Study of the Electric and Frequency Characteristics of the Current

An experimental setup (Fig. 1) was worked out to investigate the processes of current passage in an electrolytic media and of dielectric material processing. It consists of a relaxation generator decoupled galvanically from the circuit, a system of fine supply of the electrode instrument (EI) based on a stepping motor, a system of controlled rotation of this electrode with a pressure compensator, and a container with the specimen holder into which a damping element was introduced (it isn't shown in the figure).

The system of the compensator with the damper allows one to automatically support the EI force on the specimen working surface, which shouldn't lead to its

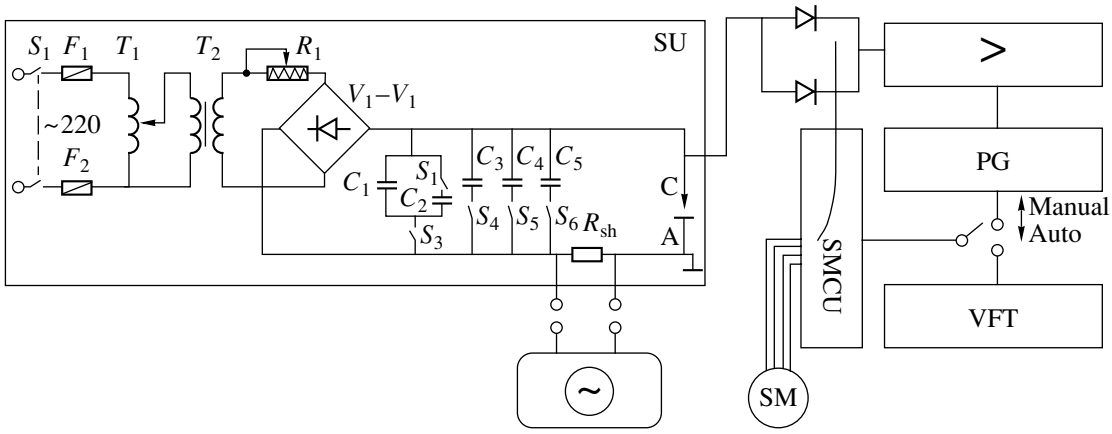

Fig. 1. Experimental bench for investigation of the electric current, frequency characteristics, and processing of the dielectrics: SU—supply unit; >—amplifier; PG—pulse generator, VFT—voltage-frequency transformer; SMCU—stepping motor control unit; SM—stepping motor.

fracture because the elements ensure the necessary EI contact with the specimen being worked.

The cathode is fastened in the holder and with the help of the supplying mechanism and can be dipped to the needed depth in the vertical plane in relation to the anode and the specimen, as well as moved in the anode horizontal plane. Rectangular plates of graphite, copper, lead, and stainless steel were used as the anode.

To measure the EI revolution frequency, an electron tachometer has been elaborated, whose block diagram is presented in Fig. 2. The tachometer consists of a transmitter that transforms the rotary motion into electric pulses, a former of rectangular pulses with a rated duration, a pulse frequency meter, and a supply unit.

To measure the CVC, the relaxation generator allows one to control the output voltage in the range of 0–400 V at a maximum load current of 10 A. The discharge current signal is determined with the help of a resistor with R = 0.5 Ohm, which is connected in series to the electrode circuit. The voltage is measured immediately in the discharge gap. CVC are obtained with the help of an XY recorder; the configuration of the current and voltage is observed simultaneously using a double-trace memory oscillograph. The interelectrode spacing and the cathode area were noted during the investigation. NaCl, NaOH, and KOH aqueous solutions of different concentrations were used as the electrolyte. Tungsten rods with various diameters were employed as the cathode. The cathode area is bounded a clay pipe and may be varied over wide limits.

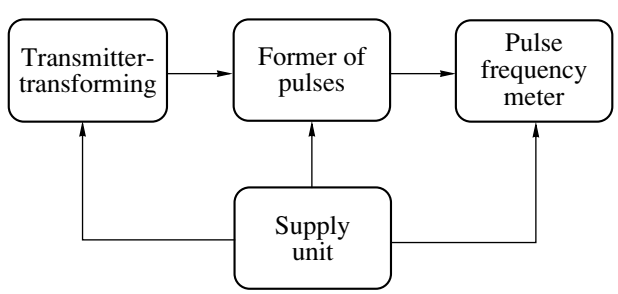

Fig. 2. Block diagram of the electron tachometer.

1.1. Examination of the Current–Voltage Characteristics

To assay the electric current passage conditions in the aqueous electrolyte solutions, current–voltage characteristics were chosen that could be investigated in the NaCl solution [6] and conveniently allow one to judge the main processes of the current passage in the solution and determine the parameters of the plasma sheath formation near the cathode. It is precisely this regime that was used later on to pierce holes in nonconducting materials.

The current evolution dynamics in the electrolyte with the variation of the voltage within the interelectrode gap in the NaOH and KOH aqueous solutions of different concentration are presented in Fig. 3 and 4. Such nature of the CVC behavior is similar to the change of the current–voltage characteristics for an NaCl electrolyte solution [6].

It should be noted that, in all the studied electrolyte solutions, the CVC didn't depend on the material; the anode was made of lead, graphite, or stainless steel. They coincide within the limits of the measurement error.

As before, four regimes the current–voltage characteristics can be recognized. Portion 1 is the region where the current linearly depends on the voltage. The normal process of electrolysis occurs in this portion. The current increases, the electrochemical processes in the electrolyte build up, and the dependence becomes nonlinear. This regime ends with the formation of a steam-and-gas bubble envelope on the cathode surface.

On further increase of the voltage, the second stage of the process begins: intense gas formation at the

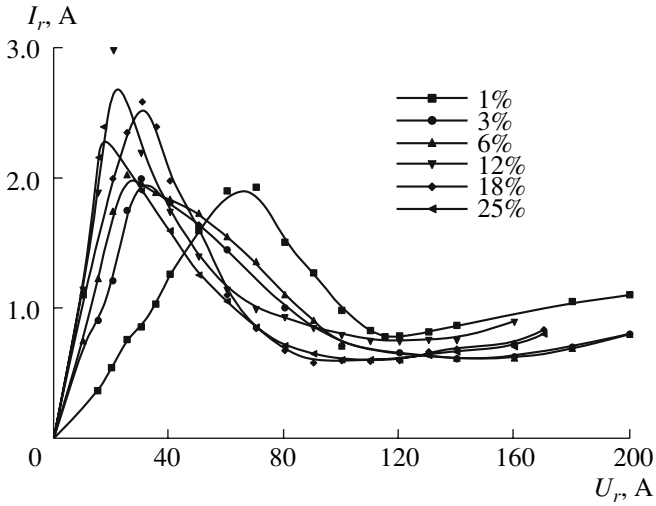

Fig. 3. CVC dependency at various concentrations of the NaOH electrolyte: $h = 3$ mm, $S_c = 2.38$ mm^2, and T = const.

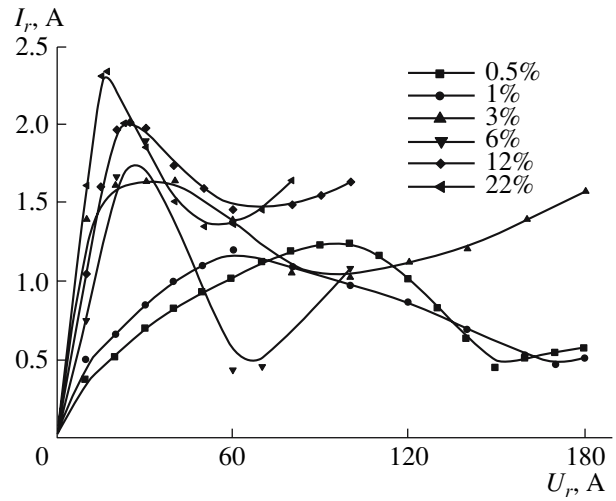

Fig. 4. CVC dependency at various concentrations of the KOH electrolyte: $h = 2.5$ mm, $S_c = 2.38$ mm^2, and T = const.

anode surface is accompanied by the appearance of separate spark discharges resulting in a drop in the current on the CVC. Its following increase builds up a constant steam-and-gas layer. The number of single discharges increases, and a plasma sheath comes into being at the cathode surface. As the experiments have shown, the beginning of the second phase is marked by the fact that the current density at which these initial discharges appear for the given concentration of the electrolyte doesn't depend on the interelectrode gap and the cathode area. This suggests that the processes of the steam-and-gas layer formation around the cathode are the governing factor determining the conditions of the current passage in the electrolyte. Namely, this layer's properties influence the parameters of the discharges and plasma sheath near the cathode.

The current densities when the initial discharges near the cathode occur are arbitrarily called critical. In Fig. 5, the critical current density is plotted against the electrolyte concentration at various amounts of dipping of the cathode into the electrolyte.

As is seen from the figure, within the concentration range of 0.05–3%, there is a rather sharp dependency of the critical current density on the electrolyte concentration, and it doesn't depend on the cathode dipping depth at any concentration. Within the concentration range of 6–20%, the critical current density (within the limits of the measurement error) virtually doesn't depend on the electrolyte concentration. It should be noted that, in electrolytes with a concentration of less than 2%, the minimum voltage at which the discharges occurs is higher in comparison with the electrolytes with a greater concentration. Apparently, this is connected with the fact that, at low concentrations of the electrolyte, hydrogen cations are generated not only near the cathode but in the whole width of the electrolyte. Moreover (as is shown in work [7]), the resistance of the weak solutions of electrolytes (less than 2%) grows sharply with the concentration decrease due to the increase of the surface tension coefficient. In this connection, higher values of voltages within the interelectrode gap are necessary to ensure the same quantity of current. The generated power determines the electrochemical processes with the resulting formation of a bubble layer around the cathode. The increase of the voltage at low concentrations and formation of gas within the whole width leads to a reduction of the current and the respective fall of the critical current density at which a discharge occurs.

At the beginning of the third stage, as a result of intensification of the gassing both from the electrolyte body and at the expense of steam generation owing to the growth of the electric power input, there comes into existence a steady continuous gaseous envelope, and

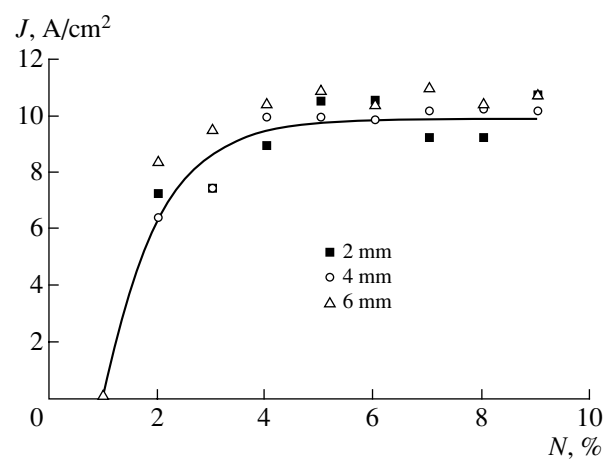

Fig. 5. Current density versus concentration at various depths of the cathode dipping.

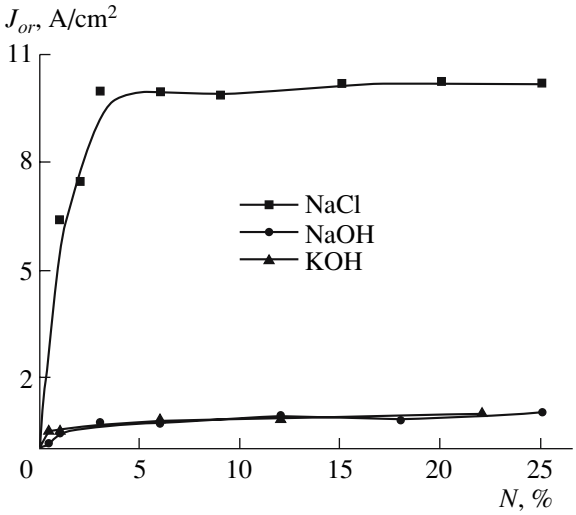

Fig. 6. Current critical density versus electrolyte concentration characteristics.

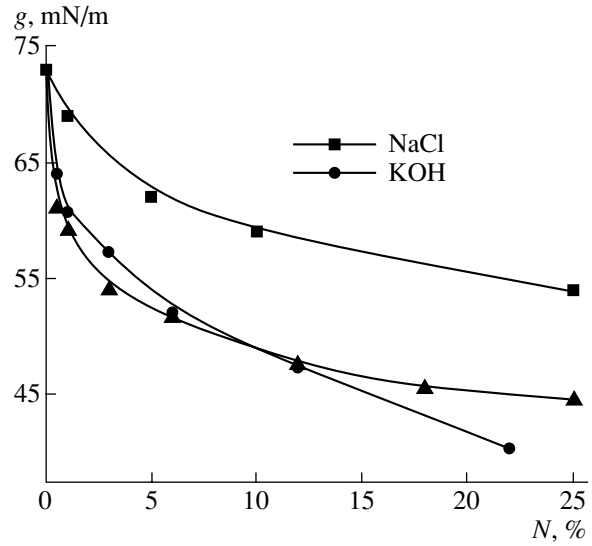

Fig. 7. Surface tension coefficient versus electrolyte concentration characteristics.

the current passes through the layer in the form of high-frequency discharges. Luminous plasma flares occur in the narrow cathode zone. Because the cathode surface is bounded by the dielectric, the plasma flares exist independently of the depth of the cathode being dipped into the electrolyte.

The voltages and current densities where the plasma flare appears, as is evident from the CVC and critical density versus the concentration characteristic for the examined electrolytes (Fig. 6), depends strongly on the electrolyte concentration and composition because of the variation of the electrolytic liquid surface tension coefficient.

The measurements of the solution surface tension coefficient by the pick-up coil method show its sharp fall with the concentration increase similar to the growth of the critical density (Fig. 7). This suggests that the continuous gaseous layer parameters depend on the electrolyte physical and chemical properties, as the change of its concentration causes a change of not only the solution surface tension coefficient but also the density, viscosity, electric conductivity, ion mobility, etc.

The creation of the solid gaseous layer and generation of the continuous high-frequency discharge are the beginning of the third phase. The cathode temperature at that moment is about 2000°C, as the thermocouple measurement showed. A further increase of voltage leads to the growth of the current and a sharp rise of the tungsten cathode temperature, its melting, and the CVC transition into the fourth phase, a regime similar to the arched one. Unlike the arched regime, it takes place at the elevated voltages in the discharge gap (from 60 V and higher, depending on the electrolyte type and its concentration).

2. Investigation of the Dependence of the Glass Piercing Weight–Space Velocity on the Technological Parameters

Previously conducted experimentation showed the possibility of hole piercing in specimens of both glass and composite ceramics. A wide selection of glass specimens both quantitatively and qualitatively (with various physical and mechanical properties and dimensions) unlike the available composite ceramics gave the opportunity to carry out the investigation with a large number of samples whose parameters could be measured. As a result, glass plates became the main object for studying the effect of the plasma sheath on dielectric articles.

The process of piercing the glass and ceramic plates was performed using the test apparatus (see Fig. 1). The plates were fixed in the holder and placed into the bath containing the working liquid (it isn't shown in the figure). Tungsten rods with different diameters were used as EI near which the steam-and-gas layer occurred. The compensator and damper automatically monitored the interelectrode spacing and mechanical load on the samples being worked. All the experiments were performed at the direct polarity of the electrodes.

The influence of the electric power input on the optical glass processing at a constant EI rotation speed of n = 2000 r/min and relaxation generator capacity of 0.5 mcF was investigated. The relationship between the velocity of the hole piercing in a glass plate 4 mm thick in an aqueous 6% NaCl solution with the electrode-instrument diameter being 1.5 mm and the input electric power is shown in Fig. 8.

The upper and lower limits are bounded by the maximum magnitude of the electric power input where the EI

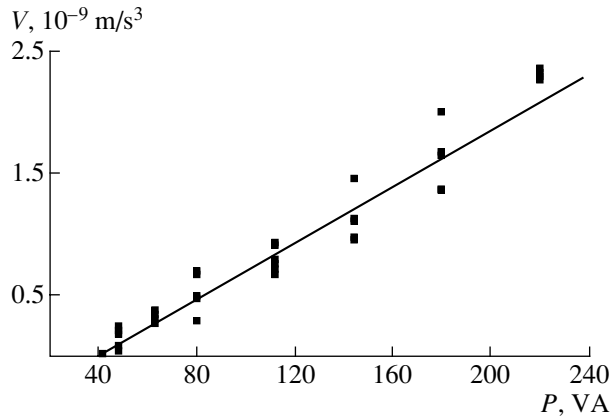

Fig. 8. Removal speed versus power characteristics for the 6% NaCl electrolyte: V = const, C = 0.5 mF.

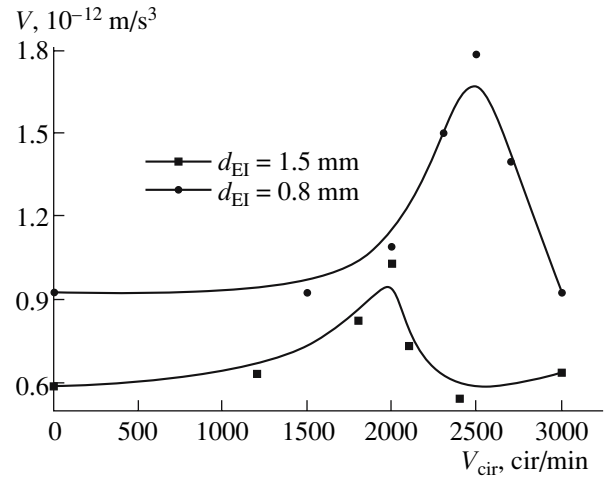

Fig. 9. Removal speed versus EI rotation characteristics for the 6% NaCl electrolyte: V = const, C = 0.5 mF, and P = 40 VA.

does not melt and the minimum value of the treatment speed. The figure shows this dependence to be linear.

Investigation of the dependence of the glass specimen volumetric piercing velocity on the EI revolution frequency has been undertaken. It has been ascertained that there is some optimum frequency of EI revolutions wherein the processing speed is maximum (Fig. 9). In the case of a constant quantity of the electric power input and the electrolyte concentration, the working speed grows with the EI diameter reduction, which could be explained by the diversity of the energy flow per unit of the surface being worked. The rise in the processing speed with the increase of the EI revolution number is determined by the abrasive effect of the tungsten electrode action and the growth of the intensity of the erosion product being dragged out from the treatment zone.

The processing velocity drop with the further increase of the EI revolution frequency is connected with the hydrodynamical effect of the steam-and-gas envelope destruction as a result of the EI rotation. This is proved by the fact that the EI diameter decrease shifts the dependence into the region of more frequencies.

The findings of the investigation of the relationship between the treatment velocity and the relaxation generator capacity presented in Fig. 10 can be used to explain the mechanism of the electric discharge action upon the dielectric. The treatment velocity grows with the reduction of the capacity magnitude and reaches the maximum value at a capacity of 0.1 mcF, wherein the characteristic frequencies are in the region of ultrasonic frequencies, which is reinforced by the oscillographic observations. It is well known that glass is worked well by using ultrasonic methods using abrasives.

Hence, cavitation, occurring as a result of ultrasonic oscillation generation in the cathode area, is one of the factors acting on the working process, along with the plasma–chemical effect, which is stimulated by a high temperature. The measurements of the dependence of the glass treatment velocity on the electrolyte concentration presented in Fig. 11 circumstantially confirm these conclusions. As has been pointed out, the surface tension coefficient decreases with the electrolyte concentration growth; owing to this, the conductivity rises and, as a consequence, the discharge gap resistance reduces. This causes the diminution of the RC generator discharge time constant and a respective shift of the characteristic discharge frequencies into the region of high frequencies. In this connection, in the region of low concentrations, according to the nature of the surface tension coefficient variation, the working speed is small and rises with the growth of the concentration.

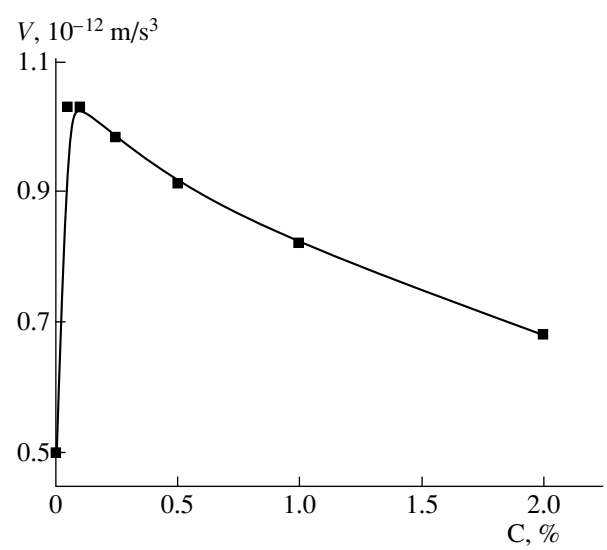

Fig. 10. Removal speed versus the condenser capacity characteristics for the 6% NaCl electrolyte: d_{EI} = 1.5 mm, T = const, and P = 40 VA.

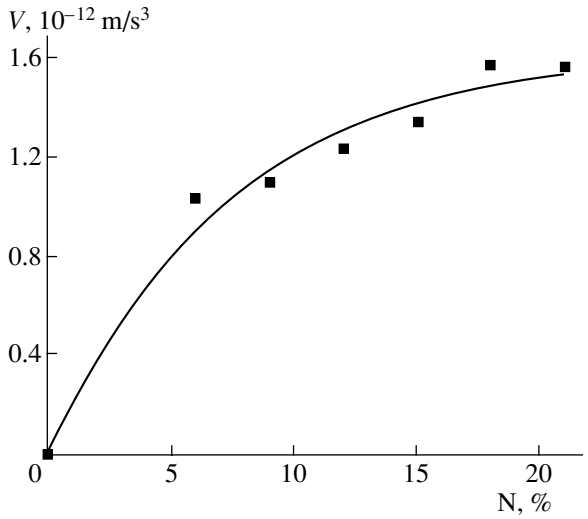

Fig. 11. Removal speed versus the NaCl concentration characteristics: T = const, C = 0.5 mF, and P = 40 VA.

CONCLUSION

Measurements of the current–voltage characteristics of the current passage reveal the general nature of the dependency with four transitional regimes. The features of the transitional regimes depend on the electric conditions and the electrolyte type and its concentration and don't depend on the interelectrode spacing. The occurrence of a plasma sheath in the cathode area at the third stage is a result of the voltage redistribution in the electrolyte circuit; the whole input energy is concentrated in this area. For every electrolyte (with the same material being used for the cathode), there exists voltages and respective current densities such that a plasma sheath comes into existence. The correlation between these parameters and the measured values of the surface tension coefficient of the examined electrolytes is found.

It is established that, under the conditions of the plasma sheath formation near the cathode in the electrolyte medium, the processing of nonconducting materials is possible. The influence of such technological parameters as the electric power input, the electrolyte concentration, the electrode-instrument revolution frequency, and the relaxation generator capacity on the speed of working such materials was investigated. It was shown that the dependence of the piercing speed upon the relaxation generator frequency and the electrode-instrument revolution frequency is of extreme character.

REFERENCES

1. Camada, H., Daiki, H., Maehata, H.K., *Hitachi Zosen Giho*, 1986, vol. 47, no. 3/4, pp. 92–98.
2. Hanreich, G., Mundleina, M., Hauser, H., Nicols, J., et al., *Sensors and Actuators*, 2001, vol. A 91, pp. 57–60.
3. June-Ho, Young-Hag Koh, and Hyoun-Ee Kim, *J. Am. Ceram. Soc.*, 1999, vol. 82, no. 11, pp. 3037–42.
4. Hideyki Horisava, Noritoshi Akimoto, and Hioraki Ashizawa, *Surface and Coating Technology*, 1999, vol. 112, pp. 389–393.
5. Horisawa et al., *Surface and Coating Technology*, 1999, vol. 112, pp. 369–374.
6. Abdukarimov, E.T., Mirkarimov, A.M., and Zaripov, A.A., *Uzbek J. Phys.,* 2003, vol. 5, no. 1, pp. 52–57.
7. Popilov, L.Ya., Heating of metals in electrolyte, in *Novoe v elekrtofizicheskoi i elektrokhimicheskoi obrabotke metallov* (News in Electrophysical and Electrochemical Processing of Metals), Moscow, 1968, pp. 124–147.

ISSN 1068-3755, Surface Engineering and Applied Electrochemistry, 2007, Vol. 43, No. 2, pp. 83–86. © Allerton Press, Inc., 2007.
Original Russian Text © V.F. Gologan, Zh.I. Bobanova, S.Kh. Ivascu, V.A. Popov, V.A. Mazur, 2007, published in Elektronnaya Obrabotka Materialov, 2007, No. 2, pp. 12–16.

ELECTRICAL SURFACE TREATMENT METHODS

Particularities of the Electroplating Process in the Case of a Single-Phase Power Supply with an Embedded Induction-Capacitance Device

V. F. Gologan[1], Zh. I. Bobanova[1], S. Kh. Ivascu[1], V. A. Popov[1], and V. A. Mazur[2]

[1] *Institute of Applied Physics, Academy of Sciences of Moldova, ul. Academiei 5, Chisinau, MD-2028 Republic of Moldova*
[2] *Center of Metrology and Automation of Scientific Research, Academy of Sciences of Moldova, ul. Academiei 3, Chisinau, MD-2028 Republic of Moldova*

Received March 6, 2007

Abstract—This paper presents experimental data on the use of a single-phase power supply and induction-capacitance device for copper electroplating. It is shown that the electrode potential and deposit structure depend on the values of the induction and capacitance through the influence of alternating components.

DOI: 10.3103/S1068375507020020

INTRODUCTION

It was found in previous investigations that, by changing the parameters of the induction-capacitance device (L, C) connected to a three-phase rectifier, one can influence the electroplating process and physical-mechanical properties of the deposits [1]. At optimal values of the induction L_{op} and the capacitance C_{op}, the metal electroplating speed (resulting from the increase of the yield of the current and the current density) and the wear resistance of the deposits increased by a factor of 1.5–2.

Preliminary tests have shown that connection of these devices to industrially produced single-phase power supplies (up to 30 mA) hinders the determination of their optimal parameters due to the construction particularities of the mentioned rectifiers. Therefore, special studies are required.

EXPERIMENT METHODS

The power supply consisted of a 40-W transformer, a rectification block, and a series connection of a parallel induction-capacitance contour. The technical characteristics were chosen so that it may be used for measurement of the polarization curves at electroplating on samples necessary for other types of tests. The induction was formed mainly by two similar throttles with L_2 = 5 H, their windings being connected in series (L_1) and in parallel (L_3).

The required capacitance was obtained by parallel connection of electrolytic condensers with a capacitance of 2200 μF.

Copper deposits electroplated from a sulfate electrolyte (250 g/l $CuSO_4$, 50 g/l H_2SO_4, t_{el} equal to 20°C, D_k equal to 2–10 A/dm^2) were studied.

The polarization curves were measured in the galvanostatic mode. The current was alternated in steps, being kept for 30 s at each step for the stabilization of the potential [2]. The influence of the contour parameters on the electrode potential was fixed starting at 5–10 mA; this satisfied the requirements of the tasks set. The deposits were electroplated on Pt samples having a surface of 0.001 dm^2.

The current value was determined by a resistance box and was registered by an M209 volt–ampere meter. For the cathode potential measurement, a B7-27A/1 volt meter was used. The current waveform was observed on the screen of a C1-55 oscillograph.

To obtain additional data on the contour influence on the copper electroplating process, alternating components in the power supply–bath circuit were studied using an SCh-56 frequency analyzer.

Influence of the induction-capacitance device parameters on the cathode potential at a current density of 10 A/dm^2

Induction L	Capacitance C, mF	Cathode potential φ, mV
–	–	313
L_1	–	323
L_2	–	368
L_3	–	315
L_2	8800	302
L_2	13200	266
L_2	17600	252
L_2	22000	291
L_2	24200	300
L_2	28600	298

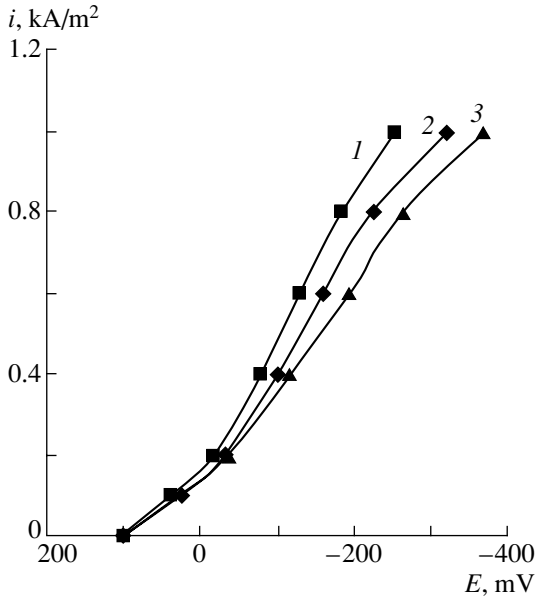

Fig. 1. Polarization curves at copper electroplating: *1*—the device is connected in the optimal mode of tuning; *2*—the device is not connected; *3*—the induction is connected.

The morphology and structure of the 0.1-mm-thick deposits were fixed on samples of a 0.042 m^2 surface using a Tesla BS-340 scanning electron microscope. For estimation of the deposit hardness, a PMT-3 microhardness tester was applied.

RESULTS AND DISCUSSION

It is found that, at connection to a rectifier of the highest induction (at a series connection by the winding of two throttles), smoothing of the pulsation in the power supply–bath circuit at a current of 80 mA occurs. Parallel connection of condensers to the induction resulted in the initial current waveform recovery if the voltage decrease on the contour did not exceed 1 V. An increase of the active induction resistance led to generation of a pulse current.

The induction-capacitance device parameters significantly influenced the cathode potential. With only the induction increasing, the electrode potential shift to the more negative side took place (Table). At connection of the condensers, the electrode potential became more positive in comparison with its values in the experiments without a contour, and the ultimate deviation was found at a maximal induction (L_{op}) and capacitance (C_{op}) of 17.600 μF (Table, Fig. 1).

Thus, it is found that, under the chosen conditions of the experiment with modification of only the induction-potential parameters, the cathode potential shifted by ~100 mV at the current density of 10 A/dm^2; that is, in parallel with the change of the solution composition and electroplating conditions (the current density, temperature, electrolyte pH, etc.), there appeared one more possibility to control the electrolytic process of electroplating and, hence, the physical-mechanical properties.

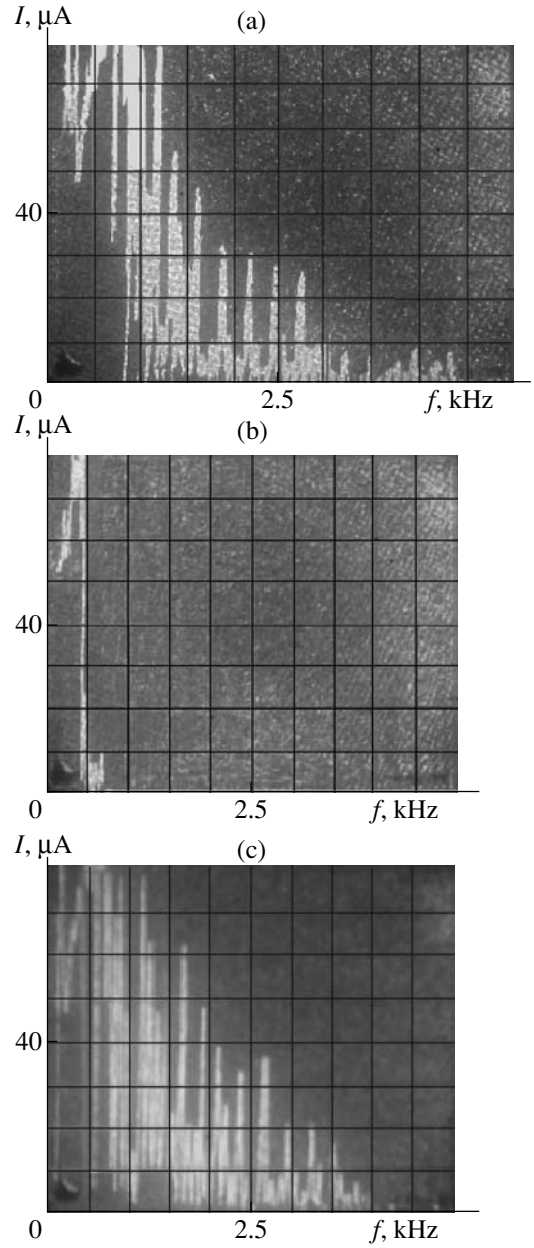

Fig. 2. Spectrum of the current alternating components at copper electroplating at D_k = 2 A/dm^2(I = 80 mA): (a) the device is not connected; (b) the induction is connected; (c) the device is connected.

The alternating components were estimated in the process of the sample electroplating at a current density of 2 A/dm^2 (I_k = 80 mA) with only the induction (L_{op}) connected with the contour (L_{op}, C_{op}) and without it (Fig. 2).

It was revealed that, at electroplating without connection of the induction-capacitance device, the alternating components were found up to 5 kHz (Fig. 2a). In this dynamic range of frequencies, their amplitude

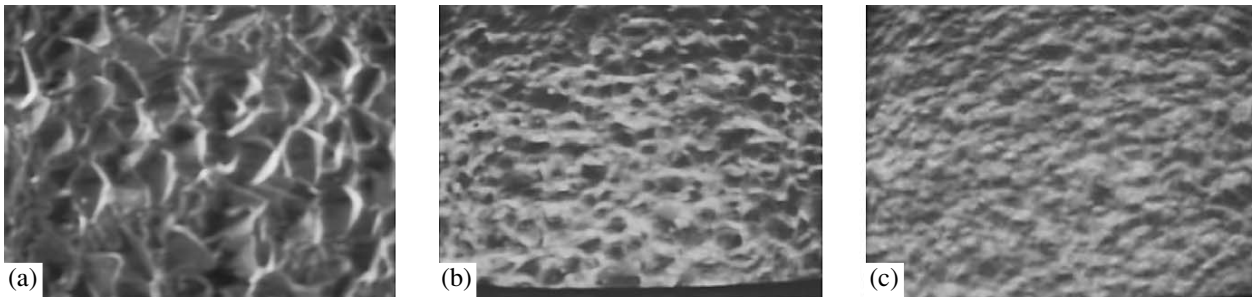

Fig. 3. Morphology of copper deposits at $D_k = 2$ A/dm^2 ($I = 80$ mA): (a) the device is not connected; (b) the induction is connected; (c) the device is connected.

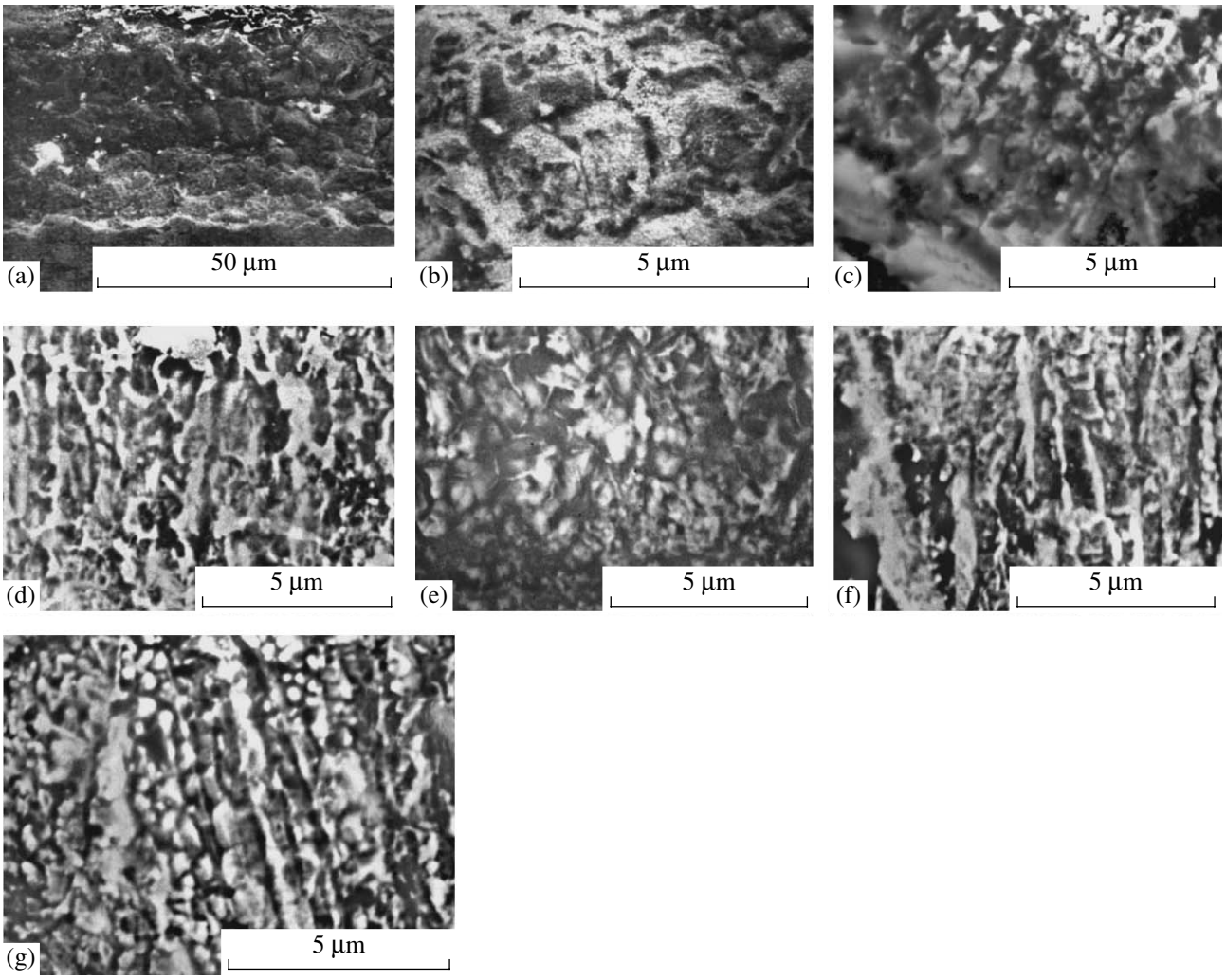

Fig. 4. Structure of copper deposits electroplated at $D_k = 2$ A/dm^2 ($I = 80$ mA): (a) ×600; (b) ×3000; (c) ×5000, the device is not connected; (d) ×3000; (e) ×5000, the induction is connected; (f) ×3000; (g) ×5000, the device is connected.

changed in a nonuniform way: at a frequency of 2.75 kHz, a sharp decrease of its value took place.

The induction connection exerted a significant influence on the spectrum of the alternating components: they were only observed at low frequencies (Fig. 2b). The capacitance connection favored the noise amplitude increase by a factor of 1.5, the spectrum broadening up to 6 kHz, and their ordering (Fig. 2c).

These conditions of the electrolysis also differently influenced the morphology of the copper deposits (Fig. 3). At electroplating without a contour, a uniform pyramidal growth of the deposits all over the surface

was observed (Fig. 3a). Connection of only the induction considerably influenced the character of the deposit growth: the prominent faces of the "blocks" significantly decreased in value, their configuration became smooth, and they uniformly spread over the surface (Fig. 3b). Connection of the condensers resulted in an increase of the mentioned faces (Fig. 3c).

The above mentioned conditions of the electroplating exerted an analogous influence on the structure of the copper, which was analyzed on transverse sections (Fig. 4). In the case of the contour-free electroplating, the deposits were formed of blocks that were appreciably different in their dimensions (Figs. 4a and 4b). The blocks themselves consisted of crystallites of small dimensions (Fig. 4c). The induction connection resulted in a decrease of the blocks, distortion of their form, and an absence of clearly defined boundaries (Figs. 4d and 4e). They were also formed of small crystalline aggregates of indistinct orientation. The deposits obtained with the contour were little dispersed with a tendency to columnar growth. Bigger aggregates had a chiefly elongated form and were located perpendicular to the interface (Figs. 4f and 4g).

The presented results of the investigations show a significant influence of the inductance-capacitance device parameters on the kinetics of the electroplating of copper deposits and their structure.

The analysis of the experimental data has shown that, as in previous research [1, 3], changes of the cathode potential and the alternating components are interrelated: the amplitude increase and the noise spectrum broadening were observed at the potential shift to the positive side. Under the usual conditions of electrolysis, such a potential shift is possible only as a result of the electrolyte composition change and its temperature increase due to the current density decrease. Therefore, application of the induction-capacitance device allows increasing the electroplating efficiency due to the current density increase [1, 3].

The observed decrease of the block dimensions at connection of only the induction is apparently caused by the more negative potential of the cathode; these experimental data are in agreement with conventional ideas on the electrode potential influence on the deposit structure [4]. The considerable narrowing of the alternating components of the spectrum frequency under these experiment conditions confirms V.A.Tyagai's statement about the relation of the noises and kinetics of the electrode processes [5], as well as the possibility to control the spectrum of the alternating components by selection of the induction-capacitance device parameters [3].

The induction connection, despite the potential shift to the more positive side, favored decreasing the dimensions of the crystalline aggregates and the formation of a disperse structure. An analogous influence was exerted by the contour at the electroplating of chromium deposits [1, 6].

These results are apparently caused by the electrodynamic conditions of the near-cathode layer formation, thus, promoting crystal growth restrictions not as a result of periodic passivation of the surface but entirely due to the nucleation velocity increase [2, 4].

Thus, the results have shown that, when designing single-phase power supplies for application in galvanic technological processes, one should take into account the influence of some construction laws on the electroplating process. In addition, it is efficient to use special induction-capacitance devices. By selecting their parameters (L, C), it is possible to increase the process efficiency and to improve the physical-mechanical properties of the deposits.

REFERENCES

1. Gologan, V.F., Electrochemical Process Control by Induction–Capacitance Devices (Review), *Elektronnaya Obrabotka Materialov*, 2006, no. 6, pp. 39-43.
2. Vagramyan, A.T. and Zhemagortsyants, M., *Elektroosazhdenie metallov i ingibiruyushchaya adsorbtsiya* (Metal Electroplating and Inhibiting Adsorption), Moscow, 1969.
3. Ivascu, C., Particularitatile cinetice a procesului de cromare cu utilizarea obiectului de resonanta. *Tehnologii moderne. Calitate. Restruturare* (Modern Technologies. Quality. Reconstruction), Chisinau: UTM, Tehnico–info, 1999, vol. 2, pp. 302–304.
4. Frumkin, A.I., Andreev, V.N., Boguslavskii, L.I., et al., *Dvoinoi sloi i elektrodnaya kinetika* (Double Layer and Electrode Kinetics), Moscow, 1981.
5. Tyagai, V.A., *Elektrokhimiya*, 1975, vol. 10, no. 1, pp. 3–24.
6. Ivascu, C., Contribuţiă obiectului de resonanţă asupra variaţiei unor parametri fizico-mecanice al depunerilor de crom, *Tehnologii moderne. Calitate. Restruturare* (Modern Technologies. Quality. Reconstruction), Chişinău: UTM, Tehnico–info, 1999, vol. 2, pp. 305–307.

ISSN 1068-3755, Surface Engineering and Applied Electrochemistry, 2007, Vol. 43, No. 2, pp. 87–89. © Allerton Press, Inc., 2007.
Original Russian Text © P.V. Peretyatku, 2007, published in Elektronnaya Obrabotka Materialov, 2007, No. 2, pp. 17–19.

ELECTRICAL SURFACE TREATMENT METHODS

The Effect of Quasi-Regular Oscillation of the Mass Transfer Intensity at Electrospark Alloying in a Magnetic Field

P. V. Peretyatku

A. Russo Beltsy State University, Pushkin str. 38, Beltsy, MD-3110 Republic of Moldova

Received March 6, 2007

Abstract—The effect of quasi-regular oscillation of the mass transfer intensity under electric spark doping in a magnetic field has been found. The ESD process has been studied using materials with different magnetic properties as electrodes. The possibility to control the process of covering formation on the cathode by changing the magnetic field induction has been shown.

DOI: 10.3103/S1068375507020032

The investigation of the process of electrospark alloying (ESA) in a magnetic field allowed revealing an interesting phenomenon of quasi-regular oscillation of pulse discharge craters (dents) caused by the alternation of focusing and defocusing of the discharge spot under changes of the magnetic field induction or discharge energy [1]. In this connection, it was supposed that the magnetic field influence must affect the mass transfer in the spark discharge. The experiments on the repeated spark discharge action on the metal backing confirmed the existence of quasi-regular oscillation and stability of the magnetic field effect on the mass transfer in the spark discharge.

In the mentioned work, the researchers studied the ESA process in a magnetic field with the purpose of revealing the quasi-regular oscillation effect on the mass transfer in the spark discharge for materials different in their magnetic properties (ferromagnetic and diamagnetic).

At the first stage, the ESA process was examined using electrodes of ferromagnetic materials in the form of bars with a size of $4 \times 4 \times 40$ mm (nickel; chromium-nickel alloy VJL-14; and hard alloys based on tungsten carbide VC8 and VC20 containing 8 and 20% tungsten, respectively); plates of St. 3 and St. 45 with a size of $4 \times 15 \times 15$ mm served as the cathodes. The ESA was carried out with the discharge energy being from 0.1 to 1.0 J and the magnetic field intensity varying within 0.0 to 0.1 Tl.

The investigation of the kinetics of the cathode mass buildup under ESA by nickel corroborated the existence of the effect of quasi-regular oscillation of the intensity of the material transfer from the anode to cathode (Fig. 1). As can be seen from Fig. 1a (curves *1* and *2*), the quantity of the transferred anode material to the cathode surface in ESA of two minutes and with the intensity of the magnetic field imposed on the treatment zone being 0.069 Tl is twice as large as at ESA under the same regime without the field. When the field intensity is increased only by 0.006 Tl, the transferred material amount reduces by nearly half and becomes comparable with the amount transferred at ESA in the absence of a field (Fig. 1, curves *3* and *1*). With the next intensity

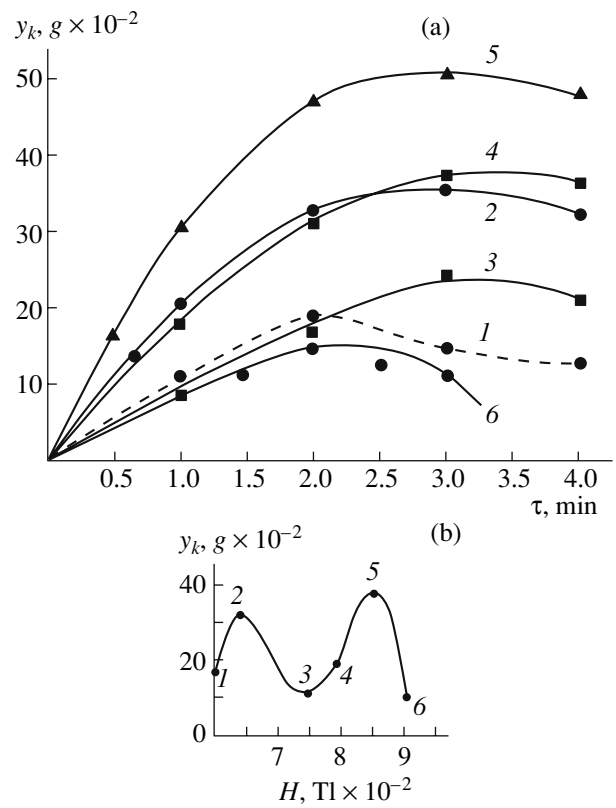

Fig. 1. Variation of steel St. 3 cathode mass buildup with time against the intensity value of the magnetic field imposed on the ESA zone (a) and the dynamics of the cathode mass increase after treatment for 2 min for the same values of the field intensity (b) Tl: (*1*) 0, (*2*) 0.069, (*3*) 0.075, (*4*) 0.081, (*5*) 0.086, (*6*) 0.091. Anode—Ni; discharge energy—0.3 J.

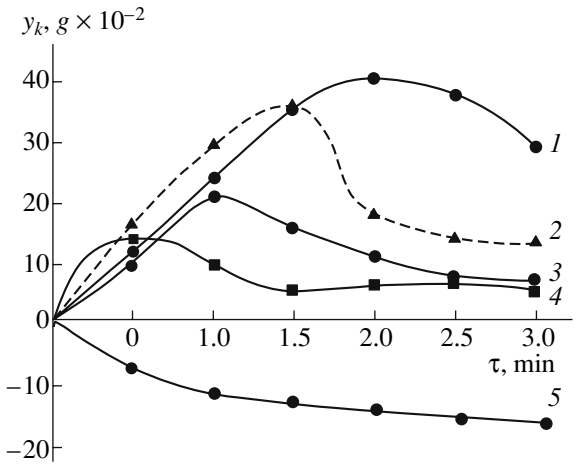

Fig. 2. Variation of the titanium cathode mass buildup with time against the intensity value of the magnetic field imposed on the ESA zone B, Tl: (*1*) 0.066; (*2*) 0.07; (*3*) 0.074; (*4*) 0.078; (*5*) 0.

increase to 0.086 Tl, the transfer of the anode eroded mass to the cathode grows again and lowers at the magnetic field intensity of 0.091 Tl (Fig. 1, curves *6*).

The quasi-regular oscillation effect shows itself clearly at any other values of the discharge energy. In so doing, only the maximum points shift in the cathode mass buildup curves $K = f(t)$. Depending on the electrode material, the nature of these points is achieved in more or less time of the ESA. For instance, within the regime with the discharge energy being 0.3 J with the field intensity values being in the range of 0.0–0.1 Tl, the maximum point of the $K = f(t)$ curve is achieved at the third minute.

At the same time, within a similar energy regime with anodes of the VJL-14 chromium-nickel alloy or the VC8 and VC20 hard alloys being used, the maximum of the $k = f(t)$ curve is achieved at approximately the sixth minute. This is accounted for by the difference of the erosion resistance and chemical activity of the mentioned materials.

Let us consider the case when the anode (electrode being treated) is a ferromagnetic material (Ni) and the cathode (Ti) is a nonferromagnetic one. On the face of it, the surface layer formation dynamics don't differ from those at ESA by other materials (Fig. 2). However, if we take into account the results of works [2, 3], in which it is established that, in the initial stage of ISA of titanium by nickel, there is observed the effect of strong erosion of the titanium cathode dominating over the nickel anode erosion and continuing for 8 minutes of treatment, whereupon the anode material deposition begins, it becomes clear that the magnetic field has substantially influenced the "suppression" of the intensive cathode erosion effect.

It can be supposed that, under such conditions with this combination of the discharge energy value and the magnetic field intensity, the electron exchange between the anode (Ni) and cathode (Ti) materials declines, thus, assisting the deposition of nickel on the cathode surface.

From the practical standpoint, the suppression of the effect of titanium providing strong erosion at the ESA by the nickel anode is very important at the hardening of the titanium alloys, as it prevents the reduction of their geometrical dimensions. In work [3], the above mentioned adverse factor was eliminated with the help of the prepassivation of the titanium backing surface by sparking it with a graphite electrode in a lower energetic regime. However, in our case, this problem is solved by the imposing on the ESA zone of a magnetic field with an intensity varied in the range of 0–0.1 Tl. In spite of the presented particularities of ESA of titanium by nickel, under the influence of a magnetic field, the effect of quasi-regular oscillation of the anode erosion mass transfer to the cathode is clearly revealed (Fig. 2).

The investigation of the ESA process in a magnetic field when both the anode (Ag) and cathode (Cu) are diamagnetic materials permitted obtaining new and interesting results. Firstly, all other factors being equal, the amount of transferred silver on the copper surface at ESA in a magnetic field differs moderately from that in the absence of a magnetic field. At some values of the field intensity, the amount of the transferred silver on the copper cathode is even slightly less than under conventional ESA without a magnetic field. However, the quality of the surface layers formed at ESA of copper by silver in a magnetic field is much higher. Also noteworthy are the layer thickness continuity and uniformity, which are achieved, as was mentioned in [1], due to the better moistening of the liquid phase under the effect of the Ampere forces arising in the ESA zone in the magnetic field.

Secondly, in spite of the difference in the amount of silver transferred to the cathode in the magnetic field, the effect of the quasi-regular oscillation of the mass transfer from the anode to the cathode reveals itself even in the absence of a magnetic field. At some values of the field intensity (0.04, 0.08, and 0.1 Tl), there is observed the violation of the silver plating process stability. Superficially, it is manifested in the form of a change of the spark, which becomes barrel-shaped testifying to the widening of the discharge passage. As a result, there is observed the sputtering of the vapor component of the silver anode erosion mass into the surrounding medium with its substantial part depositing on the poles of the electromagnet with whose help a magnetic field is created in the ESA zone. Evidently, at the mentioned values of the magnetic field intensity, there occurs the defocusing of the electron–ion beam with the result that a considerable part of the ionized particles, vapors, and silver liquid phase don't reach the cathode surface. Ultimately, during the same treatment

time, the cathode mass buildup grows with a rate that is less by half than that in the absence of the field. Meanwhile, at a field intensity equal to 0.07 Tl, there occurs electron–ion beam focusing resulting in pinching of the discharge passage and a consequent increase of the energy density in it, thus, promoting an increase in the amount of the erosion mass transferred to the cathode. Hence, the imposition of a magnetic field on the ESA zone substantially influences the process of mass transfer in the spark discharge and opens new possibilities to control the process of coating formation on the cathode.

REFERENCES

1. Mihailov, V.V., Dushenko, V.F., and Peretyatku, P.V., *Surface Eng. Appl. Electrochemistry*, 2000, no. 5, pp. 49–52.
2. Mihailov, V.V., Investigation of particularities of electrospark alloying of titanium and its alloys, *Extended Abstracts,* Kiev, 1976.
3. Mihailov, V.V., Bachu, K.A., Pasinkovskii, E.A., and Peretyatku, P.V., *Surface Eng. Appl. Electrochemistry*, 2006, no. 3, pp. 106–111.

ISSN 1068-3755, Surface Engineering and Applied Electrochemistry, 2007, Vol. 43, No. 2, pp. 90–93. © Allerton Press, Inc., 2007.
Original Russian Text © L.A. Kuz'micheva, Yu.V. Titova, A.I. Maksimov, 2007, published in Elektronnaya Obrabotka Materialov, 2007, No. 2, pp. 20–23.

ELECTRICAL PROCESSES
IN ENGINEERING AND CHEMISTRY

Generation of Chemically Active Oxidative Particles in Electrolyte Solutions under the Action of Glow and Diaphragm Discharges

L. A. Kuz'micheva, Yu. V. Titova, and A. I. Maksimov

Institute of Solution Chemistry, Russian Academy of Sciences, Russia

Received November 20, 2006

DOI: 10.3103/S1068375507020044

INTRODUCTION

Plasma-solution systems are used for sterilization of water, for water solutions and different objects [1], for water purification from organic impurities [2], and for modification of the surface of polymer materials [3, 4]. Knowledge of the nature of the active particles and, first of all, of the oxidative particles arising in solutions under discharge action is necessary for the development and optimization of these processes.

At the action of glow discharge on a solution of an electrolyte (Fig. 1), the surface of the solution directly contacting with the plasma (region of the cathode spot) is subjected to bombardment by positive ions from the plasma zone. The ion bombardment causes dissociation and ionization of water molecules and the appearance of primary active particles in the region of the cathode spot, such as atomic hydrogen, hydroxyl radicals, and solvated electrons:

$$H_2O \xrightarrow{\text{discharge}} OH^* + H^*;$$

$$H_2O \xrightarrow{\text{discharge}} H_2O^+ + e;$$

$$e \longrightarrow e_{sol}.$$

$$H_2O^+ + H_2O \longrightarrow H_3O^+ + OH^*;$$

$$OH^* + OH^* \longrightarrow H_2O_2.$$

The dimerization of hydroxyl radicals leads to the formation of hydrogen peroxide in the solution [5]. As a rule, hydrogen peroxide is considered to be a relatively stable secondary oxidative agent formed upon the gas discharge treatment of water solutions. In our opinion, the basic mechanism of its formation is the above indicated dimerization of OH radicals, although, in [6], a mechanism of H_2O_2 formation omitting the intermediate stage of formation of OH radicals was proposed and the assumption that ozone in the liquid phase is formed in the process of gas discharge treatment of water solutions and that ozone also takes part in the oxidation process were stated.

In our opinion, the processes observed under the action of both diaphragm and glow discharges are close. Indeed, a diaphragm discharge is initiated in a solution volume at electrical breakdown of steam bubbles formed in a small hole (diaphragm) in a dielectric partition dividing a plasma-solution cell (Fig. 2) with the current density increasing up to the critical value. At this point, the current flow is stopped and all the external emf turns out to be applied to the originated steam gap. If its value is sufficiently big, then an electrical breakdown takes place and an electrical discharge is originated in a bubble. The bubble collapses, the circuit is closed again, and the process described is repeated. As a result, a quasi-periodic (diaphragm) discharge arises inside the volume of the solution. In the active period of burning of the diaphragm discharge, its structure is close to the structure of a glow discharge with the same role in the region of the cathode drop. The main difference between them lies in the fact that the strong acoustic wave propagates at the collapse of the plasma zone of the diaphragm discharge in the solution, the

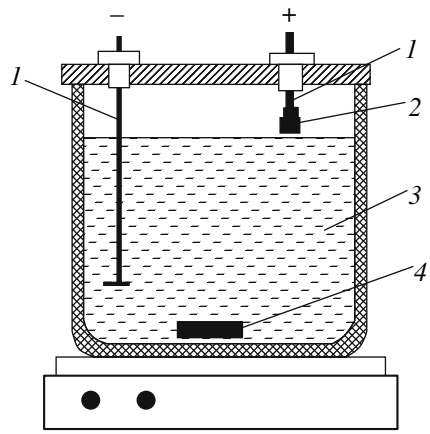

Fig. 1. Principle scheme of a cell for glow discharge: (*1*) electrodes, (*2*) plasma zone, (*3*) electrolyte solution, (*4*) magnetic mixer.

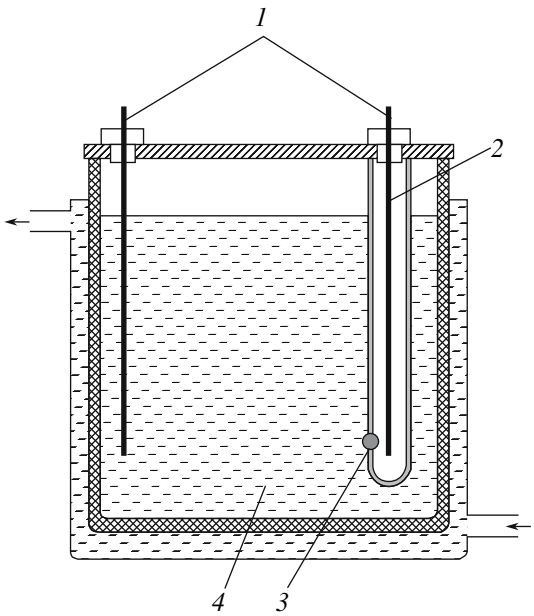

Fig. 2. Principle scheme of a cell for diaphragm discharge: (*1*) electrodes, (*2*) diaphragm, (*3*) plasma zone, (*4*) electrolyte solution.

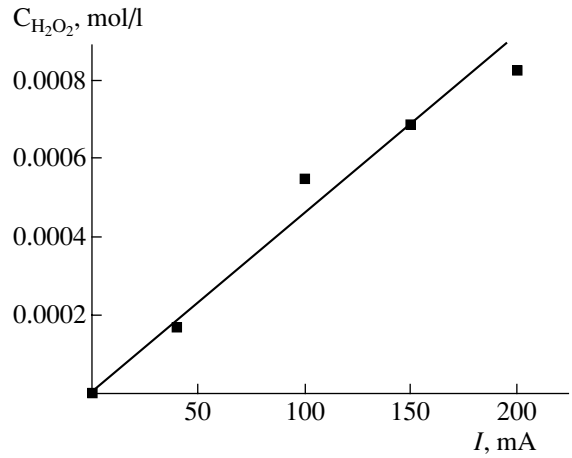

Fig. 3. Dependence of the accumulation of hydrogen peroxide on the discharge current under the action of diaphragm discharge. Experimental conditions: electrolyte—0.01 M Na_2SO_4; volume of solution—400 ml; treatment time—8 min; electrodes—graphite and stainless steel.

physicochemical effect of which may be put into practice [1].

The aim of this paper is the comparison of the efficiencies of the accumulation of hydrogen peroxide in solutions under the action of glow and diaphragm discharges and analysis of the possible role of ozone in the initiation of the oxidative processes in these systems.

EXPERIMENTAL

In the case of the diaphragm and glow discharges, solutions of natrium sulfate of various concentrations (from 0.01 to 0.1 mol/l) were used. The volume of the treatment solution composed 400 ml. The investigations were conducted in glass cells whose schemes are presented in Figs. 1 and 2. The discharge current in the case of the diaphragm discharge composed 40, 100, 150, and 200 mA; in the case of the glow discharge, it composed from 10 to 40 mA. As the electrode materials, stainless steel and graphite were used.

The accumulation of hydrogen peroxide in the solution under the action of the gas discharges was measured with the help of spectrophotometric analysis (the scheme of the experimental setup is presented in [7], and $\lambda = 253.7$ nm) and also with the help of iodine titration with molybdate ammonium.

Since the ozone was determined using spectrophotometric analysis in the same region as the hydrogen peroxide was determined, a system of analytical methods [8] was used for its detection.

1. The H_2O_2 content in the solution was determined by permanganate titration (the peroxide is determined as a regenerator; the O_3 is not determined).

2. The H_2O_2 was determined by iodine titration with molybdate ammonium ($(NH_4)_2MoO_4$ is used as a selective catalyst for the reaction of iodine ions with hydrogen peroxide, O_3 does not hinder the determination).

3. The joint presence of oxidants in the solution was determined by iodine titration using the standard methods (H_2O_2 and O_3 were determined).

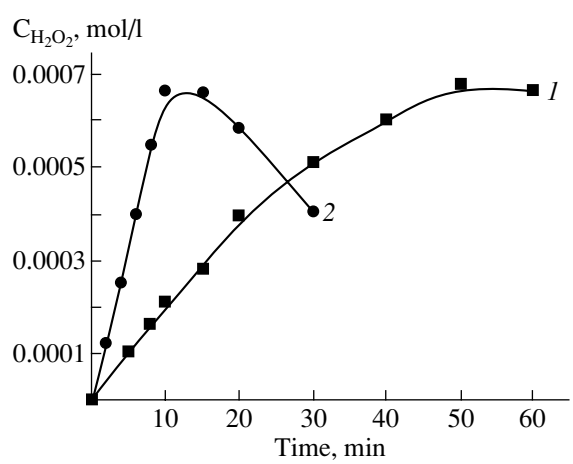

Fig. 4. Kinetic dependence of the accumulation of hydrogen peroxide in a solution under the action of diaphragm discharge at different currents, mA: (*1*) 40; (*2*) 100. Experimental conditions: electrolyte—0.01 M Na_2SO_4; volume of solution—400 ml; electrodes—graphite and stainless steel.

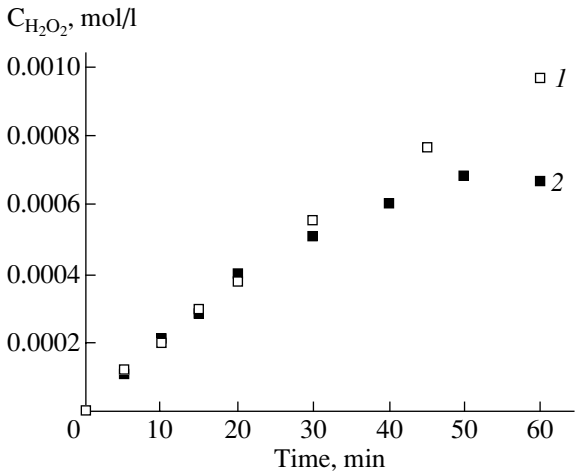

Fig. 5. Influence of the electrodes' material on the accumulation of hydrogen peroxide under the action of diaphragm discharge. Experimental conditions: electrolyte—0.01 M Na_2SO_4, volume of solution—400 ml, current—40 mA; electrodes: (*1*) graphite–graphite, (*2*) graphite–stainless steel.

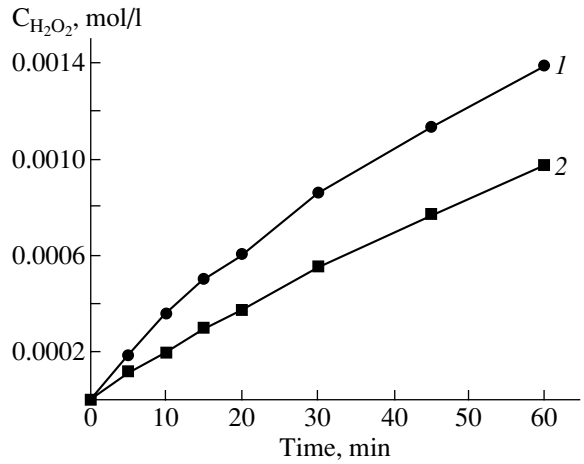

Fig. 6. Accumulation of hydrogen peroxide under the action of glow (*1*) and diaphragm (*2*) discharges. Experimental conditions: electrolyte—0.01 M Na_2SO_4; volume of solution—400 ml; discharge current—40 mA; electrodes—graphite–graphite.

RESULTS

In this paper, the dependence of the H_2O_2 accumulation in the electrolyte solution under the action of a diaphragm discharge on the discharge current was investigated. During the comparatively short time of the discharge action on the solution, the velocity of the accumulation of the hydrogen peroxide increases with an increase of the discharge current (Fig. 3). However, during treatment over a long period of time, the content of hydrogen peroxide in the solution begins to decrease (Fig. 4), which is obviously associated with its thermal decomposition under the more intensive discharge treatment. In addition, at a diaphragm discharge burning, the destruction of the cathode takes place and the electrode material enters into the solution. With the increase of the discharge current and the duration of its action, the intensity of the cathode destruction increases and, accordingly, the content of its material in the solution increases. In this experiment, a cathode made of stainless steel was used, as it is well known that the iron ions that accumulate in the solution during the gas discharge treatment are a catalyst for the decomposition of the H_2O_2.

The electrode material, in the case of both a glow discharge [7] and a diaphragm discharge, influences the formation of H_2O_2 in the solution. In Fig. 5, the kinetic curves of the accumulation of hydrogen peroxide when using electrodes made of graphite and stainless steel are presented. In the case of a glow discharge, only the material of the cathode essentially influences the H_2O_2 decomposition, since the anode is removed into the gas phase region and does not contact the solution. As is seen from the figure, in the case of using graphite electrodes, the H_2O_2 content in the solution is higher than when using electrodes made of stainless steel. We obtained analogous results for a glow discharge.

We compared the efficiency of glow and diaphragm discharges relative to the process of accumulation of H_2O_2. As shown in Fig. 6, the speed of the accumulation of H_2O_2 is higher under the action of a glow discharge compared to a diaphragm discharge, all other factors being the same (the discharge current and the volume and concentration of the solution).

Comparative results of titration of electrolyte solutions by different methods

Treatment time, min	Content of oxidants in solutions after discharge treatment $C \times 10^{-4}$ (mol/l)					
	glow discharge (0.01 Mol Na_2SO_4, 200 ml, 30 mA)			diaphragm discharge (0.01 Mol Na_2SO_4, 400 ml, 100 mA)		
	method 1	method 2	method 3	method 1	method 2	method 3
5	3.7^4	3.5	3.8	3.3	3.3	3.3
15	9.5	9.0	9.0	6.8	6.6	6.6
30	12.6	12.7	12.9	4.1	4.1	4.2

In solutions subjected to the action of glow and diaphragm discharges, the contents of both hydrogen peroxide and ozone were determined. Comparing the results of titration according to method 3 (joint presence of oxidants) with the results of the hydrogen peroxide determination according to methods 1 and 2, the quantity of O_3 in the solution can be estimated.

Our experiments showed that the titrations according to all three methods gave practically the same results, which are presented in the table. The observed differences in the values do not exceed the error of the experimental titration methods. Therefore, under the conditions of our experiments, hydrogen peroxide is only a stable secondary product forming under the action of diaphragm and glow discharges in the electrolyte solutions.

ACKNOWLEDGMENTS

This work was supported by the Russian Foundation for Basic Research, project no. 06-03-96316.

REFERENCES

1. Stroikova, I.K. and Maksimov, A.I., *Elektron. Obr. Mater.*, 2002, no. 6, pp. 43–49.
2. Ivannikov, A.A., Lelevkin, V.M., Tokarev, A.V., and Yudanov, V.A., *Khimiya Vysokikh Energii*, 2003, vol. 37, no. 2, pp. 148–151.
3. Titov, V.A., Shikova, T.G., Maksimov, A.I., and Titova, Yu.V., *Electron. Obr. Mater.*, 2004, no. 3, pp. 22–28.
4. Zheleznov, K.N. and Maksimov, A.I., *Menedeleev Communication*, 2005, no. 5 pp. 214–215.
5. Pikaev, A.K., Kabakchi, S.A., and Makarov, I.E., *Vysokotemperaturnyi radioliz vody i vodnykh rastvorov* (High-Temperature Radiolysis of Water and Water Solutions), Moscow: Energoatomizdat, 1988.
6. De Baerdemaeker, F., Monte, M., and Leys, C., *Czechoslovak J. Phys.*, 2004, vol. 54, pp. 1062–1067.
7. Kuz'micheva, L.A., Titova, Yu.V. and Maksimov, A.I., *Elektron. obr. mater.*, 2004, no. 4, pp. 51–67.
8. Skug, D. and West, D., *Osnovy analiticheskoi khimii* (Fundamentals of Analytic Chemistry), vol. 1, Moscow: Mir, 1979.

ISSN 1068-3755, Surface Engineering and Applied Electrochemistry, 2007, Vol. 43, No. 2, pp. 94–99. © Allerton Press, Inc., 2007.
Original Russian Text © E.V. Kuvaldina, D.A. Shutov, 2007, published in Elektronnaya Obrabotka Materialov, 2007, No. 2, pp. 24–30.

ELECTRICAL PROCESSES
IN ENGINEERING AND CHEMISTRY

Kinetic Characteristics of the Interaction of Oxygen Atoms with Certain Polymers

E. V. Kuvaldina and D. A. Shutov

Ivanovo State Chemical–Engineering University, Ivanovo, Russia

Received November 2, 2006

DOI: 10.3103/S1068375507020056

INTRODUCTION

Etching of polymers in oxygen plasma is widely used for modification of their surfaces. Optimization of etching processes and modification calls for knowledge of their mechanisms and, specifically, rate constants of interaction of individual chemically active components of plasma with a processing material.

The atoms in ground state $O(^3P)$ and metastable molecules in the states $a^1\Delta_g$ and $b^1\Sigma_g^+$ can be considered as the major neutral chemically active particles of oxygen plasma [1, 2]. The basic charged particles are the electrons and ions O^- and O_2^+ [3]. Ultraviolet radiation (λ = 130.4 nm) is associated with highlighting of the 1st resonance level $O(^3S)$ [4].

It is difficult to separate the action of individual active agents due to the self-consistency of the system. However, such a procedure may be realized by conducting experiments in the zone of streaming plasma afterglow using the distinctions of the characteristic life time for different particles relative to their heterogeneous decay on the reactor walls. The estimations performed show that the concentrations of all the plasma components except for $O(^3P)$ and $O_2(a^1\Delta_g)$ essentially decreased.

The area of streaming afterglow of oxygen plasma is usually used for determination of the kinetic characteristics of the interaction of oxygen atoms with materials. It is assumed that the O_2 molecules do not interact with the polymers [5–7]. The evidence for the last statement, in our opinion, is controversial. The existence of the limitative stage associated with the reactions of O atoms does not eliminate the action of other active plasma agents at the intermediate stages of a process. The molecular oxygen in the O_2 ground state ($x^3\Sigma_g^-$) may be a reagent at the stages following the initiation stage.

Generally, the most employed investigation of the recombination probability of $O(^3P)$ atoms on different surfaces is the EPR method. However, there are few data about the probability of oxygen atoms decaying on polymers obtained by the EPR method [8]. In paper [9], another method for the determination of the kinetic characteristics of the interaction of oxygen atoms with polymers, where the continuity equation for the flow of atoms is used by the authors as a basis, was proposed. The rate of the sample mass decrease was measured in the experiment; at the same time, the concentration of the atoms was being changed, with the concentration of the molecular oxygen being constant, by varying the discharge parameters. The values for the rate constants and probabilities of the kinetic interaction of atoms with the surface of polyimide films [9], polyethylene terephthalate [10], polymer films [11], polyethylene [11], and a lavsan textile [12] were determined with the help of this method.

The aim of this paper is the determination of the kinetic characteristics of the interaction of oxygen atoms with a polyethylene film (PE) and also with a number of materials based on polyethylene terephthalate with the help of a simplified variant of the method proposed by the authors in [9].

EXPERIMENTAL TECHNIQUE

Experiments were carried out on the setup whose scheme is presented in [9]. The plasma was created by the initiation of a direct current discharge in a cylindrical reactor made of type S-49 glass. The pressure of the plasma forming gas in the reactor was varied from 50 to 300 Pa, and the current strength was changed from 20 to 110 mA. The flow velocity of the gas was constant and equal to 30 cm/s. The sample was located in a ring form with a width of 6 cm and a length of 9.4 cm along the generatrix of the reactor in a thermostatically controlled zone of the discharge afterglow at a distance of 3 cm from it. The temperature of the sample was given by the external heat exchanger and was varied from 292 to 353 K. The value of the temperature on the sample surface was measured with the help of a copper-constantan thermopair passing along the wall of the reactor to minimize the disturbance of the plasma.

After processing, the sample was cut up in the direction of the gas flow z into six equal pieces. The measurement of the sample mass loss rate as a whole and of each piece separately was carried out by its periodic weighing on a WA-34 balance with an accuracy of 10^{-4} g.

The mass loss rate was calculated by the formula $W = \Delta m/(S\tau)$, where Δm is the sample mass change under the etching process, τ is the sample processing time in the plasma, and S is the sample area.

The solution of the continuity equation taking into account the transport of atoms by the gas flow, their radial and axial diffusion, and heterogeneous decay gives the next expression for the average concentration over the reactor cross section Q at the distance l from the cylinder boundary formed by the polymer:

$$[O_1] = [O_0]\exp/1/2(\tau_d/\tau_k) - \{(1/2(\tau_d/\tau_k))^2 + k\tau_d\}^{1/2}. \quad (1)$$

In expression (1), Q is the average concentration of atoms over the cross section of the reactor at the entry to the polymer cylinder, and the constant k takes into account the total loss of atoms both in the heterogeneous chemical reaction and as a result of recombination. The diffusion time τ_d and contact time τ_k are determined by the relationships

$$\tau_d = l^2 D, \quad \tau_k = l/V_z, \quad (2)$$

where D is the atom diffusion coefficient, and V_z is the linear velocity of the gas flow.

Assuming that the etching reaction rate in the section of the sample with the coordinate $z = l$ is W, from the data of the weight measurements, using expressions (1) and (2), we determined the rate constant of the heterogeneous decay of the atoms on the surfaces of the investigated material at given parameters of the discharge (the pressure and the current):

$$k = Dt_g^2\alpha - V_z t_g \alpha, \quad (3)$$

where α is the inclination of the line $\ln(W) = f(l)$.

The probability of the heterogeneous decay was calculated by the formula

$$\gamma = (2Rk)/V, \quad (4)$$

where R is the radius of the reactor, k is the Boltzmann constant, V is the thermal velocity, and $V = 0.363 \times 10^4 T^{1/2}$.

TEST SUBJECTS

In this work, high-density polyethylene 100 μm thick was used.

The materials based on polyethylene terephthalate chosen for the investigation were the following: a 35 mm film (GOST 24234-80), an Italian textile consisting of mono-filament threads with the trade mark "SST," and a domestic lavsan textile made of composite threads characterized by an average thickness of 124 μm (Standard 81476).

Table 1. The parameters of the textile on the basis of polyethylene terephthalate

Material	Diameter of the thread, μm	The gap between threads, μm	Specific density, mg/cm^2
SST textile	40	20	4.40
The polyester textile	220*	50	7.20

* Mean diameter of the thread (mean diameter of a monofilament in the thread 18.5 μm).

The parameters of the investigated textiles determined using a raster electron microscope (Tesla BS-300) are presented in Table 1.

The ratios of the atomic concentrations of the elements C, O, and H in the samples corresponded within the accuracy of the elemental analysis to the structure of the elementary unit in polyethylene terephthalate.

DISCUSSION OF THE RESULTS

The experiments showed that the etching speed of all the investigated materials in the indicated range of the discharge decreased exponentially with the rise of the z coordinate. The selected results are shown in Fig. 1. The unified exponential dependence indicates that, at least within the accuracy of the statistical straggling of the initial experimental data, the process (possibly multichannel) may be described by one effective rate coefficient. Its value can be found from the formula for the etching rate dampening taking into account the solutions of the continuity equation for the atomic flow (1).

This method presumes that the mass loss is only determined by atomic oxygen and that a direct linear dependence between the mass loss rate and the atomic flow to the material surface exists. Three variants are possible:

1) The interaction of the atoms with the polymer is predominantly chemical.

2) The recombination interaction is predominant.

3) The chemical and recombination interactions both contribute significantly to the atom loss.

In Figs. 2 and 3, the kinetic characteristics of the interaction of the atoms as a function of the pressure of the plasma forming gas at a discharge current of 80 mA and material temperature of 333 K (Fig. 2), as well as a function of the discharge current at a pressure of 100 Pa and at the same temperature (Fig. 3), are shown. Our attention is drawn to the fact that, in almost all the cases, more or less defined dependences of the rate coefficients and probabilities on the parameters of the discharge are displayed. Thus, the determined rate

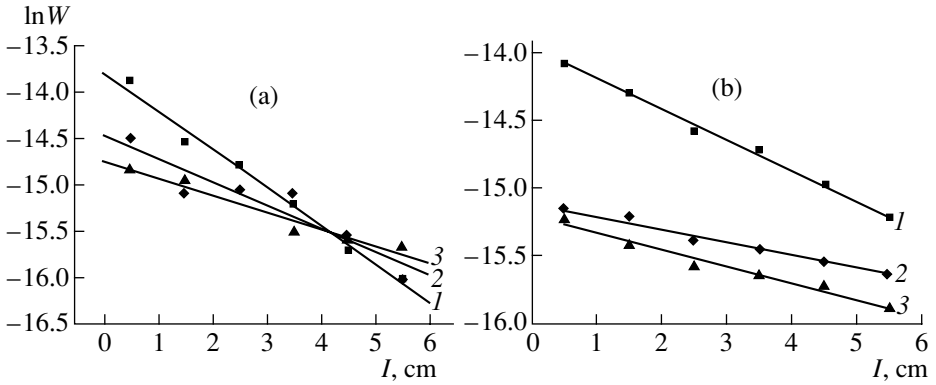

Fig. 1. Variation of the material mass loss rate in the direction of the gas flow: (a) Polyethylene film: (*1*) P = 200 Pa, I_p = 80 mA, T = 333 K; (*2*) P = 100 Pa, I_p = 40 mA, T = 333 K; (*3*) P = 100 Pa, I_p = 80 mA, T = 313 K. (b) SST textile: (*1*) P = 200 Pa, I_p = 80 mA, T = 333 K; (*2*) P = 100 Pa, I_p = 20 mA, T = 333 K; (*3*) P = 100 Pa, I_p = 80 mA, T = 323 K.

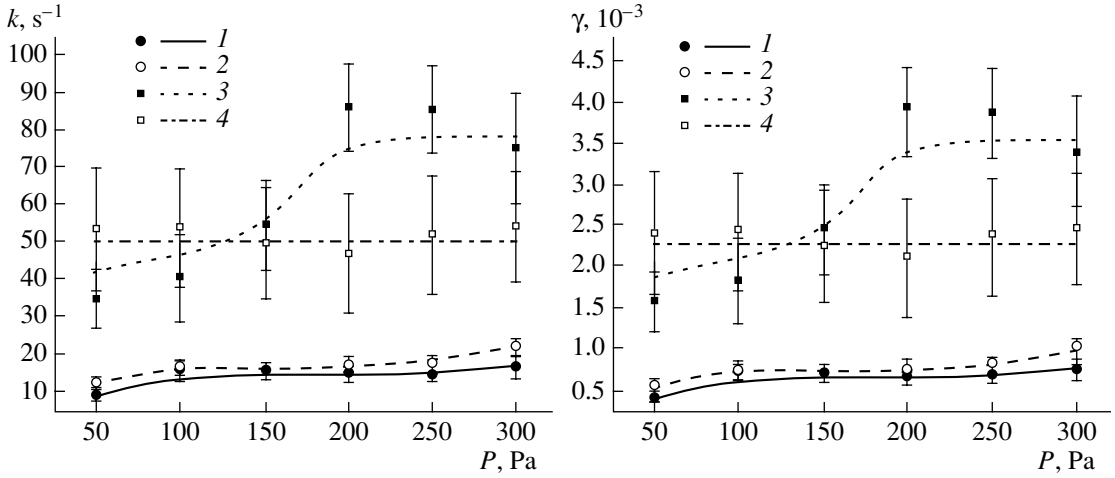

Fig. 2. The rate constants of interaction reactions (a) and the probabilities of heterogeneous decay (b) of oxygen atoms with polymers in dependence on the oxygen pressure (I_p = 80 mA). (*1*) polyethylene terephthalate film; (*2*) SST textile; (*3*) complex textile; (*4*) polyethylene film.

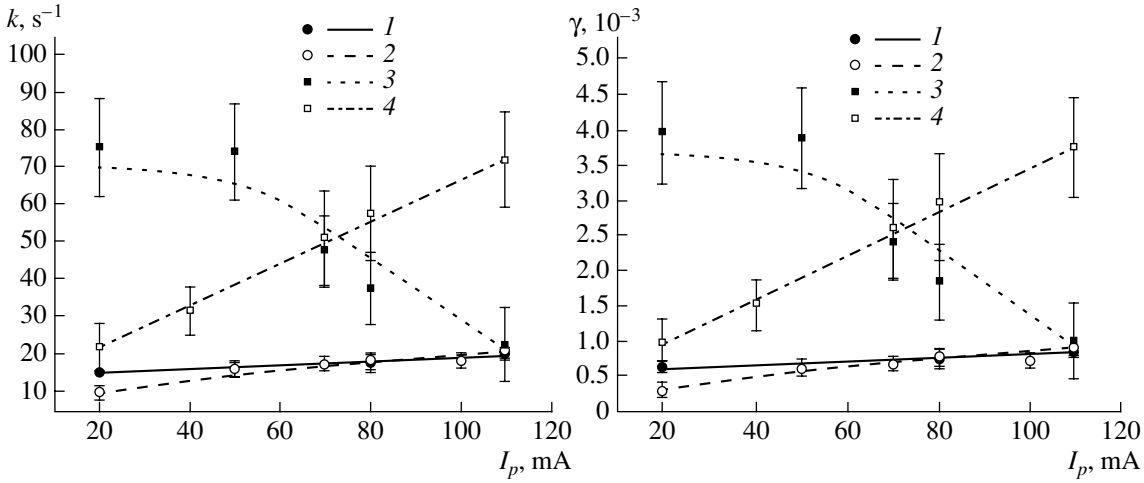

Fig. 3. The rate constants of interaction reactions (a) and the probabilities of heterogeneous decay (b) of oxygen atoms with polymers in dependence on the discharge current (P = 100 Pa). (*1*) polyethylene terephthalate film; (*2*) SST textile; (*3*) complex textile; (*4*) polyethylene film.

coefficients cannot be called constants in the sense that classic chemical kinetics operate by them.

The polyethylene terephthalate is related to the class of aromatic polymers, which are more stable under the influence of active oxygen than polyolefines, whose representative is polyethylene. Indeed, the results obtained show that the probabilities of the oxygen death on the polyethylene terephthalate film are several times less than on a polyethylene film.

We concentrated on materials on the basis of polyethylene terephthalate having a similar chemical structure but strongly differing in their effective (real) area. For the film and the monofilament and lavsan textiles, for the same geometrical areas, the ratio of their effective areas comprises 1 : 4 : 8.

It was shown previously that, over a wide range of discharge parameters, the relationship between the rates of the plasma oxidative decomposition, the oxygen expenditure from the gas phase, and the formation of basic gaseous products of the reactions for these materials is about equal to the ratio of their effective areas [13]. As is seen, the ratio of the coefficients obtained does not correspond to the ratio of the effective areas. The probabilities of death of atoms on the polyethylene terephthalate film and the SST textile are close to each other, but, on the complex textile, it is not higher than 5 times. The coefficients for the materials of the different structures as a whole variously depend on the discharge parameters; i.e., their ratio varies with the change of the parameters.

It is hardly possible to analyze in detail the dependences obtained. However, the following can be assumed. Firstly, the recombination of atoms on the surface essentially contributes to the total process of the interaction of atoms with the materials of various structures. Clearly, such parameters of a textile as the size of the reach-through holes and (or) the ratio between the fiber diameter and the reach-through hole width should influence the relationship between the probabilities for different channels of atom deaths. It is possible that the material thickness is of importance. Secondly, the atomic oxygen is not the only reagent in the streaming afterglow of the discharge; the polymer decomposition is a multichannel process. The coefficients found reflect this multichannel process; i.e., they are effective and have evaluative meaning. However, in the absence of other information, these results are of both practical and scientific interest.

We compared the coefficients found for the oxygen death with the analogous data determined in [10–12]

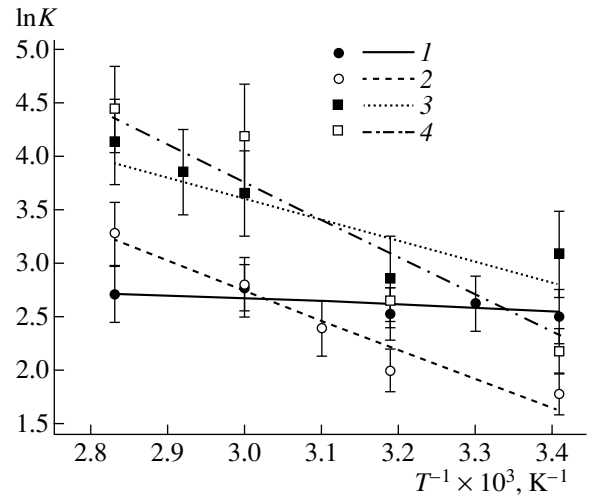

Fig. 4. The rate constants of interaction reactions of oxygen atoms with polymers on inverse temperature (P = 100 Pa, I_p = 80 mA). (*1*) polyethylene terephthalate film; (*2*) SST textile; (*3*) complex textile; (*4*) polyethylene film.

under the conditions when the comparison is possible. This showed good agreement only for the lavsan textile. For the polyethylene and polyethylene terephthalate films, the results of our measurements are, on average, 4–6 times greater. The possible reasons for such a lack of coincidence may be the following: (1) The inhomogeneity of the industrial polymers that we worked with. Their properties depend on the prehistory of the material, the presence of possible impurities, and the fabrication technology. (2) The influence of the condition of the reactor walls on the probability of death of oxygen atoms on the glass and, owing to the self-consistency of the system, on the probability of the death atoms on the polymer.

In Figs. 3 and 4, the coefficients for the rates of the interaction of oxygen atoms with the polymers as a function of the discharge current (Fig. 3a) and the temperature of the material (Fig. 4) at P = 100 Pa and I_p = 80 mA are presented. The data obtained within the accuracy of the measurements are straightened in the arrhenius coordinates, which allowed us to calculate the effective (apparent) activation energy of the process of the oxygen decomposition. The results calculated are presented in Table 2 together with the data presented earlier.

Note that the presented ΔE are far below the activation energies of the reactions observed at the thermal-

Table 2. Effective energies of activation (ΔE, kJ/mol) observed at the influence of the afterglow oxygen plasma on a polymer

Polymer	Polyethylene terephthalate film	SST textile	Polyester textile	Polyethylene film	Reference
ΔE, kJ/mol	3.6 ± 1.2	22.3 ± 2.8	16.9 ± 5.1	37.1 ± 6.5	Our data
	41 ± 3	–	19 ± 2	21 ± 2	[10–12]

oxidative decomposition of the polymers taking place under the quasi-equilibrium conditions (~100 kJ/mol).

As the data from the table attest, the values obtained for the activation energy of the plasma oxidative decomposition of the monofilament and complex textiles are close to each other, but they far above than the corresponding value for the polyethylene terephthalate film. This once again confirms the assumption that the structure of the woven material can influence the relationship of the channels of heterogeneous decay of active particles.

The activation energies obtained by different methods coincide within the measurement error in the case of the polyester textile, differ approximately by two times for the polyethylene, and differ by almost ten times for the polyethylene terephthalate film. The results of our work showed that the process of plasma oxidation in a streaming afterglow of a discharge cannot be described by one chemical reaction, it is multichannel and multistage. The temperature variation of the sample leads not only to the increase of the fraction of the reagent particles, which are able to overcome the potential barrier as in quasi-equilibrium chemical kinetics, but it also changes the relationship of the channels by which the reaction can proceeded. For each possible process (channel), its own activation energy corresponds, firstly, in the general case, to the temperature dependences for the rates and may not be described by the unified Arrhenius equation; secondly, the apparent activation energy may depend on the discharge parameters.

Deviation from the arrhenious dependence was noted in the literature for a number of materials that were processed in nonequilibrium plasma: polyimide [14], polyethylene terephthalate [15], polyvinylchloride [8, 16, 17], and polymethyl methacrylate [18].

The given papers [11] attest to the difference in the activation energies of the absorption process of O_2 at plasma processing of polyethylene in experiments with strong differing of the gas pressure (55 Pa – $\Delta E = 26 \pm 8$ kJ/mol; 188 Pa – $\Delta E = 7 \pm 2$ kJ/mol).

The observed difference in the activation energies presented in Table 2 may be a result of such factors.

In addition, the possible reason for the difference in the rate coefficients and activation energies following from different investigations may be caused by the dependence of the probability of the atoms' death on the processing time. Consequently, the authors of [19] showed that the coefficient of the atoms' death on the polyvinylchloride film reached quasi-stationary values in only 3–4 hours of treatment; in this time interval, it decreased by a factor of three.

CONCLUSIONS

The process of oxidative decomposition in activated oxygen in a discharge afterglow is multichannel and multistage. As a result, its effective kinetic characteristics (k and γ) depend on the discharge parameters. If these kinetic characteristics are described in terms of the rate coefficients of the of oxygen atoms' reactions with the materials, then the corresponding values in the range of pressures for O_2 from 50 to 300 Pa and discharge currents from 20 to 110 mA at the polymer's temperature of 333 K lie in the range of 6 to 20 s^{-1} for the polyethylene terephthalate film and monofilament textile and in the range of 20 to 90 s^{-1} for the polyethylene film and lavsan textile.

These coefficients depend only slightly on the temperature. In view of the mentioned fact that the process is multichannel and multistage, the activation energies depend on the external parameters. It is likely that, in such conditions (little generation of heat, low activation energies), the process of plasma oxidation of polymers should be sufficiently stable.

The data obtained allow us to predict, at least in order of value, the decomposition rates of materials in afterglow conditions and to take into account, as a first approximation, the rate change at separation of materials from the generation zone of active particles.

REFERENCES

1. Gousset, G., Trousseau, M., Vialle, H., and Ferreira, C.M., *Plasma Chem. Plasma Process*, 1989, vol. 9, no. 2, pp. 189–206.
2. Maksimov, A. and Rybkin, V.V., *Zh. Prikl. Spektros.*, 1982, vol. 37, no. 1, pp. 33–38.
3. Brederlow, G., *Ann. Phys.*, 1960, Bd. 5, F.7, H.7-8, pp. 414–428.
4. Grinevich, V.I. and Maksimov, A.I., Etching of Polymers in Low-Temperature Plasma, in *Primenenie nizkotemperaturnoi plazmy v khimii* (Application of Low-Temperature Plasma in Chemics), Polak, L.S., Ed., Moscow: Nauka, 1981, p. 135.
5. Maccallum, J.R. and Rankin, C.T., *Macromol. Chem.*, 1974, vol. 175, pp. 2477–2482.
6. Cook, J.M. and Benson, B.W., *J. Electrochem. Soc.*, 1983, vol. 130, no. 2, pp. 2459–2467.
7. Egitto, F.D., *Pure Appl. Chem.*, 1990, vol. 62, no. 9, pp. 1699–1708.
8. Menagarishvili, V.M., *Kinetics and Mechanism of Interaction of Active Oxygen with Polymer Films*, Extended Abstract of Cand. Sci. Dissertation, Ivanovo, 1990.
9. Kuvaldina, E.V., Lubimov, V.K., and Rybkin, V.V., *Khimiya Vysokikh Energii*, 1992, vol. 26, no. 5, pp. 475–478.
10. Kuvaldina, E.V., Rybkin, V.V., Terekhina, E.A., and Titov, V.A., *Khimiya Vysokikh Energii*, 1994, vol. 28, no. 4, pp. 359–360.
11. Shikova, T.G., *Physicochemical Mechanisms of Interaction of Low-Temperature Plasma with Certain of Polymer Materials*, Extended Abstract of Cand. Sci. Dissertation, Ivanovo, 2001.
12. Kuvaldina, E.V., et al., *Khimiya Vysokikh Energii*, 1995, vol. 29, no. 3, pp. 219–222.

13. Kuvaldina, E.V., Rybkin, V.V., Titov, V.A., and Ivanov, A.N., *Khimiya Vysokikh Energii*, 2000, vol. 34, no. 6, pp. 456–459.

14. Kuvaldina, E.V., Lubimov, V.K., Maksimov, A.I., and Rybkin, V.V., *Khimiya Vysokikh Energii*, 1990, vol. 24, no. 5, pp. 471–474.

15. Kuvaldina, E.V., Rybkin, V.V., Terekhina, E.A., and Titov, V.A., *Khimiya Vysokikh Energii*, 1994, vol. 28, no. 4, pp. 422–435.

16. Brovikova, I.N., Menagarishvili, S.D., and Rybkin, V.V., *Khimiya Vysokikh Energii*, 1992, vol. 26, no. 4, pp. 381–382.

17. Menagarishvili, S.D., and Rybkin, V.V., *Khimiya Vysokikh Energii*, 1994, vol. 28, no. 2, pp. 187–188.

18. Mokrousov, K.Ya. and Orlikovskii, A.A., *Investigation of Etching Process of PMMA in Low-Temperature Plasma, Proceedings of General Physics Institute*, Russ. Acad. Sci., Moscow, 1987, vol. 8, pp. 115–125.

19. Maksimov, A.I. and Titov, V.A., Determination of the Probability of Heterogeneous Decay of Oxygen Atoms on PVC Films Surface at their Processing in Afterglow Oxygen Plasma, *Vsesoyuznaya nauchno-tekhnicheskaya konferentsiya "Fizika i tekhnologiya tonkoplyonochnykh polimernykh system"* (All-Union Conf. on Physics and Technology of Thin-Film Polymer Systems), Gomel, 1991, Part I, pp. 35–37.

ISSN 1068-3755, Surface Engineering and Applied Electrochemistry, 2007, Vol. 43, No. 2, pp. 100–106. © Allerton Press, Inc., 2007.
Original Russian Text © T.V. Kuchuk, 2007, published in Elektronnaya Obrabotka Materialov, 2007, No. 2, pp. 31–38.

ELECTRICAL PROCESSES
IN ENGINEERING AND CHEMISTRY

Cross Flow Around a Cylinder at Periodic Disturbances in the Boundary Layer by Electrolysis Bubbles

T. V. Kuchuk

Institute of Applied Physics, Academy of Sciences of Moldova, ul. Academiei 5, Chisinau, MD-2028 Republic of Moldova

Received September 5, 2006

Abstract—Particularities of dynamic flow control in an open-loop system around a cylinder with a boundary layer by means of periodic generation of microbubbles are presented. Experiments were carried out in the range of Reynolds numbers of Re = (0.3–1.2) × 10^5. It is shown that this method provides very similar results as in the case of continuous generation of microbubbles; however, the energy expenditure is two times less. The effect can be explained by the delayed response of the boundary layer separation on the disturbance cutoff. Lock-in modes of the natural vortex shedding frequency f_N and the frequency of forced oscillations f_E, as well as superposition of these frequencies, are registered. Maximal values of the amplitude of the drag and lift oscillations are registered in the range of low frequencies ($f_E/f_N < 0.07$).

DOI: 10.3103/S1068375507020068

1. INTRODUCTION

In recent years, research in fluid mechanics on the flow control around those bodies for which the shift of the separation point of the boundary layer occurs has become more intensive. This trend of research is promising, since, by flow control alone, it is often possible to attain the necessary performance of this kind of bodies in various technical applications, in particular, to intensify the heat exchange processes, to reduce the drag and vibrations in heat exchangers, to increase the efficiency of burning, and so on.

The streamlining of bluff bodies, for example, a cylinder, may be altered by passive or active flow control methods [1]. In the first case, the energy necessary to transform the flow regime in the boundary layer is directed from a free stream using a turbulence generator. Some passive control methods (roughness, turbulence of an external stream) have become classical and are widely used in various power installations. Among the latest achievements in this domain, methods of passive control should be mentioned based on the formation of an ordered system of vortex structures on the body surface. Such a system enables a substantial intensification of the convective heat exchange with minimal energy expenditure [1–3].

In the case of active flow control, the energy input required to transform hydrodynamic and heat exchange parameters of bluff bodies is supplied from the outside. This energy may be directed for blowing or suction of the boundary layer [4], for heating or cooling of the body surface [5], for generating microbubbles in the boundary layer [6, 7], and for producing rotational motion of the body or its separate parts [8]. The main characteristic feature of active flow control methods is that they may be applied both in the steady-state and dynamic regimes. In the steady-state regime, the parameters of the action of an external disturbance source are not time dependent. The optimal control parameters should be defined to increase the efficiency of the active flow control methods in a steady-state regime. In this context, active and passive methods do not differ much.

In the case of dynamic control, the action of periodic disturbances directly influences the processes of the boundary layer separation and formation of the vortex wake past a bluff body. Feedforward or feedback systems are used for the dynamic control.

In the case of a cross flow around a cylinder, methods were used of longitudinal and transversal forced vibrations of a cylinder [9] or some separate parts of its surface [10] with the aim to control the hydrodynamic performance in open-loop systems of active dynamic control. This principle of control is also implemented on the basis of such methods as a periodic disturbance in the incident flow [11], superposition of acoustic disturbances [12], periodical jet blowing into the boundary layer [13], local heating and cooling of the cylinder front area [14], and torsion vibrations of a cylinder [15].

In the majority of investigations, the main attention was given to searching for the effect of synchronization of the natural vortex shedding frequency f_N with the frequency of forced oscillations in the flow around a cylinder (lock-in mode). In particular, it is reported in [9, 15] that the frequency synchronization (lock in) near the natural vortex shedding frequency $f_N = f_E$ was observed. A similar effect was reported in [11] for $f_N = f_E/2$ and in [9] for $f_N = f_E/3$. Nevertheless, in a number of publications, only smooth behavior in the lock-in mode was reported for $f_N = f_E$ [16]. The results of investigations on the influence of the frequency and ampli-

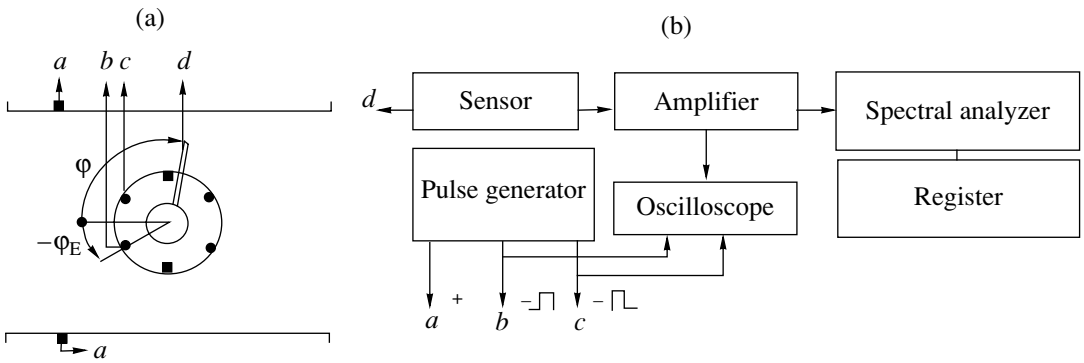

Fig. 1. Scheme of the working chamber (a) and a schematic diagram of the control loop (b).

tude of forced disturbances on the flow around a cylinder beyond the regime of the frequency synchronization or the lock-in mode disagree more significantly. For example, although a similar method was applied for flow control around a cylinder, an increase in the drag is mentioned in [12], while its decrease is reported in [17].

The feedback dynamic flow control around a cylinder was the subject of theoretical and experimental studies [16, 18–19]. Applying this principle of flow control implemented in the method of acoustic disturbances in [18], a decrease in the level of the velocity pulsations exceeding 30 dB was attained. A substantial reduction in the cylinder drag was found in [16] when this principle was used in the method of active control over torsion vibrations of a cylinder. Some characteristic features of the application of the feedback flow control principle have been obtained via numerical modeling of a flow around a cylinder [19].

In the present study, the main attention is given to the development of an active flow control method around a cylinder based on the boundary layer disturbance by electrolysis bubbles. Some features of a steady flow control around a cylinder using this method are presented in [20]. The aim of the work is an experimental investigation of the effect of periodic disturbances in the boundary layer by electrolysis bubbles on the development of vortex shedding in the cylinder wake.

2. EXPERIMENTAL SETUP AND METHOD

A closed-type hydrodynamic tunnel and a working chamber with a cross section of 150×70 mm^2 was used for the experimental investigations. The Reynolds numbers varied in the range of $Re = (0.3–1.2) \times 10^5$. The principle scheme of the working channel and the cylinder inserted in it is shown in Fig. 1a. Six electrodes 70 mm long and 1.2 mm wide were mounted with spacing of 60 degrees over the surface of a cylinder with a diameter of 22 mm made of an organic glass. The required angle of the electrode arrangement and the pressure piezosensor relative to the front critical point may be adjusted via rotation of the cylinder around its axis. The electrodes located along the cylinder generatrix and on the walls of the working channel were connected to a step-pulse generator. The active dynamic flow control around the cylinder was performed by sequential application of negative square pulses at one or two electrodes symmetrical relative to the front critical point. In the case of two electrodes, the pulses were supplied in turn at the first and second electrodes at equal time intervals.

The pulse current density changed to 200 mA/cm^2, and the pulse frequency varied in the range of (0.2–150) Hz.

A schematic diagram of the control loop over the flow and measuring equipment, which includes the step-pulse generator, pressure sensors, and instruments, is shown in Fig. 1a. An LKh-610A sensor was used to measure the pressure pulsations. Spectral analysis was performed using an SK4-56 spectral analyzer.

For flow visualization, the method of electrolysis bubbles and stroboscopic lighting was used. The cylinder drag and lift force was computed by integrating the pressure distribution along the cylinder perimeter.

3. RESULTS AND DISCUSSION

Electrolysis hydrogen bubbles generated in the boundary layer over the entire cylinder surface may substantially increase the heat and mass transfer in the case of free convection [21] or cross flow around a cylinder in the range of critical Reynolds numbers [22]. In particular, it was shown that, at the flow disturbance around the cylinder surface by electrolysis bubbles, a threefold increase in the heat-transfer coefficient was attained [21]. In the case of forced convection ($Re = 10^4–10^5$), the effect of microbubbles on the cylinder heat transfer is weaker (about 40%), but the drag decreases substantially (down to 50%) [20]. In both cases, the results may be elucidated by the turbulence generation due to microbubbles at their growth, separation, and motion through the cylinder boundary layer.

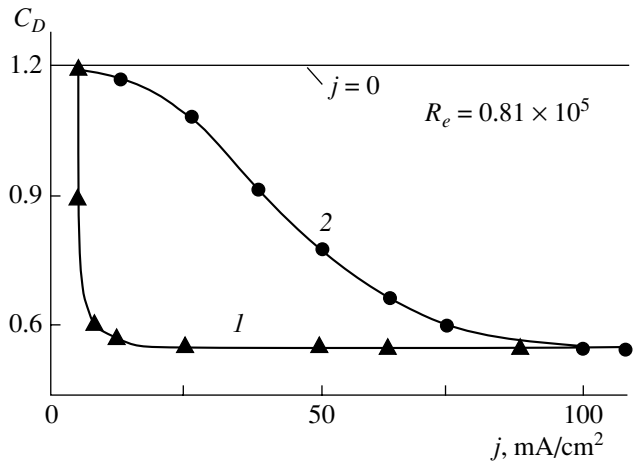

Fig. 2. Influence of microbubbles on the cylinder drag: (*1*) continuous generation of microbubbles around the entire cylinder surface; (*2*) local symmetric generation ($\varphi = \pm 30°$).

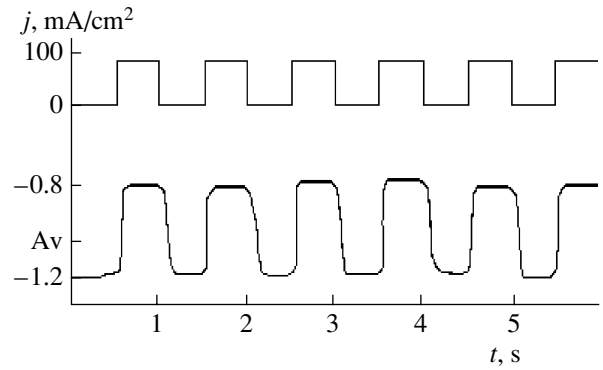

Fig. 3. Temporal variation of the pressure coefficient on the cylinder surface (φ_2 = 140°) for f_E/f_N < 0.07, J = 100.0 mA/cm^2, and $\varphi_E = \pm 30°$.

The efficiency of the active flow control around the cylinder using continuous generation of microbubbles into the boundary layer increases substantially when the process is localized in the front part of the cylinder. As the analysis of Fig. 2 shows, at the localization of the point where microbubbles are introduced in the boundary layer ($\varphi = \pm 30°$), a smooth decrease in the cylinder drag is possible when the current density changes in the range from 3 to 100 mA/cm^2, whereas, in the case of generation of microbubbles over the entire cylinder surface, an abrupt stepwise change occurs at J = 11 mA/cm^2.

The method of local disturbances in the boundary layer by microbubbles was used to model an asymmetric cross flow around a cylinder [22]. When the flow regime in the boundary layer alters by the electrolysis bubbles on one side of the cylinder only, an asymmetric pressure profile with various locations of separation points of the boundary layer forms on the cylinder. This results in the cylinder drag decreasing; however, the lift force increases dramatically. In this case, the greater the current density, the more drastic the changes observed in the cylinder hydrodynamic performance are.

At the local periodic generation of microbubbles on one side of a cylinder, the laminar to turbulent transition of the flow regime in the boundary layer at this side occurs when the current pulse is applied to the respective electrode. The laminar regime completely restores at the moment when the pulse is interrupted. It should be noted, however, that this occurs exclusively for frequencies of current pulses much less than the natural vortex shedding frequency ($f_E < 0.07 f_N$).

In the range of $f_E/f_N < 0.07$, symmetric ($J = 0.0$) and asymmetric ($J \neq 0.0$) profiles of the pressure distribution arise on the cylinder surface over certain time intervals. Figure 3 shows the distribution diagram of the temporal variation of the pressure coefficient over the cylinder surface for the point located at the angle φ = 140°. Analysis of the diagram suggests that the delay in the pressure restoration occurs after the current pulse is interrupted at the cylinder side where disturbances in the boundary layer are produced.

For greater frequencies f_E, the pressure distribution over the cylinder surface becomes asymmetric at the phase of the zero current pulse as well. When f_E increases, the location of the separation point of the boundary layer shifts downstream approaching the separation point for continuous asymmetric generation of microbubbles into the boundary layer (Fig. 4). In this case, the phase practically disappears when the symmetric pressure profile restores, despite the fact that

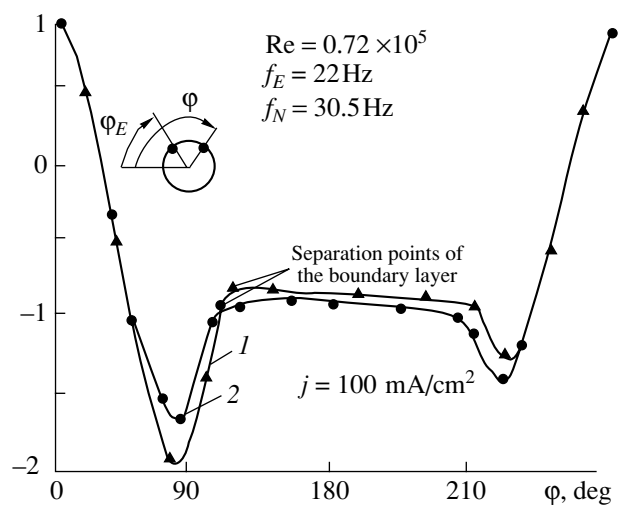

Fig. 4. Effect of periodic generation of electrolysis bubbles on the distribution of the pressure coefficient over the cylinder surface: (*1*) continuous generation of microbubbles, (*2*) periodic generation ($\varphi_E = \pm 30°$).

there is no effect of microbubbles (J = 0.0 mA/cm) on the boundary layer.

The observed phenomenon may be explained by the delayed response (hysteresis effect) of the boundary layer to the disturbance pulse cutoff, which results in the deceleration of the upstream motion of the separation point of the boundary layer relative to the moment when the process of the turbulence generation in the layer terminates. This phenomenon may be compared with an hysteresis effect due to creation (collapse) of a separation bubble in the boundary layer at one side or the other of a cylinder when the flow velocity increases (decreases) [23]. However, in the case of the flow control around a cylinder by generation of electrolysis bubbles, no separation bubbles were observed. The disturbances in the boundary layer are so strong that, when going through the critical regime, a direct transition to the supercritical flow regime occurs, which is characterized by an unstable flow accompanied by fluctuations in the vortex shedding frequency. The delay in the response of the boundary layer on the disturbance cutoff may be imagined as a "memory effect" of this disturbance. Whatever the nature of this effect is, it provides vast opportunities for development of dynamic flow control methods, because the same end result (drag lowering, lift enhancement, and heat and mass exchange process intensification) may be obtained at substantially less energy expenditure than applying the steady-state methods.

At local periodic disturbance in the boundary layers at both sides of the cylinder by alternate application of electric pulses at the symmetrical electrodes in the front part of the cylinder, various regimes of the effect of an external disturbance on the processes of vortex generation and shedding past the cylinder may be observed. For illustration, diagrams are presented in Fig. 5 that show the temporal dependence of the pressure at the cylinder surface (Fig. 5a) and the respective amplitude–frequency spectra (Fig. 5b). The regime when synchronization occurs of the vortex shedding frequency with the frequency of the forced disturbance in the boundary layer is clearly evident in the diagrams. In comparison with the cross flow around the cylinder without disturbance (Fig. 5a, diagram *1*; Fig. 5b, spectrum *1*), when the synchronization regime is attained, the steady vortex shedding frequency is observed; the amplitude of the pressure oscillations increases abruptly and practically does not change with time (Fig. 5a, diagram *2*; Fig. 5b, spectrum *2*). In the synchronization regime, the maximal magnitude of the amplitude of the pressure oscillations was found when the frequency of the forced disturbances coincides with the natural vortex shedding frequency ($f_E = f_N$).

When the frequency of the generation of electrolysis bubbles in the boundary layers of the cylinder differs from the frequencies f_S of the synchronization regime, in the $p(t)$ diagrams (Fig. 5a, diagrams *3*, *4*) and spectra (Fig. 5b, spectra *3*, *4*), both the natural vortex shedding frequency f_N and the frequency of the forced oscillations f_E are clearly evident. In this case, as follows from diagrams *3* and *4*, a superposition of these oscillations occurs. The only difference is that, for $f_E < f_S$ (diagram *3*), the f_E frequency dominates and, for $f_E > f_S$ (diagram *4*), oscillations with frequency f_N dominate. At the same time, for $f_E < f_S$, oscillations with the frequency $f_E + f_N$N can be observed in the spectra (Fig. 5b, spectrum *3*). Similar pulsations were registered in [24], where the method of torsion vibrations was applied for the dynamic flow control.

Figure 6 shows the effect of the current density on the range limits for which the regime of the synchronization of the vortex shedding frequency and the frequency of forced disturbances of the boundary layer establishes. The synchronization regime arises when the critical density magnitude is reached $J = J_C$, which is dependent on the Reynolds number, the cylinder diameter, the roughness, and other parameters. In particular, for our experimental conditions (d = 22 mm, Re = 0.72×10^5, and a polished electrode surface), the critical current density is equal to 11 mA/cm^2. With the current density increase, the synchronization range extends, and, for $J > 73$ mA/cm^2, it stabilizes between frequencies of $f_{\min} = f_E/f_N = 0.68$ and $f_{\max} = f_E/f_N = 1/43$.

The effect of a periodic disturbance in the boundary layer of a cylinder by electrolysis bubbles on the cylinder drag may be evaluated by analyzing the dependence of the mean value of the coefficient of the base pressure C_{Pb} on the frequency of the current square pulses f_E shown in Fig. 7. In the function $C_{\mathrm{Pb}}(f_E/f_N)$, four ranges are clearly evident with various types of the pressure variation in the base part of the cylinder under the action of microbubbles. In the first range ($0 < f_E/f_N < 0.07$), the cylinder drag is practically the same as that observed in the regime with continuous asymmetric disturbance in the boundary layer for equal current density. In the ranges $0.15 < f_E/f_N < f_{\min}$ and $f_E/f_N > f_{\max}$ at the current density J = 100 mA/cm^2, C_{Pb} increases to 0.62 and 0.58, respectively, due to the delayed response of the restoration of the separation point of the laminar boundary layer on the disturbance cutoff.

The $f_{\min} < f_E/f_N < f_{\max}$ range represents a special case in the $C_{\mathrm{Pb}}(f_E/f_N)$ dependence that corresponds to the synchronization regime. In this range, the cylinder drag increases and reaches its maximal value at $f_E/f_N = 1$. It should be noted, however, that, despite the pronounced decrease of C_{Pb} in the synchronization regime, its magnitude is substantially greater than for the case of the flow around the cylinder with the laminar boundary layer (undisturbed regime). Due to the delayed pressure restoration on the cylinder surface when the disturbance is interrupted, the separation point of the boundary layer shifts downstream, and this shift is greater for greater disturbance frequencies. This may elucidate that the base pressure increases with an increase in the frequency of the current pulses in the ranges beyond the synchronization regime. In the synchronization range, a

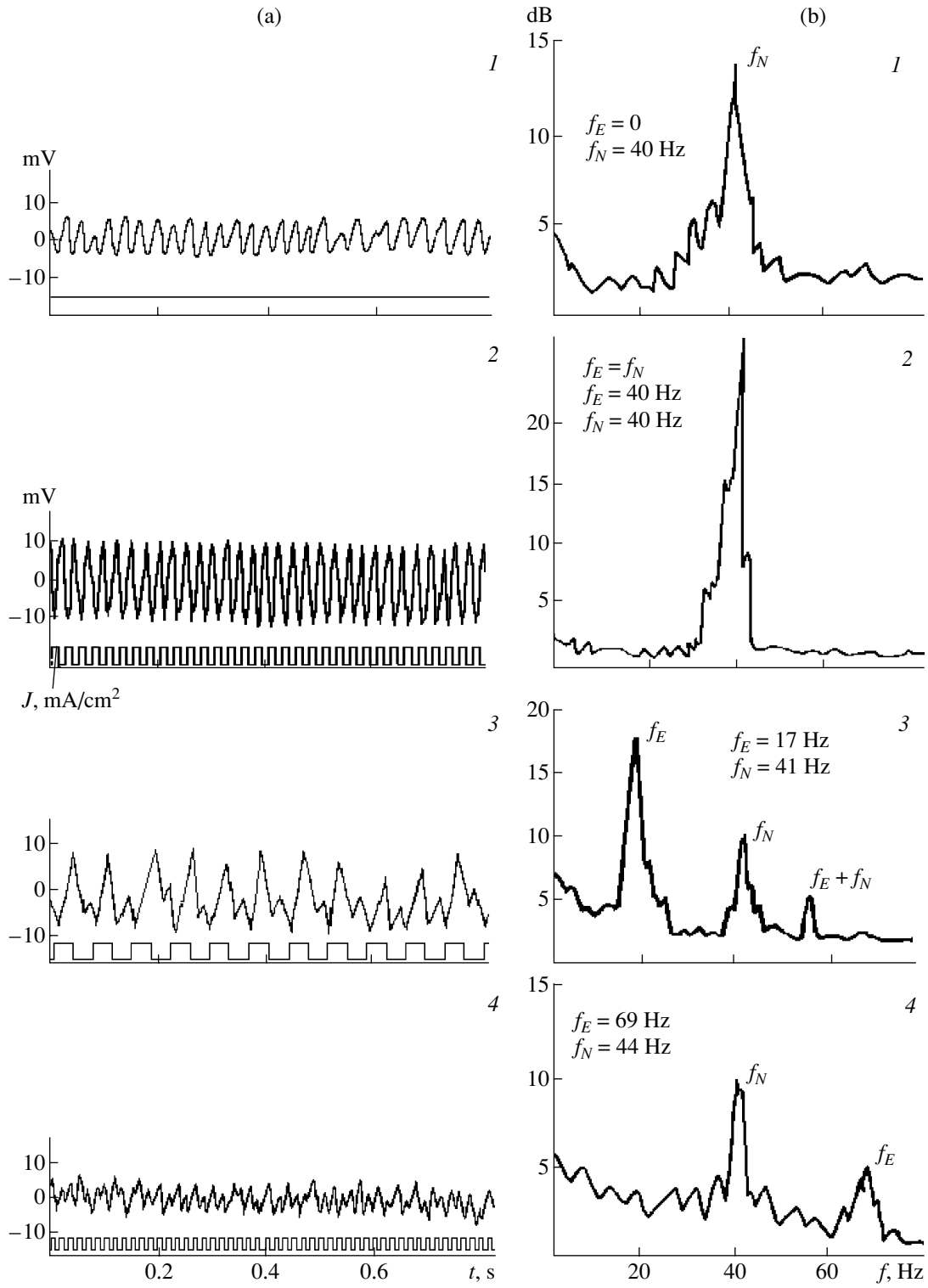

Fig. 5. Diagrams of temporal variation of the pressure on the cylinder surface (a) and the respective amplitude–frequency spectra (b). $\varphi_2 = 140°$. Ordinate–arbitrary scale.

steady vortex shedding establishes past the cylinder with its pronounced frequency, while, at the same time, the intensity of these vortices increases. This results in an increase of the wake width, and the separation point of the boundary layer somewhat shifts upstream. This behavior of the separation point of the boundary layer markedly influences the cylinder drag for the given range where the frequency of the current pulses

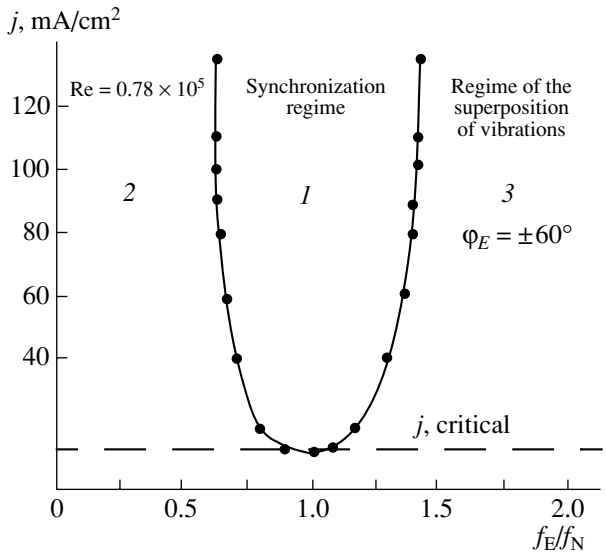

Fig. 6. Influence of the electric current density on the range of frequency synchronization. $\varphi_E = \pm 60°$.

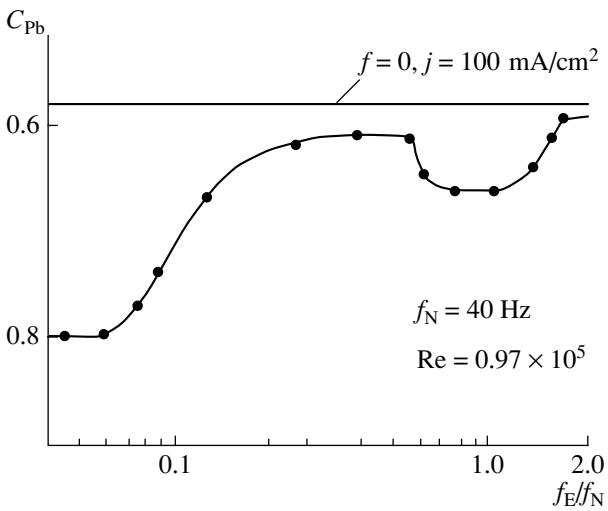

Fig. 7. Influence of the frequency of generation of electrolytic bubbles on the base pressure coefficient. $\varphi_2 = 180°$.

changes. In this context, the flow control method around a cylinder using periodic generation of microbubbles into its boundary layer has some common features with the method of torsion vibrations of a cylinder [9].

The effect of dynamic flow control around a cylinder using microbubbles on the lift force of the cylinder is substantial in the range of low frequencies ($f_E/f_N <$ 0.07), where the change of the laminar and turbulent regimes on various sides of the cylinder is performed with the frequency of the forced disturbances and at the maximal amplitude of the shift of the separation point of the boundary layer. In this range of frequencies, the amplitude of the oscillations of the lift force may exceed by 2 or 3 times the cylinder drag.

4. CONCLUSIONS

Analysis of some characteristic features of the dynamic flow control method around a cylinder using periodic generation of electrolysis bubbles into its boundary layer is given. The following principle results have been obtained.

In the range of low frequencies ($f_E/f_N < 0.07$), a periodic local generation of microbubbles both from one and two sides of the cylinder leads to a transition from a laminar flow regime in the boundary layer to a turbulent regime during the phase when the pulse is applied; the laminar regime restores at the disturbance cutoff. A delayed response of the boundary layer to the disturbance cutoff has been found.

In the range of frequencies $f_E/f_N < 0.07$, for generation of microbubbles on one side of the cylinder, the asymmetric profile of the pressure distribution is also retained in the phase of the disturbance cutoff.

The synchronization regime of the frequency of generation of electrolysis bubbles with the vortex shedding frequency has been found. The frequency range where this regime establishes extends with an increase in the current density.

The cylinder drag increases in the synchronization regime and reaches its maximal value at $f_E/f_N = 1$.

In the range of $f_E/f_N < 0.07$, the amplitude of the oscillations of the lift force is 2 to 3 times greater than the cylinder drag.

REFERENCES

1. Gad-el-Hak, M., *Appl. Mech. Review,* 1989, vol. 42, pp. 261–293.
2. Wetzel, T.G. and Simpson, R., *J. Aircraft*, 1998, vol. 35, no. 3, pp. 370–379.
3. Berezent'yv, M.Yu., Guvernyuk, S.V., Zubin, M.A., Zubkov, A.F., and Mosin, A.F., *Aeromekh. Gaz. Dinamika*, 2001, no. 1, pp. 11–17.
4. Sun, M. and Hamadani, H., *AIAA Journal*, 2001, vol. 39, no. 4, pp. 735–737.
5. Waka, R. and Yoshino, F., *Trans. JSME, Ser. B*, 1994, vol. 53, no. 490, pp. 1704–1708.
6. Bologa, M.K., Paukov, Yu.N., and Kuchuk, F.V., *Modelling, Simulation and Control, Ser. B*, AMSE Press, 1986, vol. 6, no. 4, pp. 37–50.
7. Watanabe, H., Hara, A., and Onuma, S., *J. Fluids Eng.*, 1990, vol. 112, pp. 67–73.
8. Kimura, T., Tsutahara, M., and Wang, Z., *AIAA Journal,* 1991, vol. 30, no. 2, pp. 555–556.
9. Stansby, P.K., *J. Fluid Mechanics*, 1976, vol. 74, pp. 641–665.
10. Bar-Saver, A., *AIAA Journal*, 1989, vol. 27, pp. 820–821.
11. Ito, S., Tanaka, E., and Yamashita, S., *Trans. JSME,* 1994, vol. 60, no. 572, pp. 1118–1124.

12. Hasio, F.B. and Shyu, J.Y., *J. Fluids and Structures*, 1991, vol. 5, pp. 427–442.
13. Biringen, S., Active Control of Transition by Periodic Suction-Blowing, *Phys. Fluids,* 1984, vol. 27, no. 6, pp. 1345–1347.
14. Ladd, D.M., and Hendricks, E.W., *Experiments in Fluids*, 1988, vol. 6, pp. 69–70.
15. Fujisawa, N. and Kawaji, Y., *Trans. JSME, Ser. C*, 1995, vol. 61, no. 585, pp. 1832–1836.
16. Khan, M.J. and Ahmed, A., *AIAA Journal*, vol. 31, no. 1, pp. 208–209.
17. Bera, J.-C., Comite-Bellot, G., and Sunyach, M., *C.R. Acad. Sci.Paris, Ser. IIb*, 1998, vol. 326, pp. 859–865.
18. Frowcs Williams, J.E., *J. Fluids and Structures,* 1989, vol. 3, no. 2, pp. 115–122.
19. Park, D.S., Ladd, D.M., and Hendricks, E.W., *Phys. Fluids*, 1994, vol. 6, no. 7, pp. 2390–2405.
20. Bologa, M.K., Kuchuk, T.V., and Paukov, Yu.N., *Energetika (Lithuania)*, 1992, no. 1, pp. 44–56.
21. Zhan-Geng, G., Warmeuberung bei freier Konvektion unter Einfluss von elektrolitisch erzengten Wasserstofblasen, *Doctoral (Eng.) Dissertation,* Fak. Verfahrenstrechen, Stuttgart Univ., 1992, p. 114.
22. Kuchuk, T., and Bologa, M., Influenta perturbarii asimetrice a stratului limita asupra curgerii in jurul unui cilindru, *Lucrarile conferintei nationale de termotehnica* (Proc. of National Conference on Heat Engineering), X. Sibiu, Ed., 2000, pp. 13–18.
23. Kamiya, N., Susuki, S., Nakamura, M., and Yoshinaga, T., Some Practical Aspects of the Burst of Laminar Separation Bubbles, *Proc. 12th Congress Int. Council Aeron. Sci. (ICAS), S1*, Munich, 1980, pp. 417–428.
24. Williams, D.R., *Phys. Fluids,* 1998, vol. 10, no. 6, pp. 1243–1245.

ISSN 1068-3755, Surface Engineering and Applied Electrochemistry, 2007, Vol. 43, No. 2, pp. 107–109. © Allerton Press, Inc., 2007.
Original Russian Text © S.A. Baranov, O.Yu. Keloglu, 2007, published in Elektronnaya Obrabotka Materialov, 2007, No. 2, pp. 39–42.

ELECTRICAL PROCESSES
IN ENGINEERING AND CHEMISTRY

Temperature Effect on Reversible and Irreversible Phase Transitions by the Example of Studying Magnetic Properties of Cast Amorphous Microwire

S. A. Baranov and O. Yu. Keloglu

Institute of Applied Physics, Academy of Sciences of Moldova, ul. Akademiei 5, Chisinau, MD-2028 Moldova

Received November 1, 2006

DOI: 10.3103/S106837550702007X

INTRODUCTION

It is known that the theories of nucleation and magnetic-phase formation have much in common; therefore, the study of magnetic phenomena can be an addition to the solution of problems of nanoparticle crystallization. On the other hand, as is shown further, it is also possible to derive common regularities of the theory of magnetism from the common representations of the nucleation theory.

Cast glass-coated amorphous microwire (CGCAM) with a positive magnetostriction has a rectangular hysteresis loop, which is characterized by a coercive-force stable magnitude H_s. In this case, the coercive force characterizes a new-phase-nucleation switching field and has (as has already been noted) a direct analogy with the nanoparticle nucleation. The coercive-force magnitude (or the nucleation switching field) and the fluctuations of this quantity with the temperature and heat-treatment conditions are of theoretical and practical interest.

The temperature dependence of the switching field in the low-temperature range is defined by the residual stresses considered in detail in [1]. At high temperatures, there are thermal-relaxation processes, which are investigated in this paper. First, we consider the temperature dependence disregarding the structure relaxation but with taking into account the residual-stress change. These changes in the switching field have a reversible character; i.e., after returning to the initial temperature, all the switching-field parameters are restored. It can be relevant both at reasonably low temperatures and for high heating rates. A heat treatment (or annealing), i.e., the sample aging at a particular temperature for a certain time during which the structure relaxes, is an irreversible process. Therefore, the result of the heat treatment can be measured by returning to the initial temperature while also taking into account the reversible temperature processes. In reality, both processes proceed simultaneously in amorphous materials, which we discuss below and in the conclusions.

Let us also note that the principal difficulty in investigating the indicated phenomena arises due to the fact that the amorphous states are metastable and quasi-degenerate. For this reason, in this study, we restrict ourselves only to using the first principles for the possible construction of the theory.

In contrast to magnetic phases, for nucleation phases, we are usually interested only in the irreversible nucleation product. However, as becomes clear below, the irreversibility of these processes can be investigated from unified positions.

1. TEMPERATURE DEPENDENCE OF THE SWITCHING FIELD IN CGCAM AT LOW TEMPERATURES

For the temperatures ranging from the crystallization onset ($T_1 \sim 500$ K) to low temperatures (close to those of liquid nitrogen), the experimental dependence for the switching field H_s (or the coercive force) on the temperature (if one disregards the temperature-relaxation processes) can be approximated by a linear function

$$H_s/H_{s0} \sim (T^* - T)/(T^* - T_0), \tag{1.1}$$

where the temperature T^* is defined as the temperature of the glass–metal seal (more than 1000 K) in a microwire.

As T_0 and H_{s0}, it is possible to take an arbitrary point. For definiteness, we take the lowest temperature T_0 for which there is still a linear dependence (1.1) and the highest H_{s0} corresponding to this temperature. At low temperatures ($T_0 \sim 100$ K), this dependence transforms into that close to the exponential dependence. We use the elementary theory proposed in [1]; for this reason, we repeat certain arguments of the indicated work.

The stresses arising on the microwire surface (see [1]) are

$$P = C(T^* - T), \tag{1.2}$$

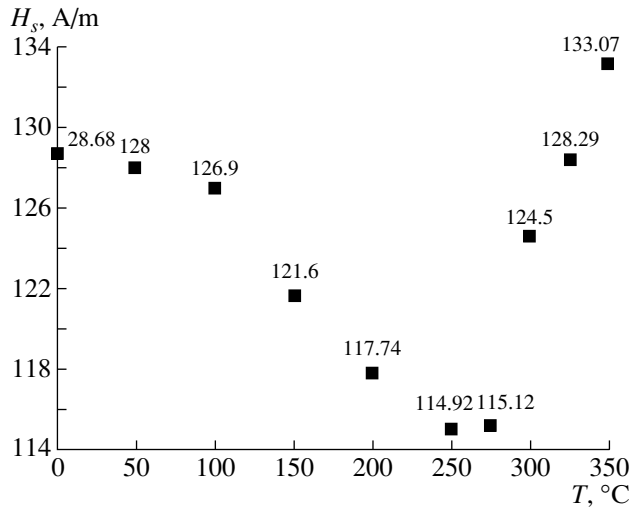

Fig. 1. Temperature dependence of the switching field H_s (according to [5]).

where

$$C \sim (1\text{–}10)\ \text{J/deg m}^3. \tag{1.3}$$

The residual stresses at the microwire center, where the new domain nucleates, are considered one order of magnitude lower. Therefore, for the energy difference $E_{1.2}$, which a domain wall overcomes, it is possible to write the following formula according to [1]:

$$E_{1.2} \sim CV(T^* - T), \tag{1.4}$$

where V is the volume of the new-domain nucleus, which is estimated below.

Let us consider the theory in [1], where the relative probability of the transition between two (*1* and *2*) oppositely directed magnetic states $w(1, 2)$ is defined as follows:

$$w(1, 2) \sim \exp\{-E_{1,2}/kT\}, \tag{1.5}$$

where k is the Boltzmann constant.

Formula (1.5) is the Arrhenius approximation. It defines the probability of the quantum transition of a particle from lower to upper states under the action of the temperature. The relative magnitude H_{sw}/H_{s0} is inversely proportional to w (*1*, *2*).

Experimentally, the temperature dependence of the coercive force was studied in [2]. The theoretical curve was calculated in [3] (from the theory that uses Eq. (1.5) [1, 3]) and fully corresponds to experiments from [2].

Let us note that, in the proposed theory, the problem of the thermal relaxation of the structure, which seems to be very urgent for amorphous materials at high temperatures, is not considered. An arbitrary amorphous material is in a metastable state and, hence, is thermally unstable. On heating, it can also transform into a metastable state. In this case, the coercive force should also vary. In the following paragraphs, we consider these processes.

2. THE ANNEALING-TEMPERATURE EFFECT ON THE SWITCHING FIELD AND ITS FLUCTUATIONS

In alloys with a reasonably high magnetostriction, stress relaxation resulting in lowering the switching field H_s takes place at annealing. In the case of the CGCAM, it is of interest to anneal at a temperature at which the microcrystal nucleation begins (~300°C) because, at a temperature higher than 300°C, the CGCAM loses its amorphism and nucleation and the microcrystalline-phase growth [4, 5] are observed.

From the results of observation of two hundred cycles of magnetization, we plotted the graphical temperature dependence of the average coercive force H_s and its fluctuations σ_{Hs} [4, 5]. These values were measured for samples from an alloy on the basis of $(CoFeNi)_{73}B_{16}Si_{11}$ with positive magnetostriction before and after annealing. The annealing was performed to T = 350°C without the action of arbitrary additional external fields and stresses. As for the other amorphous alloys, we revealed that the average values of H_s noticeably decrease with increasing temperature. A coercive force appeared equal to H_s = 130 A/m under normal conditions with T = 0°C and H_s = 115 A/m at T = 250°C [5].

In addition, it was noted that the change in H_s is irreversible. For example, if the annealed samples are cooled to room temperature, the switching field is not returned to the initial value. We also note that H_s measured immediately at the annealing temperature has a lower value than that measured after the cooling.

As can be seen (Fig. 1), the further increase in temperature leads to increasing H_s, which can be associated with the occurrence of a crystalline microstructure [4]. At T = 350°C (H_s = 133 A/m), an excess of the initial value of the switching field occurs.

We singled out three factors explaining the effect of the annealing on the change in the magnetic properties of the amorphous materials: the residual-stress relaxation, the domain-wall stabilization, and the precrystallization effects and crystallization [4].

For the CGCAM, it is possible to explain the changes in H_s occurring in the temperature range of 0°C ≤ T ≤ 250°C by the residual-stress relaxation.

The tendency to lowering the switching-field fluctuations σ_{Hs} with increasing the annealing temperature is obvious, and it is also maintained after the microcrystal-nucleation point (T ~ 300°C). The fluctuations σ_{Hs} = 1.23 A/m (0.96%) at room temperature (Fig. 2), σ_{Hs} = 0.6 A/m (0.52%) at T = 250°C, and σ_{Hs} = 0.47 A/m (0.35%) at T = 350°C. It is possible to assert that the relaxation process proceeds in the system to a more stable state in which the magnetic fluctuations of the system are less expressed.

3. THEORY OF THE TEMPERATURE DEPENDENCE OF THE PHASE NUCLEATION BY THE EXAMPLE OF STUDYING THE SWITCHING FIELD

For the theoretical description of the above phenomena, we generalize Eq. (1.5) to the case of the structure change. Then, based on the theory proposed in [1, 2, 6], we write the following with exponential accuracy:

$$H_s/H_{s0} \sim \exp(E_{1.2}/kT)/\{1 + \exp(-G/kT)\}, \quad (3.1)$$

where the first multiplier in the formula describes the low-temperature processes with the activation energy $E_{1.2}$ (see Eq. (1.5)), and the second multiplier is responsible for the high-temperature processes for which G is the change in the Gibbs energy due to the processes of irreversible phase transitions associated with the amorphous-state crystallization. In the classical theory of nucleation (Bekker–Volmer), it is conventional to use a reciprocal value that defines the nucleation rate.

At low temperatures, the value $\exp(-G/kT)$ is small; therefore, it suffices for Eq. (1.5). At high temperatures, we present Eq. (3.1) as

$$H_s/H_{s0} \sim \exp(E_{1.2}/kT)/\exp(G/kT). \quad (3.2)$$

Now, the principal dependence is defined by the multiplier $\exp(G/kT)$, which just determines the irreversible relaxation. We note that it is possible to assume in the proposed model that

$$G(T) \sim T\Delta(S_1 + S_2), \quad (3.3)$$

where S_1 is the entropy, which decreases during the relaxation of an amorphous state to a more stable amorphous state, and S_2 is the entropy, which increases during the transition of an amorphous state into a stable polycrystalline state [7]. Because the system transfers to a more stable state with increasing entropy, the switching-field fluctuation (Fig. 2) decreases.

Let us formulate the final conclusions. The proposed theory can enable us to evaluate the thermodynamic function of the state of the system (calculating the values $\Delta(S_1 + S_2)$ from experimental data, which seems to be very important as an alternative approach for studying the properties of metastable states. The magnetic phase transitions represent a simpler model for studying the nucleation; therefore, the idea of constructing the general theory that describes these processes can prove to be fruitful for the study of the physics of the indicated phenomena.

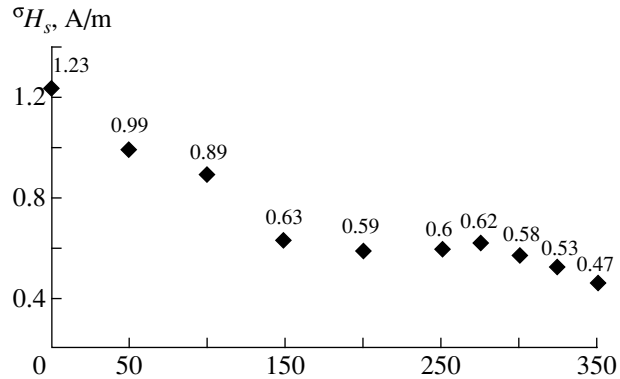

Fig. 2. Temperature dependence of the switching-field fluctuations σ_{Hs} (according to [5]).

ACKNOWLEDGMENTS

The authors thank Professor A.I. Dikusar for guidance of this work and also for valuable discussions and remarks. This work was supported in part by the RFFI–Moldova Program (grant no. 06.11CRF).

REFERENCES

1. Baranov, S.A., Baskes, M., Garsia, K.L., and Usenko, V.P., *Elektron. Obrab. Mater.*, 2004, no. 6, pp. 81–87.
2. Varga, R., Garcia, K.L., Luna, C., et al., *Non-Crystalline Solids*, 2003, vol. 3, pp. 85–91.
3. Baranov, S.A., Laroze, D., Vargas, P., and Vazquez, M., *Physica*, 2006, vol. B372, pp. 324–327.
4. Baranov, S.A., Bashev, V.F., Boiko, L.S., Zotov, S.K., Larin, V.S., and Torkunov, A.V., Structure and Properties of Quickly Quenched Fe(Co, Ni, Mn)–B–Si–C-based Microwire, *Sborn. Nauchn. Trudov: strukt. i svoist. bistro okhl. splavov* (Collection of Papers "Structure and Properties of Quickly Cooled Alloys"), Dnepropetrovsk, 1988, pp. 67–69.
5. Karimova, G.V., Bistable Cast Amorphous Glass-Coated Microwire from Fe and FeCo Alloys and its Application in Magnetometry, Extended Abstract of *Cand. Sc. Dissertation*, Izhevsk, 2006.
6. Köster, U. and Herald, U., *Kristallizatsiya metallicheskikh stekol: sbornik statei "Metallicheskie stekla"* (Crystallization of Metallic Glasses: Collection of Papers "Metal Glasses"), Moscow: Mir, 1983, pp. 325–371.
7. Bal'makov, M.D., Blinov, L.I., and Pocheptsova, I.S., *Pis'ma Zh. Tekh. Fiz.,* 1998, vol. 24, no. 3, pp. 12–17.

ISSN 1068-3755, Surface Engineering and Applied Electrochemistry, 2007, Vol. 43, No. 2, pp. 110–115. © Allerton Press, Inc., 2007.
Original Russian Text © G.A. Barbashova, V.V. Shomko, 2007, published in Elektronnaya Obrabotka Materialov, 2007, No. 2, pp. 43–48.

ELECTRICAL PROCESSES
IN ENGINEERING AND CHEMISTRY

Cyclicity Effect of the Electrical Energy Input in a Channel of the Underwater Spark Discharge

G. A. Barbashova and V. V. Shomko

Institute of Pulse Processes and Technologies, National Academy of Sciences of Ukraine, pr. Oktyabrskii 43a, Nikolaev, 54018 Ukraine

Received October 11, 2006

Abstract—The cyclicity effect of the electrical energy input on the hydrodynamic characteristics of the plasma channel and its radius, expansion velocity, and specific pressure force pulse is investigated for oscillating modes of the underwater spark discharge. A methodology of numerically determining the hydrodynamic characteristics for electrohydropulse processing facilities employing the power of an electric discharge in oscillating modes is recommended.

DOI: 10.3103/S1068375507020081

INTRODUCTION

From many experiments on photorecording the development of channels of underwater spark discharges (see, e.g., [1, 2]), it was learned that the front of the pressure wave generated in the fluid separates from the channel at the initial stage of its development. The analytical [3] and empirical [4, 5] dependences of the parameters of a pressure wave with amplitude P_m and duration τ_+ of the positive phase are therefore expressed, as a rule, in terms of the energy and time characteristics of the electrical power supplied in the channel. In the great majority of instances, analytical solutions [3, 6] and results of numerical experiments [2, 7] were based on setting the power supplied in the discharge channel in the monopulse mode. The effect of the following power pulses on the hydrodynamic processes under the discharge oscillating modes was considered much less [5, 8]. The effect was supposed a priori to be insignificant, and, in the physical experiments [5], any one-to-one correspondence between the oscillating mode of the underwater spark discharge (cyclicity of the electrical energy input) and the parameters of the initial pressure wave emitted was undiscovered. Therefore, the goal of this research is to elucidate the effect of the electric power pulses that follow after the first one on the hydrodynamics of the oscillating modes of the underwater spark discharge by means of physical and numerical experiments.

EXPERIMENTAL

To investigate the energy characteristic of the underwater spark discharge, an experimental technique described in detail in [9] is applied. The energy source was a pulse current generator equipped with a capacitor of capacitance $C = 3 \times 10^{-6}$ F, which was charged to the voltage $U_0 = 2 \times 10^4$ V. The generator was controlled by an air gap. The discharge circuit inductance was $L = 3.4 \times 10^{-4}$ H, and the accumulated energy was $W_0 = CU_0^2/2 = 600$ J.

The discharge was realized within a vessel $0.5 \times 0.5 \times 0.5$ m^3 in volume, which was filled with distilled water. To eliminate power loss at the stage of forming the cylindrical plasma channel, the discharge was initiated by an aluminum conductor 11 μm in diameter. The electric power $N(t)$ and energy $W(t)$ that were released in the discharge channel were determined by the discharge current and voltage, which were recorded with an oscillograph. The measurement accuracy was checked by the energy balance in the discharge channel by comparing the accumulated energy W_0 with the sum of the electrical energy released in the plasma channel and the power circuit. The energy balance in the experiment was maintained with an accuracy of 8%, which was recognized as the upper limit of the experimental uncertainty.

The energy characteristics for two oscillating modes of the underwater spark discharge are shown in Fig. 1. The modes differ in the interelectrode distance l: l = 0.04 (mode *I*, solid curve of $N(t)$) and 0.055 m (mode *II,* dashed curve of $N(t)$).

At the modes, the power pulsations of the i-th pulsation energy $W_i < 0.01\ W_0$ are not taken into consideration. As a result, at the mode *I*, the energy is supplied in six power cycles at the energy criterion [5] $\eta = W_1/W_0 \leq 0.4$; at the mode *II*, the energy input cycle number is 4 at $\eta \approx 0.7$. The characteristic property of mode *I* as compared with mode *II* is the lesser rate of the first pulse power rise (1.6×10^{13} W/s to 2.3×10^{13} W/s) and the higher one (by 1.4–2 times) at the following pulsations. At that, the specific (per unit length of the discharge gap) values of the rate of the first pulse power rise are in close agreement; for the following pulses, they are higher (about by 2–3 times) at the mode *I*.

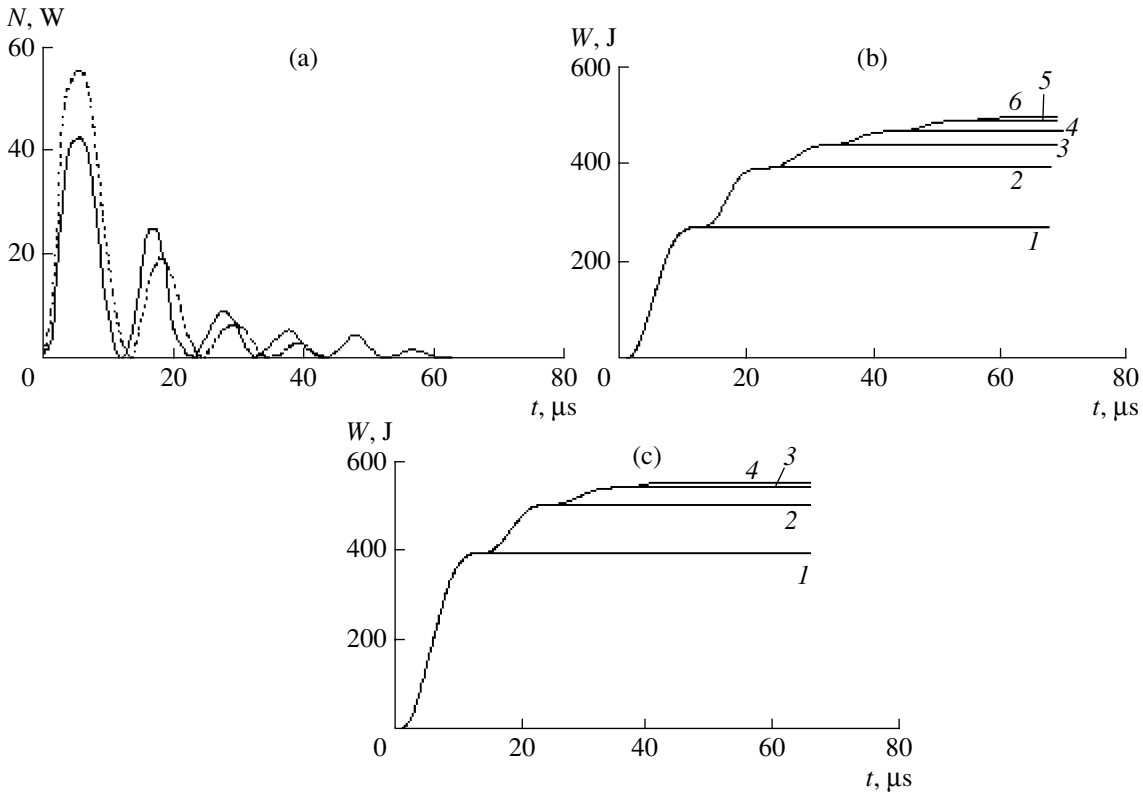

Fig. 1. Electric power (a) and energy released in a discharge channel ((b) is the base mode *I*, and (c) is the base mode *II*) as a function of time and the number of accountable power pulsations.

MATHEMATICAL FORMULATION OF THE PROBLEM AND RESULTS OF THE NUMERICAL EXPERIMENT

The plasma discharge channel is modeled by an acoustic radiating cylindrical element of finite length in which the electric power $N(t)$ is supplied at the time τ during its expansion. In the region bounded by the plasma–water contact discontinuity and the shock wave, one can solve a set of two-dimensional nonlinear gas dynamics equations in [10]:

$$\begin{cases} \dfrac{\partial(r\rho)}{\partial t} + \dfrac{\partial(r\rho v_z)}{\partial z} + \dfrac{\partial(r\rho v_r)}{\partial r} = 0, \\ \dfrac{\partial(r\rho v_r)}{\partial t} + \dfrac{\partial(r\rho v_z v_r)}{\partial z} + \dfrac{\partial[r(\rho v_r^2 + P)]}{\partial r} = P, \\ \dfrac{\partial(r\rho v_z)}{\partial t} + \dfrac{\partial[r(\rho v_z^2 + P)]}{\partial z} + \dfrac{\partial(r\rho v_z v_r)}{\partial r} = 0, \\ \dfrac{\partial(re)}{\partial t} + \dfrac{\partial[r(e+P)v_z]}{\partial z} + \dfrac{\partial[r(e+P)v_r]}{\partial r} = 0, \end{cases} \quad (1)$$

where τ is the time; r and z are the cylindrical coordinates; v_r and v_z are the radial and axial components of the fluid velocity vector; P is the pressure; ρ is the density; $e = \rho[\varepsilon + (v_r^2 + v_z^2)/2]$; ε is the internal energy of the fluid mass unit, where $\varepsilon = [P - c_0^2(\rho - \rho_0)]/[\rho(\kappa - 1)]$; ρ_0 and c_0 are the density and the sound speed of the fluid at rest; and $\kappa = 7.15$.

At the inner boundary of the calculation region, namely, the plasma–water contact discontinuity, the energy balance condition is set [2]:

$$\frac{1}{(\gamma - 1)}\frac{d(P_a V_a)}{dt} + P_a\frac{dV_a}{dt} = N(t), \quad (2)$$

At the outer boundary, namely, the shock wave, the dynamic compatibility conditions are [10]

$$[\rho]D - [\rho v_n] = 0,$$

$$[\rho v_n]D - [\rho v_n^2 + P] = 0, \quad (3)$$

$$[\rho(\varepsilon + v_n^2/2)D] - [\rho v_n(\varepsilon + v_n^2/2) + P v_n] = 0,$$

where P_a and V_a are the pressure in the discharge channel and the channel volume, $\gamma = 1.26$, v_n is the normal component of the fluid velocity vector, D is the shock wave velocity, $[f] = f_1 - f_2$, and f_1 and f_2 are the values of the function on the left and right of the shock wave.

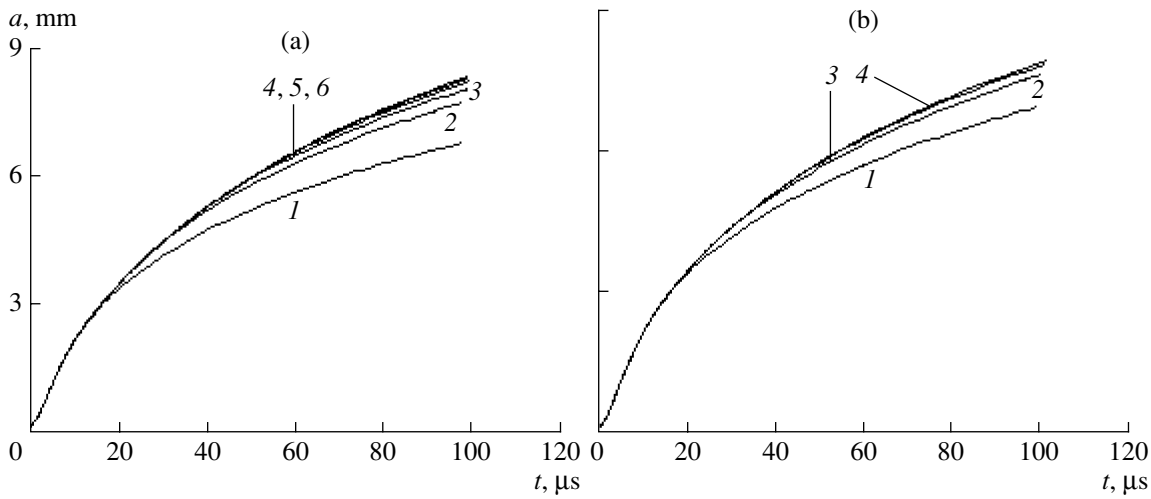

Fig. 2. Radii of the middle section of a discharge channel as a function of time and the number of accountable power pulsations: (a) are variants of the base mode *I*, and (b) are variants of the base mode *II*.

The initial values of the hydrodynamic parameters of the fluid surrounding the channel are equal to their values in the undisturbed medium, and the initial values of the radius, expansion rate, and pressure in the discharge channel are calculated by method [11].

Problem (1)–(3) was solved using the Godunov finite-difference method using the late-design algorithm [10]. In particular, we analyzed the hydrodynamic characteristics of the discharge channel (radius $a(t)$, expansion rate $\dot{a}(t)$ of the middle section, pressure $P_a(t)$, and specific impulse of the pressure force $I_a(t) = \int_0^1 P_a(\tau)d\tau$) and the fluid (pressure $P(t)$ and $I(t) = \int_0^t P_a(\tau)\,d\tau$) at a point in the equatorial plane of the discharge channel $r = 0.08$ m from the channel symmetry axis.

The energy release variants under condition (2) are chosen to enable one to analyze the effect of each following pulse of the electric energy input on the characteristics investigated. Therefore, for the experimental modes of the energy release, which are shown in Fig. 1a and recognized as basic, added variants are formed whose numbers correspond to the accountable cycle number of the electrical energy input in the discharge channel. The data from Fig. 1b, c represent information on the value of the electrical energy supplied into the discharge channel for each variant. For the convenience of comparison of the calculation results of the specific impulse of the pressure force, the upper limit of the integral of the pressure is limited by the time of the energy input for the base modes. It is acceptable, since, later on, the pressure weakly dampens; therefore, the value of the integral of the pressure increases slowly. The specific impulse of the pressure force tends to a value achievable in a time of about 1/10 of the pulsation period of the electroblasting cavity [12].

For six and four variants formed on the basis of base modes *I* and *II,* respectively, the calculated hydrodynamic characteristics of the electric discharge are shown in Figs. 2–6. In all the figures, the curve numbers are equal to the number of accountable power pulses.

From an analysis of the $a(t)$ relationships in Fig. 2, it follows that the discharge channel radius distinctly "responds" to an added energy input when the value of the energy being supplied is no less than 10% of the energy already supplied in the channel (variants *1–3* in Fig. 2a and *1–2* in Fig. 2b). At that, a sensible increase in the radius occurs under supplying about half of the energy of the next pulsation. Thus, the curves of the radius relationships of the fourth (Fig. 2a) and third (Fig. 2b) variants, whose energy increases by 6 and 7.5%, respectively, coincide essentially with the curves of the preceding variants. Application of the monopulse approximation of the six-pulse mode of energy release results in a decrease in the discharge channel radius by 15% at the time of termination of the energy release at the base mode. The difference increases with time. The deviation value increases with an increase of the number of energy input cycles (discharge cyclicity rate). It should be noted that taking into account the second energy addition introduces the basic amendment into the calculated radius in the monopulse approximation. Consideration of all the following power pulsations results in an increase in the radius of no more than 5%.

Additional (even very small) energy supplies affect the discharge channel expansion velocity more greatly than the radius (see variants *4*, *5* in Fig. 3a and *3*, *4* in Fig. 3b). The next energy input cycle already distinctly affects the rate in the power increase stage. From the analysis of the above results, it follows that, at the

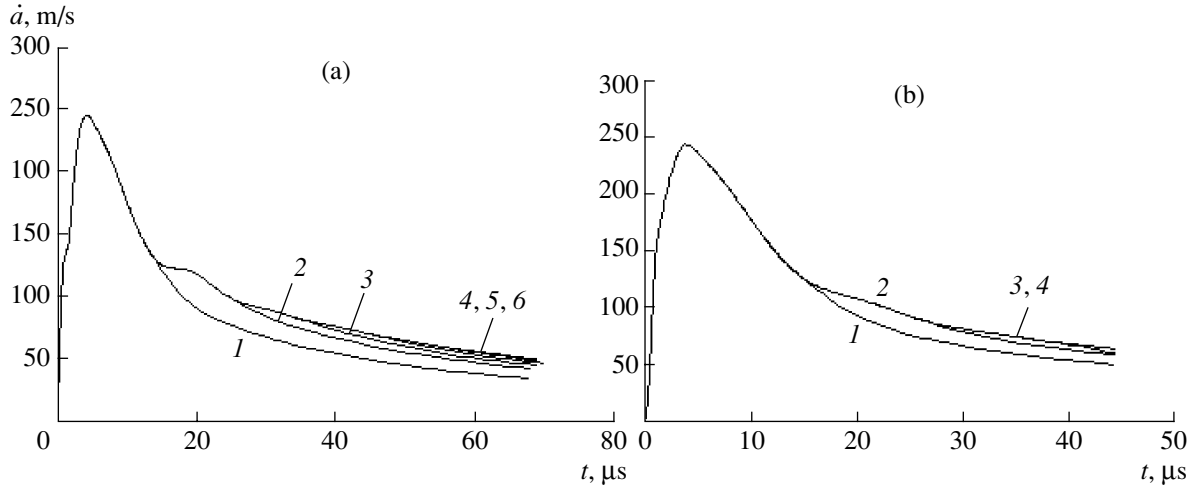

Fig. 3. Discharge channel expansion velocity in the middle section as a function of time and the number of accountable power pulsations: (a) are variants of the base mode *I*, and (b) are variants of the base mode *II*.

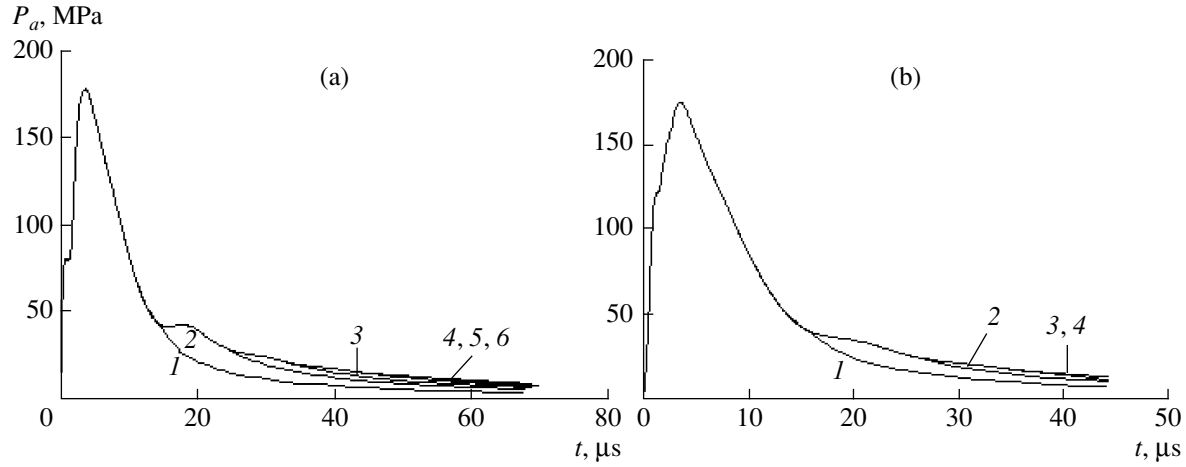

Fig. 4. Pressure in a discharge channel as a function of time and the number of accountable power pulsations: (a) are variants of the base mode *I,* and (b) are variants of the base mode *II*.

monopulse approximation, the channel expansion rates decrease on their decaying curves depending on the discharge cyclicity rate and the velocity fixation time by 15–50%. In the case of the strongly oscillating modes of the discharge (Fig. 3a), taking into account the power pulsation following the second one gives above the same velocity increase as the second pulsation. In such discharge modes, the supplied energies have comparable values at the second and all the following power pulsations (Fig. 1b).

The pressure pattern in the discharge channel (Fig. 4) and the fluid (Fig. 5) is qualitatively similar to the channel expansion velocity. However, the following energy supplies affect the pressures higher than the velocity. Thus, only taking into account the second power pulsation results in an increase in the pressure level in the channel in the relaxation section of more than 40% at base mode *II* (Fig. 4b) and above 70% at mode *I* (Fig. 4a). Towards the end of the energy release, that is, when taking into account all the power pulsations, the increase of pressure in the channel is 65 and 210% and that of the fluid pressure is 60–80%. The most increase occurs taking into account the energy supplies at the second and third pulsations.

Curves of the specific impulse of the pressure force (Fig. 6a–d) qualitatively repeat the shape of the curves of the channel radii (Fig. 2a, b) but differ significantly in the various variants. At that, the maximum divergences of the specific impulses in variants *1*, *4* (Fig. 6b, d) and *1*, *6* (Fig. 6a, b), representing calculated data for the monopulse and base discharge modes, respectively, are 15–25% for the discharge channel and 15–30% for the fluid.

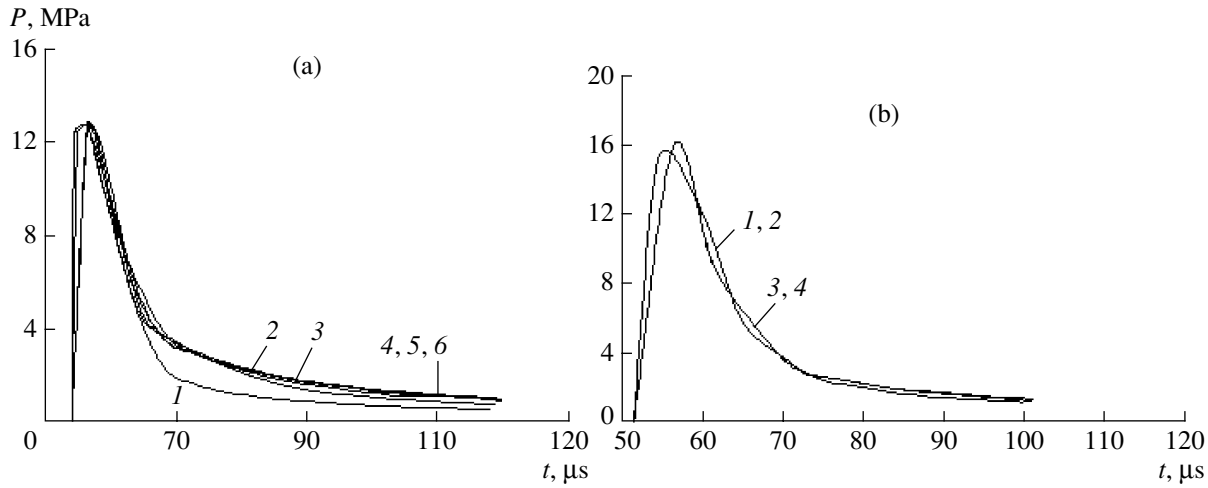

Fig. 5. Pressure profile in a fluid as a function of time and the number of accountable power pulsations: (a) are variants of the base mode *I*, and (b) are variants of the base mode *II*.

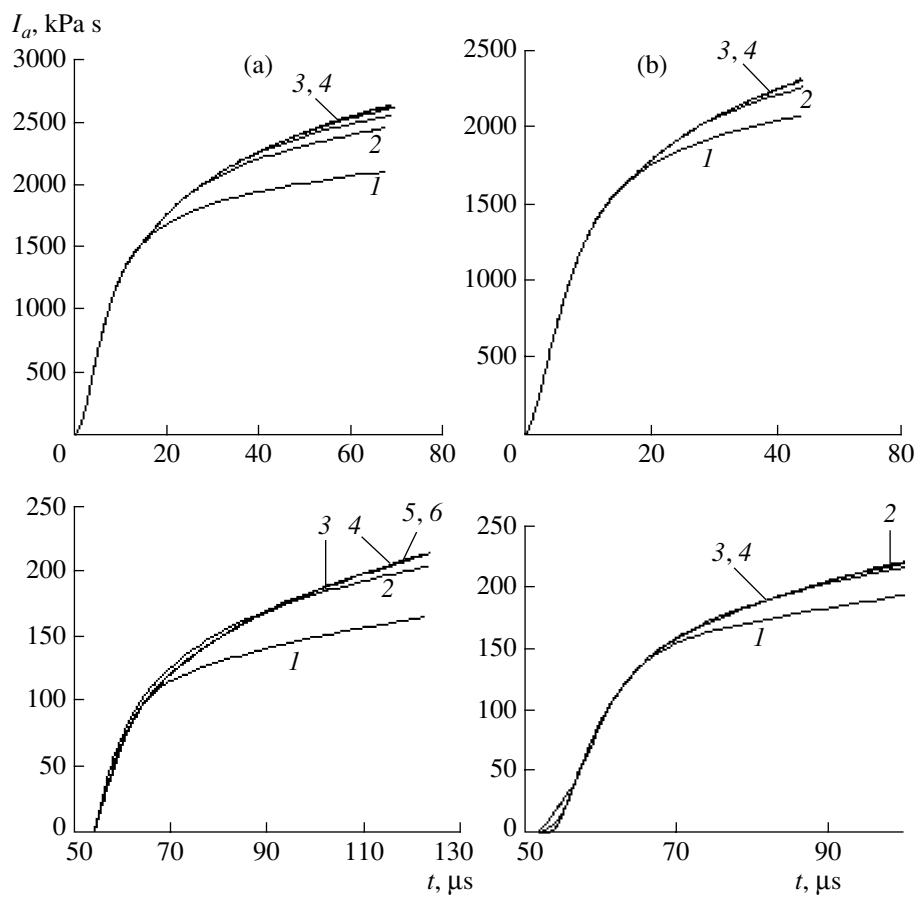

Fig. 6. Specific impulse of the pressure force for a channel ((a) is the base mode *I*, and (b) is the base mode *II*) and a wave in a fluid ((c) is the base mode *I*, and (d) is the base mode *II*) as a function of time and the number of accountable power pulsations.

CONCLUSIONS

An analysis of the above results snows that the employment of the monopulse energy input at the oscillating modes of the underwater spark discharge in the numerical experiment decreases the value of the discharge channel radius by the time of the end of the electric energy release by more than 10%, the channel

expansion velocity by 15–50%, the pressure in the channel during its relaxation stage by 65–210%, the pressure downstream of the shock wave front by 60–80%, and the specific impulse of the pressure force by 10–30%. Consequently, when numerically determining the characteristics of electrohydropulse processing facilities employing the energy of discharge oscillating modes, for which the pressure or the specific impulse of the pressure force are dominant contributors (see, e.g., [5, 9, 13]), the calculation model should take into account all the power pulsations. In the case of weakly oscillating discharge modes ($\eta > 0.7$), it is desirable to take into account at least the first two power pulsations, and, in the case of highly oscillating discharge modes ($\eta < 0.6$), it is desirable to take into account at least the first three pulsations.

REFERENCES

1. Komel'kov, V.S., *Dokl. Akad. Nauk SSSR*, 1959, vol. 129, no. 6, p. 1273.
2. Naugol'hykh, K.A. and Roi, N.A., *Elektricheskie razryady v vode* (Electrical discharge in water), Moscow: Nauka, 1971.
3. Arsent'ev, V.V., *Zh. Prikl. Math. Teor. Fiz.*, 1965, no. 5, p. 51.
4. Okun', I.Z., *Zh. Teor. Fiz.*, 1967, vol. 37, no. 9, p. 1729.
5. Krivitskii, E.V. and Shamko, V.V., *Perekhodnye protsessy pri vysokovol'tnom razryade v vode* (Transient Phenomena in a High-Voltage Discharge in Water), Kiev: Naukova Dumka, 1979.
6. Krutikov, V.S., *Pis'ma Zh. Tekh. Fiz.*, 2005, vol. 31, issue 12, p. 88.
7. Shamko, V.V., Vovchenko, A.I., Kamenskaya, L.A., and Barbashova, G.A., *Elektr. Obrab. Mater.*, 2005, no. 1, p. 61.
8. Barbashova, G.A., Vovchenko, A.I., Kamenskaya, L.A., and Shamko, V.V., *Akustichnii Visnik*, 2004, vol. 7, no. 4, p. 3.
9. Shamko, V.V. and Kucherenko, V.V., Theoretical Foundations of Engineering Calculations of the Energy and Hydrodynamic Parameters of Underwater Spark Discharge, *Preprint of Inst. of Pulse Processes and Technologies, Natl. Acad. of Sci. of Ukraine*, Nikolaev, 1991, no. 20, p. 51.
10. Barbashova, G.A. and Ivanov, A.V., *Gidromekhanika,* 1986, issue 53, p. 16.
11. Vovchenko, A.I., *Pratsi IED NANU. Elektrodinamika: zb. nauk. pr.: K: NAN Ukraini*, 2001, p. 117.
12. Koul, P., *Podvodnye Vzryvy* (Underwater Explosions), Moscow: Izd. Inostr. Lit., 1950, p. 494.
13. Yurchenko, E.S., Polovinko, V.D., and Barbashova, G.A., Effect of Pressure Pulse Parameters on the Drop of Residual Stress, *Materialy VI mezhdunarodnoi nauchnoi shkoly-seminara* (Proc. VI Int. Sci. School-Seminar), Nikolaev, 2005, p. 30.

ISSN 1068-3755, Surface Engineering and Applied Electrochemistry, 2007, Vol. 43, No. 2, pp. 116–118. © Allerton Press, Inc., 2007.
Original Russian Text © A.R. Rizun, Yu.V. Golen', T.D. Denisyuk, 2007, published in Elektronnaya Obrabotka Materialov, 2007, No. 2, pp. 49–51.

ELECTRICAL PROCESSES
IN ENGINEERING AND CHEMISTRY

Initiation of Electrical Discharge by Exothermal Compositions at Destruction of Firm Soils

A. R. Rizun, Yu. V. Golen', and T. D. Denisyuk

Institute of Impulse Processes and Technologies, NAN, Ukraine

Received October 11, 2006

DOI: 10.3103/S1068375507020093

INTRODUCTION

The development of new efficient environmentally safe methods and technologies for destruction of dense and firm seabed soils and rocks of shores for hydraulic engineering construction and reconstruction of sea and river ports, terminals, housing, and coastal constructions is an extremely real problem.

The existing traditional mechanical methods do not satisfy all the requirements and needs of exploitation and applications. They are characterized by the quite complex operations of self-floating structures positioned above a region, where construction works need to be fulfilled under conditions of limitation of the working depth and low productivity when working with rocky soils. For soils with high solidity (above 20 MPa), mechanical methods are unacceptable.

Underwater shock dredging is a more efficient method; however, it has limitations, for example, close to hydraulic engineering and coastal constructions, cable sites, hydraulic hookups, and if navigation in the safety zone cannot be stopped. Not only coastal ports and nearby port installations, berths, passing ships, and buildings can suffer during explosions but also mass annihilation of fish is possible.

As shown by investigations [1], the electrodischarge method for destruction of firm soils and shore rocks will allow an essential decrease in the building and reconstruction costs of ports, levees, and all kinds of hydraulic engineering and shore housing construction.

However, its wide-ranging application and exploitation may only be realized provided that the productivity of the process is increased up to 3–5 m^3/h for soils with a solidity of more than 30 MPa using mobile compact electrodischarge equipment adapted for work in a marine environment. The achievement of such productivity ratings is possible provided that the stored electrodischarge energy is increased by a factor of 3 to 5. Investigations on the enhancement of the electrodischarge showed that, by using exothermal compositions (EC), its energy can be increased by several times. The mass and dimension characteristics of the electrotechnical systems can also be decreased.

The aim of this work is to increase the efficiency of electrodischarge destruction of firm soils by using exothermal compositions.

The main idea of the investigations is the use of the complex action of electrodischarge and exothermal compositions for the destruction of firm seabed soils.

Electrodischarge (ED) has a number of advantages in comparison with explosives, namely, the absence of pollution, the considerably small velocities of the shock waves, and the possibility to use ED in the immediate vicinity of industrial buildings, housing constructions, and other objects.

However, ED ranks below explosives in the volume of the destruction and productivity. To increase the intensity and force effect of electrodischarge, systems for supplying aluminum-bearing exothermal compositions (EC) into the inter-electrode gap of the electrodischarge setup were developed [2]. As EC, substances are used that are capable of an exothermal transformation. A liquid mixture of an oxidant and a fuel may be chosen as such a medium. The exothermal mixture is bound to ignite easily under the action of a spark discharge and release a quantity of energy, as far as possible, at combustion. Such an active medium should not detonate under the action of force shock waves and should have the property of combustion at atmospheric pressure.

As the investigations showed [3], a mixture made up of 40% fuel and 60% oxidant is the most appropriate working medium for electrodischarge. When working out the composition of the discharge medium, the safety of the process and the mixture activity degree were considered first of all. First, industrial tests showed a threefold increase of the electrodischarge energy with equipment using the EC with the discharges initiated by a wire in the optimal regime. As further investigations showed, at the destruction of ferroconcrete items by high discharge energies (within 100 kJ) with the help of the electrodischarge setup "Basal't," the use of the EC allowed a substantial

Table

No.	*W*, kJ	*V*, m^3/h (without EC)			V, m^3/h (30 g of EC)		
		30 MPa	40 MPa	60 MPa	30 MPa	40 MPa	60 MPa
1	12.5	0.14	0.12	0.07	2.28	1.72	1.16
2	25.0	0.25	0.19	0.12	2.44	1.80	1.20
3	37.5	0.39	0.30	0.25	2.60	1.96	1.32
4	50.0	0.50	0.47	0.30	2.72	2.0	1.38
5	62.5	0.64	0.59	0.40	2.88	2.12	1.44
6	75.0	0.90	0.70	0.47	3.0	2.20	1.48
7	87.5	1.0	0.82	0.55	3.08	2.36	1.52
8	100.0	1.27	0.92	0.62	3.28	2.44	1.60

decrease of the setup dimensions and an increase of the efficiency of its work. It was established experimentally that the power intensity of the developed EC comprises from 5 to 8 kJ/g depending on the aluminum percentage.

The rheological, physiological, and chemical properties of the EC can be changed in dependence on one or another of the requirements for the technological processes and also by taking into account the parameters of the electrohydraulic plants (EHP). The EC is characterized as being fire-safe and explosion-proof, as well as easy ignited by an electrodischarge. These properties of ECs allow us to use them for the initiation of discharges at plants working at active production and allow the increased mobility of the plants owing to the decrease of their mass and overall dimensions, which essentially increases the working efficiency of EHP.

Because the electrodischarges at the destruction of firm seabed soils in the area of ports and levees takes place in blast holes (with closed and constant volumes, V = const), the total energy from the electrodischarge and the combustion of the EC can be estimated. The EC essentially increases the effect of the destruction due to the increase of the pressure amplitude in the steam-gas cavity and the increase of the frequency of its pulsation. As in the case of an electroexplosion, the energy of the reaction products can be checked using the formula

$$E = \frac{PV}{\gamma - 1}, \quad (1)$$

where E is the energy of the reaction products, P is the pressure, V is the volume, and γ is the ratio of the specific heats = 1.26.

However, in actual practice, because it is made up of an electrical energy release and a subsequent chemical energy release, the estimation of all the ratings becomes complicated. It is, first of all, necessary to choose an equation for the calculation of the thermodynamic parameters of the high-voltage electrochemical explosion (HECE). The expansion of the gas cavity at the HECE will cause the parameters to change and dependence (1) to take on a more complex form.

The determination of the energetic parameters of the HECE can be carried out using the final results of the destruction volumes and pressures at the complex destruction by HECE of a firm soil with σ = 30, 40, and 60 MPa and at the electrodischarge destruction in a pure form of the same objects. The resulting volumes of the destruction zones can be used for the solution of inverse problems for finding the parameters of the HECE, thus, omitting more complex and cumbrous calculations taking into account the pressures, the internal energy, the entropy, the regime of the chemical energy release in the discharge channel, etc.

The results of the experimentally obtained dependence of the volumes of the destruction zones of firm seabed soils on the total energy of the HECE at the use of 30 g of EC and the destruction zones of soils with the same solidity at a pure electrodischarge are presented in the table. The parameters of the discharge circuit were not changed.

In the figure, the diagram of the volume changes of the destruction zones depending on the energies of the electrodischarge and ECE is shown.

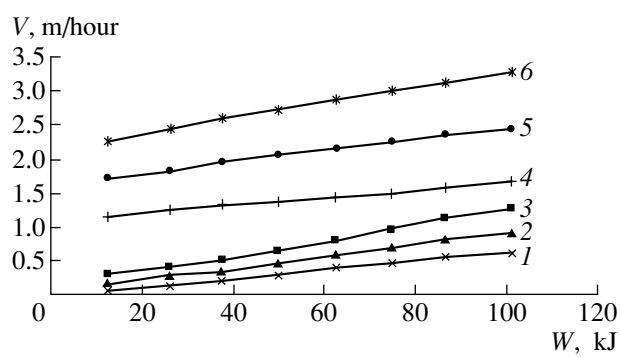

The volume of destruction of firm seabed soils with solidity of σ, MPa: (*1*) 30, (*2*) 40, (*3*) 60 (without EC); (*4*) 30, (*5*) 40, (*6*) 60 (with EC).

The established dependence of the volumes of the destruction zones on the energy of the HECE allows us to estimate the productivity of a device and the expediency of its use for objects with a soil solidity from 30 to 60 MPa.

The results of the experimental investigations were tested while conducting dredging works in the area of Sevastopol's port. The technology and a special device were developed on the basis of these results. The application of the technology will allow us to solve the problem of conducting dredging works or the destruction of coastal massif close to buildings and communication systems.

REFERENCES

1. Annikov, V.E., Vovchenko, A.I., Ivanov, V.V., and Tarutin, V.P., Active Working Medium for Electro-Hydroimpulsive Plants, in *Fiziko-tekhnicheskie aspekty elektrovzryvnogo preobrazovaniya energii* (Physico-Technical Aspects of Electro-Explosion Transformation of Energy), Kiev: Naukova Dumka, 1990, pp. 20–30.
2. Vovchenko, A.I., Posokhov, A.A., and Pozdeev, V.A., Electrochemical Characteristics of High-Voltage Electrochemical Explosion, in *Fiziko-tekhnicheskie aspekty elektrovzryvnogo preobrazovaniya energii* (Physico-Technical Aspects of Electro-Explosion Transformation of Energy), Kiev: Naukova Dumka, 1990, pp. 30–42.
3. Vovchenko, A.I. and Posokhov, A.A., *Upravlyaemye elektrovzryvnye protsessy* (Controlled Electro-Explosion Processes), Kiev: Naukova Dumka, 1992.
4. Naugol'nykh, K.A. and Roi, N.A., *Elektricheskie razryady v vode* (Electrical Discharges in Water), Moscow: Nauka, 1971.

ISSN 1068-3755, Surface Engineering and Applied Electrochemistry, 2007, Vol. 43, No. 2, pp. 119–125. © Allerton Press, Inc., 2007.
Original Russian Text © V.N. Tsurkin, A.V. Mel'nik, 2007, published in Elektronnaya Obrabotka Materialov, 2007, No. 2, pp. 52–59.

ELECTRICAL PROCESSES
IN ENGINEERING AND CHEMISTRY

System Analysis of Factors Stabilizing the Loading Parameters of Electro-Hydro-Impulsive Treatment of a Melt

V. N. Tsurkin and A. V. Mel'nik
Institute of Impulse Processes and Technologies, NAN, Ukraine
Received November 23, 2006

DOI: 10.3103/S106837550702010X

INTRODUCTION

Any technology for material treatment should assure the stability of naturally repetitive processes. Only in this case might one expect a high percentage of quality outcomes. When technology methods based on treatment by physical fields are used, the solution of this problem essentially depends on the stability of the loading parameters; i.e., the external structure forming parameters (ESFP) should be naturally and stably repeated with minimal dispersion. On the other hand, the control of the processes leading to the internal structural kinetic changes (ISKC) in the treatment object is possible by varying the ESFP. Hence, it is necessary to determine the processes that are the most sensitive to a change of one or another parameter. The physical and engineering methods used in the technological operations of the processes of material treatment are multiparametric, multifunctional, and multipurpose as a rule. Therefore, the problems of stabilization of the loading parameters in view of their regular repetition with minimal values of dispersion should be solved by a system approach when the set of all basic input and output parameters of the system is analyzed and the most sensitive connections between the ESFP and ISKC are also determined. The actuality of such an approach is obvious since revealing the stabilization conditions of naturally repeated treatment processes will permit us not only to control the stability by using them but also show us ways to increase the treatment efficiency.

The academic statement of the mentioned problem may be represented in the framework of the theory of systems. We will consider the applied aspect of the problem for the technological method of electro-hydro-impulsive treatment (EHIT) of a melt before its pouring. The technological scheme of such a method is presented in Fig. 1. The pressure field source in the treatment object (liquid metal) is the electric-discharge generator of elastic vibrations (EDGEV), which affects the melt by means of acoustic waves through the elastic transmission element (membrane with a waveguide).

The loading parameters at (EHIT) are the output characteristics of the EDGEV, which is the tool acting on the processing object. The amplitude and the shift velocity of the waveguide face, the pressure at its end, the duration and pulsing frequency, and the processing time are presented as the ESFP. The functionality of the treatment is determined by the forming of physical processes in the melt [ISKC] (generation of a nonstationary field of pressures, acoustic cavitation, formation of local acoustics fluxes and flows, etc.), providing degassing, refining from detrimental impurities, homogenization of the melt, and activation of the potential centers for nucleation owing to the variation of the loading parameters.

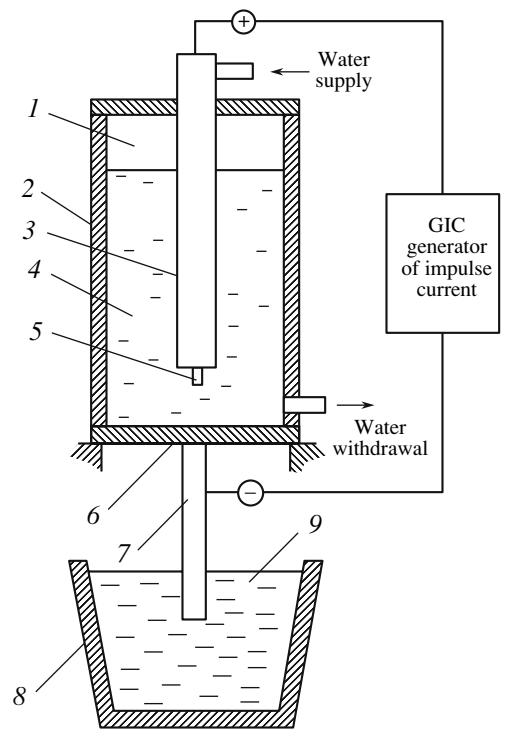

Fig. 1. Scheme of EHIT of a melt by EDGEV: (*1*) air cavity; (*2*) discharge chamber; (*3*) electrode; (*4*) working liquid; (*5*) current distributor; (*6*) membrane; (*7*) waveguide; (*8*) ladle; (*9*) melt.

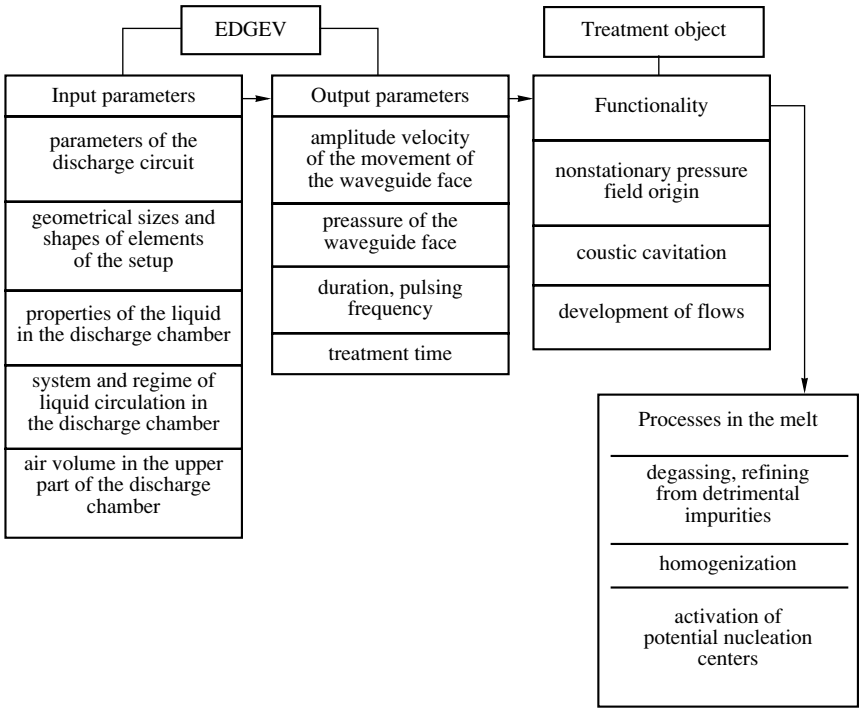

Fig. 2. System of the factors providing stability of EHIT.

The aim of this work is to conduct a system analysis of the physical and engineering factors of ESFP stabilization at EHIT of the melt and to determine the degree of their influence on the ISKC formation in the treatment object.

Notice that the formation of ISKC in the melt is a multifunctional process because the scenario of these processes is determined by the influence of many factors [1]. At the same time, modern scientific and practical experience allows us to distinguish and describe them with sufficient accuracy.

System Analysis

The minimal dispersion of ESFP may be obtained by optimal selection of the discharge circuit parameters: the geometrical sizes; the shape of the discharge chamber, the membrane, and the waveguide; the properties of the working fluid filling the discharge chamber; and the volumetric content of air in the upper part of the discharge chamber. We will denote them as the input parameters of the perturbation source. Let us show their influence on the range of ESFP variation. Assume that the lower the range of the ESFP variation at the maximal changes of the input parameters is, the higher the stability of the process is. In terms of the terminology introduced, let us represent the system of the EHIT method factors of the melt influencing the ESFP dispersion and also the cast metal quality rating in the scheme form represented in Fig. 2.

The selection of the EDGEV input characteristics for ensuring the minimal dispersion of the output loading parameters is based on the analysis of theoretical and experimental works devoted to EHIT practical application to a melt in a ladle. One must perform a detailed analysis of each of the listed input parameters of the action tool and determine their contribution to the dispersion of the ESFP.

The Influence of the Characteristics of the Discharge Circuit on the Stabilization of the Loading Parameters

The following characteristics of the discharge circuit (as was shown in [2], they exactly determine the electrical and electrodynamical characteristics of the discharge circuit and also the hydrodynamic and acoustic characteristics of the liquid in the discharge chamber) influence the stabilization of the loading parameters: the voltage on the plates U_0, the capacity of the condenser battery C, the inductance of the contour L, and the length of the interelectrode (discharge) gap l_p. The gap length corresponding to the equality of its active resistance (R_a) to the impedance of the contour ($\sqrt{L/C}$) is optimal in view of the maximal value of the electrical energy transformation efficiency.

In the papers of many authors where different technological applications of electroblasting processes in a liquid were investigated, the integral parameter of loading the stored energy $W_0 = CU_0^2/2$ is used. Its influence on the characteristics of the work materials and media in a range of variations were shown. Note that, often, the energy generation time ($\tau \sim \pi\sqrt{L/C}$) and also the relationship between R_a and $\sqrt{L/C}$ were not considered. Such an approach did not allow for a systematic character when displaying the analysis of the loading parameters influence on the treatment object characteristics. We will show this by analyzing the earlier results of the melt loading characteristics investigations at EHIT.

It is reasonable to suppose that an increase of W_0 leads to a rise of the vibration amplitude of the EDGEV work element. An experiment showed [3] that the increase of the maximum deflection of a EDGEV membrane with thickness of δ_m = 6.3 mm from 2.6 to 7 mm takes place at optimal l_p with a rise in W_0 from 0.625 to 2.5 kJ due to the increase of C from 0.5 to 2 (F at U_0 = 50 kV). In other words, the increase of W_0 by a factor of 4 leads to an increase of the deflection by 2.7 times. However, the EHIT work element is not a membrane but a waveguide face, so these results are not very informative. The theoretical investigations carried out in [4] confirmed that the vibration amplitude of the face of the waveguide A_w increases with an increase of W_0. In addition, the duration of the cavitation processes in the melt (the time intervals between the pressure pulses in the liquid metal when the pressure falls down to zero or does not exceed the initial atmospheric value) also increases. In [5], it is shown that A_w and the duration of the basic movement increase with a rise of W_0, but the frequency of the relaxation oscillations practically does not change. However, an open question remains to be answered: Is the value of l_p optimal in view of the electrical efficiency optimal for formation in the melt of the maximum possible values of the treatment force factors?

In paper [6], the dependence of the pressure pulse parameters acting on the bottom end of the rod on l_p and C is investigated using a measuring rod; i.e., only two parameters were varied from the indicated four parameters. The estimations of the average pressure in a pulse P_s and its duration τ_0 in the specified intervals of C and l_p were made by the authors. Hence, for example, at l_p = 5 mm, the highest P_s is reached at the value of C = 0.5 F but at the minimum of τ_0. At l_p = 45 mm, the maximum of P_s and τ_0 corresponds to C = 1.5 F. Analyzing these results, it may be concluded that the minimum dispersion of P_s and τ_0 is reached at a simultaneous increase of both l_p and C. This is physically quite justified because an increase in C implies a rise in W_0 and in the amplitude of the discharge current ($\sim U_0/\sqrt{L/C}$) and also an increase of its period ($\sim\pi/\sqrt{L/C}$). Within the bounds of one discharge gap length l_p, an increase of C should lead to a rise of W_0 and, as was noted in [3], to a growth of P_s. Note that the analyzing parameters in [6] correspond to the oscillatory regime of a discharge with the value of the energy fraction released during the first half-cycle of the current η [2] up to 0.4. Therefore, the practical use of these results is problematic. Note that, at $\eta < 0.4$, there is no systematic character of the results in [6]; in addition, they do not agree with the results obtained in [3].

The authors of [7], on the basis of the results of experimental investigations of a membrane deflection at a discharge in an enclosed volume, state that, under the condition W_0 = const, the elastic element executes the maximum displacement at lower values of U_0, which means at greater values of C, which emphasizes the significance of the parameter $\sqrt{L/C}$ in the formation of the membrane dynamics. At that, the difference in the displacement of a membrane with a thickness of δ_m = 12 mm and a diameter of d_m = 500 mm increases from 1.7 to 3 times at the increase of W_0 from 0.1 to 2 kJ. The analogous relationship for the regimes of a discharge with constant and different values of W_0 also remains for the accelerations corresponding to each displacement. In this paper, an estimation of the movement velocities of a central part of a membrane with dependence on W_0 is also carried out. It is established that the movement velocity depends on the regime of energy release in the discharge channel, and, at W_0 = const, the movement velocity decreases with an increase of U_0. The saturation region is found outside of which the increase of W_0 is unpractical in the view of the increase of the movement velocity. The significance of this experiment, in our case, lies in the fact that the regime of energy release η as an integral parameter of the discharge circuit influences the dynamics of an elastic element. Unfortunately, this qualitative result is not strengthened in [7] by quantitative data, which also does not provide a reason for the use of the system approach for the analysis of liquid metal loading stability.

In paper [8], the dependences of the output parameters of the EDGEV on the set of four mentioned parameters of the discharge circuit are obtained, which corresponds to the system approach in the solution of this problem and allows the ESFP stabilization methods to be clearly found and also the possibility to obtain control of the ISKC. Here, the expressions for the pressure at the waveguide face $P_w(t)$ for three regimes of energy release η (1, 0.8, 0.37) corresponding to the aperiodic, coordinated (optimal in view of the electrical efficiency), and oscillatory character of the current flowing in the interelectrode gap are presented:

$$\begin{cases} P_w(t) = 19.44\dfrac{U_0}{r^2}L^{-1.97}C^{-0.97}t^{3.44}\exp\left(-0.94\dfrac{t}{\sqrt{LC}}\right), \\ \text{at } \eta = 0.37; \\ P_w(t) = 3.1\dfrac{U_0}{r^2}L^{-2.115}C^{-1.115}t^{3.74}\exp\left(-0.86\dfrac{t}{\sqrt{LC}}\right), \\ \text{at } \eta = 0.8; \\ P_w(t) = 0.73\dfrac{U_0}{r^2}L^{-1.96}C^{-0.96}t^{3.42}\exp\left(-0.42\dfrac{t}{\sqrt{LC}}\right), \\ \text{at } \eta = 1, \end{cases} \quad (1)$$

where r is the radius of the waveguide rod.

Relationships (1) show that the pressure $P_w(t)$ should be analyzed not only in dependence on U_0, C, L, and l_p but also on r. The pressure $P_w(t)$ is the most sensitive to the change of r. The pressure P reaches its maximum values at $\eta = 0.37$, which indicates that the coordinated regime of the discharge is not optimal in view of obtaining of the maximum loading factors in the melt.

Thus, by analyzing relationships (1), the EDGEV input parameters can be ordered according to their influence on the loading stability of the melt from larger to smaller (r, U_0, C, L) irrespective of l_p.

For one setup, we accurately stabilized the values of r, U_0, and C. It is necessary to minimize the value of L in the design of the setup and achieve the maximum fastening of the connecting cables in the space since L depends on their mutual arrangement.

When formulating the problem for the relationships obtained, the voltage U_d at which the discharge is initiated was taken into account, but always $U_d < U_0$ since the losses of electrical energy arose. Therefore, for the practical use of formula (1) taking into account the engineering requirements for the conditions of the loading stabilization, it is necessary to minimize the dispersion in the difference ($U_d - U_0$), which is technically realizable.

The Dependence between the Geometrical Characteristics of the Structural Elements of the Setup and the Loading Parameters

The control of the wave components of the transmitted load at the discharge stage is appropriate to conduct at the cost of the parameters of the discharge circuit, waveguide diameter d_w, and the oscillatory component in the afterdischarge stage by varying the geometrical characteristics of the EDGEV chamber [5, 8]. As noted in [7], a characteristic of an elastic movement of a moving element under the action of a pulse load is the presence of two harmonics: the high harmonic associated with the high frequency oscillations of the central part of the membrane, and the low harmonic of its basic displacement. Such phenomenon is typical for practically any parameters of a discharge circuit; i.e., the presence of the high harmonic is caused by the structural particularities of the elastic element and does not depend on the intensity of the pulse load.

With sufficient accuracy, the diameter of the membrane d_m, the waveguide mass m_w, the properties of the working fluid and its volume, the presence of the air space above the liquid, and also W_0 can be chosen as the input parameters of the analyzed system. As was shown in [9], the pulsation dynamics of the steam–gas cavity (SGC) may be determined by taking into account the energy put into it, which is reduced to a dependence on W_0.

In [5], on the basis of numerical modeling, the estimation of A_w (the amplitudes of the relaxation oscillations of the EDGEV waveguide face) in the afterdischarge stage is carried out. The possibility for the control of the loading parameters of the liquid metal at EHIT at the cost of the EDGEV geometric characteristics was shown. The calculations were performed for values of the stored energy of 1, 2, and 3 kJ. A numerical experiment showed that the amplitude A_w decreases almost ten times with an increase of δ_m and d_w by a factor of two, while the high frequency components in the basic displacement of the membrane are displayed and the frequency of the relaxation oscillations increases. With the increase of d_m and the chamber diameter, the amplitude A_w essentially increases, the duration of the basic movement does not change, and the frequency of the relaxation oscillations significantly decreases. An increase of d_w and of m_w slightly reduces A_w and the frequency of the relaxation oscillations. The graphical dependences of the maximum oscillation amplitudes of the waveguide face $A_{\hat{a}}^{\max}$ on δ_m at fixed values of d_m and W_0 are presented in Fig. 3. It is seen from the figure that the amplitude is fitted approximately in direct proportion to the discharge energy with a change of W_0. The change of δ_m, for example, by a factor of 2 leads to the change of $A_{\hat{a}}^{\max}$ by approximately a factor of 7 to 9, i.e., almost tenfold. Thus, δ_m essentially influences the stabilization of this output parameter in comparison with W_0.

It should be noted that no noticeable changes in the values of $A_{\hat{a}}^{\max}$ take place at an increase of δ_m by more than 16 mm. Therefore, the upper limit of δ_m may be limited by this value, and the lower limit may be limited by the value at which the amplitude $A_{\hat{a}}^{\max}$ does not exceed the area of the elastic deformations.

In [3], the results of the experimental investigations of the EDGEV amplitude–frequency characteristics with a cylindrical chamber are presented. For the range of δ_m from 3 to 16 mm, the form of the dependence of the maximum displacement of the membrane on δ_m at a pulse energy of 312 J and a voltage of 50 kV is analogous to the curves presented in Fig. 3. In this paper, the spectral analysis of the EDGEV membrane displace-

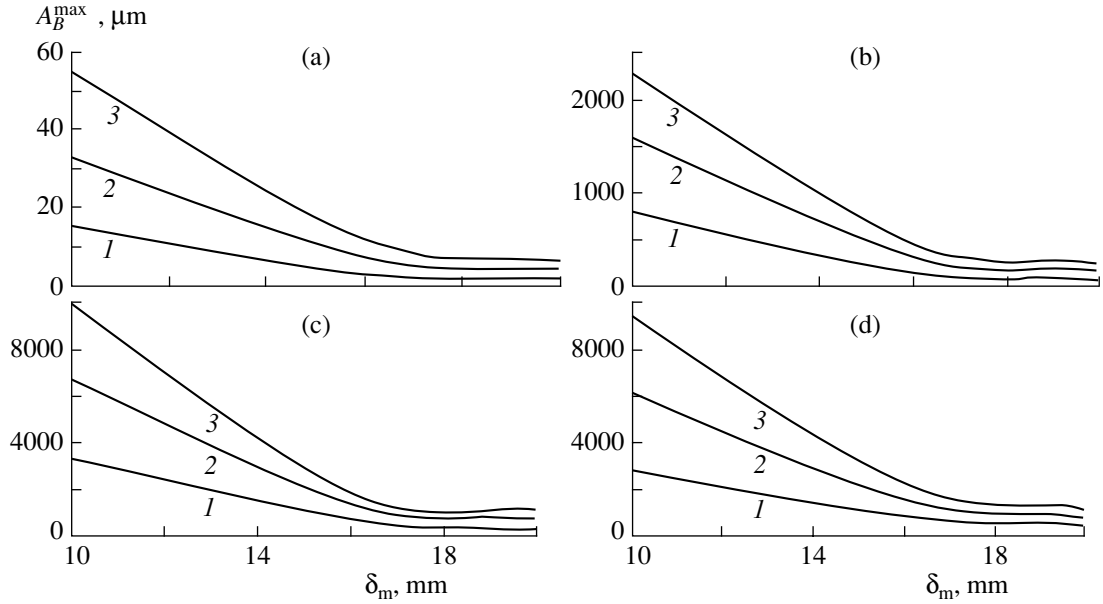

Fig. 3. The dependence of the maximum vibration amplitudes of a waveguide face on the membrane thickness at a membrane diameter δ_m (in mm) of (a) 100, (b) 230, (c) 300, and (d) 400: W_0 = (*1*) 1; (*2*) 2; and (*3*) 3 kJ.

ments is fulfilled, which allows the spectrum of the main frequencies to be determined. It is established that the placement of the spectrum maximum moves towards the high frequencies with an increase of δ_m. As the other parameters of the EDGEV change, no significant change of the spectrum maximum placement is observed. This confirms the conclusion obtained in [5, 7] that the high frequency oscillations of a membrane are determined by its thickness.

Thus, the parameters of the discharge chamber may be ordered according to the greatest influence on the loading parameters of the melt at the SGC stage in the following sequence: δ_m, W_0, d_m, d_w. The greater the value of W_0, the higher the sensitivity of the ESFP is to the change of δ_m. Taking into account that δ_m is chosen from considerations of the membrane durability, the problem of the definition of its geometry and dynamics is of current importance.

The Influence of the Properties of the Working Liquid in the Discharge Chamber on the Parameters of the Loading

As the working liquid of the EDGEV discharge chamber, water or weak electrolytes are used [3]. The characteristics of the free (no wire initiated) discharge essentially depend on the physicochemical properties of the working medium (mainly, on the specific resistance ρ_c).

In [3], comparative experimental investigations of the influence of different working liquids on the dynamic characteristics of the EDGEV transmitting element are carried out. The following liquids were investigated: industrial water (ρ_c = 8.5 (m)), distilled water (ρ_c = 150–200 (m)), and PMS-40 organic silicon (polymethylsiloxane) liquid. The pulse energy was changed from 50 to 750 J. It was shown that the value of the acceleration of an EDGEV elastic element using distilled water as the working medium is changed from 3000 to 11000 m/s2 at W_0 equal to 80 and 720 J, respectively. At this, the movement velocity changes from 0.3 to 2.5 m/s, the displacement makes up 200–800 μm, and the basic harmonics are the harmonics with a frequency of 1.25 kHz. A decrease of the oscillation parameters of the EDGEV transmitting element is observed when using industrial water. The maximum acceleration makes up 10000 m/s^2, the velocity does not exceeds 1.6 m/s, and the displacement does not exceed 600 μm. The basic harmonics have a frequency of 1.5 kHz. The values of the EDGEV parameters are significantly decreased in the case of the application of the PMS-40 liquid. Therefore, the value of the acceleration is located in the range from 1500 to 3000 m/s^2 at W_0 equal to 80 and 320 J, respectively. The movement velocity of the element made up 0.6 m/s, and the maximum displacement was changed from 50 to 150 μm. It was established that, for all the discharge parameters, the basic harmonics of the EDGEV oscillations have a frequency of 1.75 kHz.

Therefore, using PMS-40 as the working liquid, it is possible to decrease the acceleration at the external surface of the elastic element by a factor of 1.25 to 2.25 in comparison with the industrial water and by a factor of 2.3 to 3.5 in comparison with the distilled water. The energetic characteristics of the oscillation spectrum are higher than for the distilled water but somewhat lower than for the industrial water. At the same time, the

authors noted a significant increase of the stability of the EDGEV work.

Thus, the output characteristics of the setup substantially depend on the properties of the working liquid, and the loading parameters at the EHIT of the melt in a ladle can be stabilized in a given range by means of the corresponding selection of a liquid. It is best to use waters with ρ_c in the area of 20 Om m in the discharge chambers [9]. This gives satisfactory ratings of the stability and discharge efficiency, is technically simple for realization, and is economically sound.

Influence of the Volume of the Air Cavity in the Upper Part of the Discharge Chamber and the Circulation of the Working Liquid through the Interelectrode Gap on the Loading Parameters

In [10], theoretical and experimental investigations of the degree of influence of the air volume in the upper part of the discharge chamber and the water circulation through the chamber on the amplitude of the waveguide oscillations A_w were carried out. It is established that the presence of an air cavity and the liquid circulation positively influence the increase of A_w, since correctly organized circulation stabilizes the discharge and minimizes the breakdown loss, which can be related to the category of the discharge initiation, and the air cavity is a resonator for the dynamic processes of the SGC in a closed volume [9]. On the basis of the numerical modeling of the processes occurring in the discharge chamber, taking into account the accepted assumptions, it is found that the presence of an air cavity with a volume of 0.5% of the volume of the discharge chamber leads to a significant rise of the maximum amplitude of the waveguide vibration; however, on the whole, the changes of the amplitude have a statistical nature. Choosing the air volume content will allow us to regulate (within the necessary limits) the value and the character of the transmitted load on the treatment object at the stage of the redistribution in dependence on the predetermined properties of the foundries. The liquids used in the EDGEV for the EHIT of the melt should be circulated to provid cooling of the working chamber. This step is required by the high temperatures of the liquid metal, whose heat is transmitted by the waveguide into the discharge chamber. Hence, the systems and principles of the circulation influence more than the liquid itself on ESFP.

In the Institute of Impulse Processes and Technologies of NAN of Ukraine, experimental investigations of the discharge current and voltage for different l_d at both the circulation of the interelectrode gap and without it were conducted [11]. The prebreakdown losses of W_0 for different values of U_0, the rod diameter of the electrode, and l_d were determined. Three schemes for the circulation of the interelectrode gap were applied: through a hollow electrode, through a hollow current distributor, and through a hollow isolator. As the results of the investigations showed, the construction of an electrode with the circulation through the hollow isolator is the most successful and recommended for further exploitation. In such scheme, the prebreakdown losses decrease on average by a factor of 1.3 to 2.5 in comparison with the same electrode but without circulation. As a result, the possibility to increase the diameter of the electrode's rod diameter up to 12–15 mm and, therefore, to increase the working life by a factor of 2 to 3 has appeared. The circulation velocity of the interelectrode gap increases with the increase of the diameter of the rod. Therefore, for example, it is necessary to increase the effective velocity of the circulation from 3 to 5 m/s with an increase of the diameter from 8 to 15 mm. Further increase of the velocity reduces the working efficiency of the electrode. In addition, at circulation, the length of the discharge gap l_d for prebreakdown losses composing 20–30% of W_0 is greater by 30–40% than without circulation; i.e., the possibility to remove the electrode's isolator from the ruptured zone appeared, which also increases the working life of the technological setup.

Therefore, the loading parameters of the treatment object can be stabilized by means of optimal choose of V in the upper part of the chamber and also by liquid circulation with a determined velocity through the interelectrode gap.

CONCLUSIONS

1. The analysis conducted confirmed the earlier obtained data on the multiple-factor and ambiguous influence of the parameters of the discharge circuit and the EDGEV parameters on the ESFP determining the processes in the melt.

2. The system approach for the determination of the stability rating and efficiency of the ESFP is proposed, which provides the possibility for complex multifactor control of the ISKC in the melt.

3. At the channel stage, the ESFP are more sensitive to the waveguide radius and the value of the breakdown voltage U_d. If the waveguide radius is fixed, the influence of U_d has a statistical nature.

4. The ESFP dispersion can be minimized by a rational system for the liquid circulation in the discharge chamber. Liquid circulation with a determined velocity (in dependence on the diameter of the electrode's rod) through the interelectrode gap allows the prebreakdown losses to be reduced and the working life of the technological setup to be increased.

5. The ESFP at the stage of SGC are more sensitive to the membrane thickness of the EDGEV and the volume of the air cavity above the liquid. The thickness of the membrane essentially influences the stabilization of the vibration amplitude of the waveguide in comparison with the discharge energy W_0. The influence of the air cavity on the dynamics of the waveguide face has a statistical nature, and the maximum effect is reached at an insignificant change of the air volume.

REFERENCES

1. Naidek, V.L., *Protsessy vneagregatnoi obrabotki metallicheskikh rasplavov massovogo naznacheniya* (Processes of Extra-Aggregate Treatment of Metal Melts for Mass-Production), Kiev: Naukova Dumka, 1998.
2. Krivitskii, E.V. and Shamko, V.V., *Perekhodnye protsessy pri vysokovol'tnom razryade v vode* (Transient Processes at High-Voltage Discharge in Water), Kiev: Naukova Dumka, 1979.
3. Pozdeev, V.A., Tzarenko, P.I., Butakov, B.I., and Malyushevskii, P.P., *Elektrorazryadnye generatory uprugikh kolebanii* (Electric-Discharge Generators of Elastic Vibrations), Kiev: Naukova Dumka, 1985.
4. Galiev, Sh.U., Barbashova, G.A., Bilyanskii, Yu.S., Zhirnov, M.V., and Kosenkov, V.M., *Problemy Prochnosti*, 1991, no. 11, pp. 78–82.
5. Tsurkin, V.N and Mel'nik.A.V., *Elektronnaya Obrabotka Materialov*, 2006, no. 1 (237), pp. 63–69.
6. Korobov, V.A. and Tsurkin, V.N., *Elektronnaya Obrabotka Materialov*, 2002, no. 1, pp. 86–88.
7. Litvinenko, V.P., Koval', S.V., and Sysoev, V.G., Investigation of Restrained Elastic Element at Impulse Loading, in *Fiziko-mechanicheskie protsessy pri vysokovol'tnom razryade v zhidkosti* (Physical-Mechanical Processes at High-Voltage Discharge in Liquid), Kiev: Naukova Dumka, 1980, pp. 173–183.
8. Tsurkin, V.N., Sinchuk, A.V., and Ivanov, A.V., *Elektronnaya Obrabotka Materialov*, 2004, no. 1, pp. 82–87.
9. Gulyi, G.A. and Malyushevskii, P.P., *Vysokovol'tnyi elektricheskii razryad v silovykh impulsnykh sistemakh* (High-Voltage Electrical Discharge in Power Impulse Systems), Kiev: Naukova Dumka, 1977.
10. Tsurkin, V.N and Mel'nik, A.V., *Elektronnaya Obrabotka Materialov*, 2003, no. 6, pp. 63–69.
11. *Experimental Search of Methods for Discharge Initiation by Forced Circulation of Working Liquid through Interelectrode Gap* (Research Report No. 0193U024940), IIPT, NAN Ukraine, Strel'tzov, V.A., Supervisor, Nikolaev, 1994.

ISSN 1068-3755, Surface Engineering and Applied Electrochemistry, 2007, Vol. 43, No. 2, pp. 126–130. © Allerton Press, Inc., 2007.
Original Russian Text © I.V. Popova, A.I. Marinin, A.I. Ukrainets, G.A. Lezenko, V.P. Vasyliv, Yu.A. Dashkovskii, V.V. Olishevskii, 2007, published in Elektronnaya Obrabotka Materialov, 2007, No. 2, pp. 60–65.

ELECTRICAL TREATMENT
OF BIOLOGICAL OBJECTS AND FOODSTUFFS

Production of Fructose-Oligosaccharide Mixtures Using Electric-Pulse Technologies

I. V. Popova, A. I. Marinin, A. I. Ukrainets, G. A. Lezenko, V. P. Vasyliv, Yu. A. Dashkovskii, and V. V. Olishevskii

National Institute of Food-Processing Technologies, ul. Vladimirskaya 68, Kiev, 01033 Ukraine

Received September 7, 2006

DOI: 10.3103/S1068375507020111

Lately, the treatment of food stuffs and raw materials with electromagnetic fields has been attracting increasingly strong interest [1–3]. This interest is caused by the following reasons: food stuffs and semi-finished products have electromagnetic properties and electric conductivity and dielectric permittivity and magnetic permeability so that, during electric and magnetic treatment, changes occur in the distribution of the electric charges in the medium resulting in changes to the physical and chemical properties of products [4].

Electrohydraulic treatment (EHT) seems to be the most promising method for treatment of food raw materials and ready products with electromagnetic fields.

Study [5] is distinguished among the published results of the applied research. It shows that an electric charge pulse affects plant raw materials during processing in a comprehensive way. The shock wave emerging as a result of the medium breakdown actively mixes up the system. Moreover, by creating tensile forces in the fluid, it causes the creation of cavity bubbles facilitating dispersion of particles. The thermal process in the discharge channel results in the creation of a vapor-and-gas cavity whose pulsing intensifies the heat- and mass-exchange processes.

In addition, application of this technique facilitates the suppression or inhibition of the microflora of food stuffs without significant changes to the organoleptic properties of those stuffs.

We have studied the effect of electrohydraulic treatment on suspensions of inulin, a polysaccharide (whose molecule consists of residues of β-D-fructopyranose), and the process of its partial and complete hydrolysis resulting in production of fructose-oligosaccharide mixtures, which are utilized in many branches of the food-processing industry.

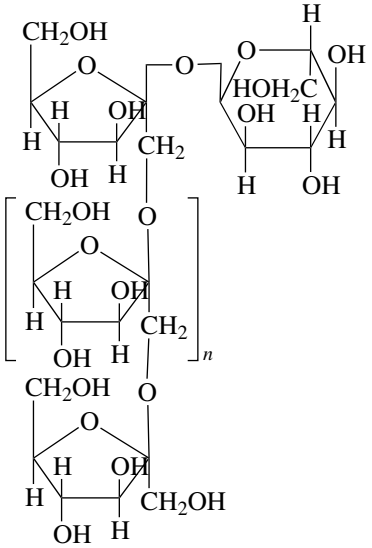

A similar study was carried out with chicory (one of the most widely spread plants with a high content of inulin), which is used in certain amounts in the food-processing industry but worthy of wider usage owing to its multiple beneficial effects on the human body.

Hydrolysis of inulin is performed most frequently by processing its solution or suspensions with mineral or organic acids and, in the majority of cases, by heating [6]. As a result, the hydrolysis products, fructose and oligosaccharides characterized by a lower polymerization degree then inulin (so called fructans), are usually contaminated by the products of dehydration, decomposition, and subsequent condensation of fructose and the coloring agents produced as a result of other secondary processes.

The use of enzymes for the production of inulin-oligosaccharide syrups, which is discussed in the literature, is also characterized by a number of disadvantages. In particular, apart from the strict observance of the requirements for medium acidity and temperature

parameters, the target product should be additionally cleaned of both the ferment substance and the producing coloring agents.

The application of electrohydraulic treatment for inulin hydrolysis ensures the neutral reaction of the initial reaction medium and the absence of other chemical agents, hence, the cleanness of the produced fructose-polysaccharide mixtures as compared to standard hydrolysis methods.

For hydrolysis, aquatic solutions or suspensions of inulin were made with the content of dry substances varying from 2 to 30%. The powders for the production of the suspensions were preliminary maintained in water for 72 hours for the polysaccharide grains to swell, thus, facilitating the more complete hydrolysis of the specimens. The prepared solutions or suspensions underwent electric pulse treatment with 5 to 75 pulse discharges at an electrode voltage of 35–40 kV.

As a result of the electrohydraulic effect and the other physical phenomena developing during the high-voltage discharge in the fluid, the glycoside bonds between the fructose structural units in the inulin molecules are mechanically disrupted and the elements of the water molecules are connected; i.e., partial hydrolysis of the inulin molecules occurs. As a result, some of the inulin molecules are transformed into the final product of complete hydrolysis, fructose. The hydrolysis effect is attained in a neutral medium without adding any chemical reagents and does not involve the production of colored by-products.

The content of the dry substances (DS) in the reaction mixture was measured by the refractometric method. The content of fructose in the hydrolizate was determined by the classic Muller method for the determination of reducing substances.

The optimal number of pulses during the electric-spark treatment was determined on the basis of the maximum content of the reducing substances in the hydrolizate, thus, indicating the most complete hydrolysis of the inulin.

Figure 1 shows, as an example, the results of an experiment where the optimal number of high-voltage pulses required for attaining the highest relative content of fructose in the final product of the hydrolysis was determined.

Most probably, if the number of pulses exceeds the optimal value, conditions are created for recombination processes in which the molecules of D-fructose (monosaccharide) that were produced at the initial stages of the hydrolysis do not transform into a more thermodynamically stable β-pyranose form (as is the case under the conditions of standard hydrolysis without the application of pulse electric treatment) but interact with each other creating dimers and, primarily,

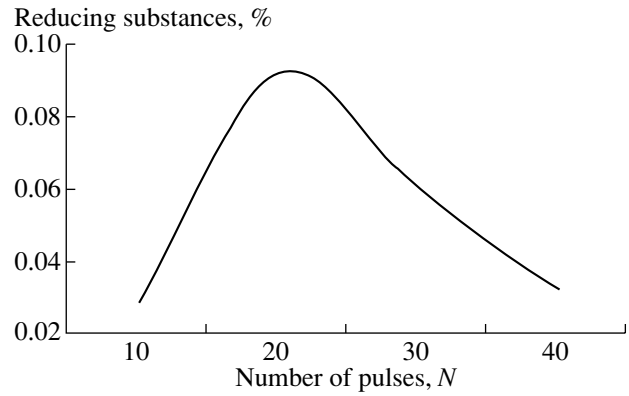

Fig. 1. Dependence of the content of reducing substances in the hydrolyzate on the number of high-voltage pulses.

1-(β-D-fructofuranosil)-β-D-fructofuranose, i.e., inulobiosis,

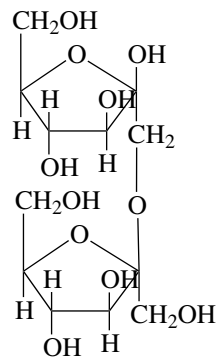

as well as trimers, tetramers, and other fructans with a lesser polymerization degree than inulin, i.e., inulo-oligosaccharides.

The table shows the results of some experiments in which the optimal parameters of the electric-spark treatment of inulin solutions and suspensions were determined.

Since chicory seems to be a more promising candidate for practical use in the food-processing industry as compared to pure inulin, a similar study was carried out to determine the dependence of the hydrolysis degree on the parameters of the electric-spark treatment with freshly minced chicory bulbs and with powders made from dried and roasted chicory bulbs. For the experiments, commercial powders manufactured by the Slavutsky chicory drying plant (Khmel'nitsk oblast, Ukraine) were used.

The prospects for the usage of chicory are based, on the one hand, on economic factors, since extraction of pure inulin from inulin-containing plants is a sufficiently complex process and requires significant additional expenses. On the other hand, the chicory root contains, in addition to the main component, i.e., inulin, other biologically active substances that may be used

Regimes of Electric Pulse Treatment of Aqueous Solutions and Suspensions of Inulin

Experiment no.	Voltage, kV	Number of pulses	Content of DS, %	Content of fructose in the obtained mixture, %	Hydrolysis degree, %	Conclusions
1	35	5	2.01	0.22	22.1	Number of pulses insufficient for inulin hydrolysis
2	40	10	2.05	1.47	48.6	Content of reducing substances in the obtained mixture increases
3	35	20	2.07	2.60	53.9	Number of pulses sufficient for partial inulin hydrolysis
5	35	50	2.2	1.55	44.5	Content of reducing substance decreases and the degree of polymerization of inulo-oligosaccharide increases
6	35	75	2.21	2.95	41	Degree of polymerization of inulo-oligosaccharides additionally increasing owing to recombination processes with a further increase in the number of pulses not being needed

for medical treatment and prophylactics, so adding them to food products in the form of chicory components should be welcomed.

For powders made of dried and roasted chicory, the studies that were conducted were similar to those for pure inulin. The optimal regimes for pulse electric treatment were determined, and they virtually coincided with the inulin-treatment regime.

In addition, the dimensions of the particles at different stages of the pulse electric treatment were determined by the method of laser-beam scattering.

The studied commercial specimen of chicory powder mainly consisted of particles with diameters ~200 μm; it also contained a significant amount of particles with a diameter of ~100–50 μm and virtually did not contain particles whose diameter was less than 1 μm.

As a result of the electrohydraulic treatment (35 kV and 10 pulses) (see Fig. 2b), the content of particles with a diameter of ~200 μm halved as compared to the initial suspension. The amount of smaller particles (10–5 μm) steeply (3- to 4-fold) increased, apparently, indicating that the macromolecule fragmented as a result of hydrolysis under the effect of the electrohydraulic treatment and fragments of olygoinulides with a lower polymerization degree and finer particles were produced as a result. A significant number of particles with a diameter of 1.0–0.5 μm appeared.

If the number of pulses was increased to 20 (Fig. 2c), the trend continued: the relative content of large particles decreased and that of finer particles (<1.0 μm) increased even more. Thus, under these conditions, the hydrolysis process continued resulting in the production of inulin olygomers with a lower polymerization degree and fructose.

If the number of spark discharges was further increased to 30 or more, the content of large and small chicory particles virtually did not change (Fig. 2d).

The behavior of inulin and inulin-containing materials under the conditions of electrohydraulic treatment may be explained as follows.

Application of electromagnetic fields is known to significantly change the magnetic properties of water [4, 7–9]. This means that this factor alone may change the conditions of the hydrolysis of organic compounds, i.e., the interaction with water of such a biopolymer as polysaccharide inulin.

It was discovered that the chemical bonds in molecules are polarized under the effect of a magnetic field [10]. The water molecules having a permanent dipole moment are aligned with respect to the magnetic-field frequency, and the rotation of dipole molecules under the effect of an alternating magnetic field corresponds to the frequency of the field variation [11]. A similar effect is also observed for organic molecules, for example, protein.

However, protein is *per se* a bipolar substance, while the nature of the studied biopolymer, polysaccharide inulin, differs from that of protein. However, the native inulin molecule is characterized by a certain distribution of the electric density, in particular, on the oxygen atoms forming glycoside bonds between individual fructose links in the inulin polymer molecule differing

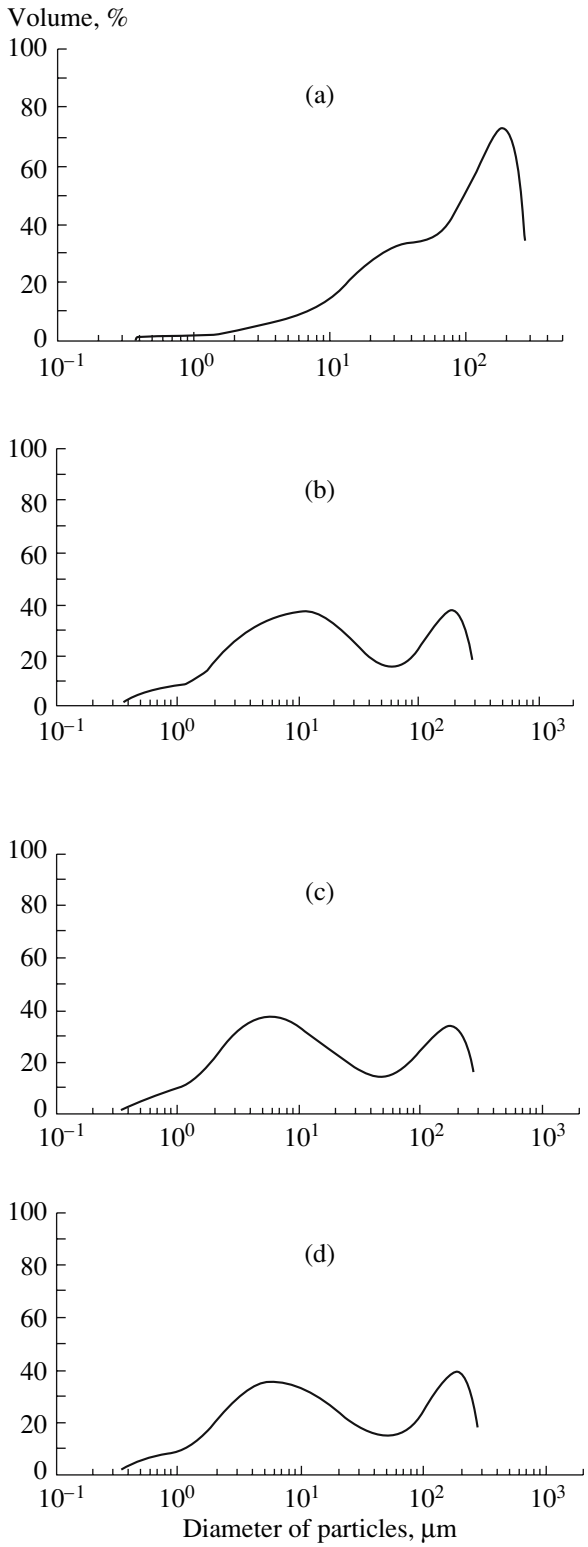

Fig. 2. Distribution of particles by sizes in the initial suspension of the chicory powder and its hydrolyzates after electrohydraulic treatment (EHT): (a) initial suspension before treatment; (b) EHT regime: 35 kV and 10 pulses; (c) EHT regime: 35 kV and 20 pulses; (d) EHT regime: 35 kV and 30 pulses.

from that on the oxygen atoms incorporated into the primary and secondary alcohol groups. An electromagnetic field apparently causes a redistribution of the electronic density in the polysaccharide molecule, including changes in the density of the effective charges on the bridging oxygen atoms. This phenomenon should, in turn, result in changes to the reaction capacity of glycoside bonds on the reaction of inulin hydrolysis.

The changes to the regimes of the electrohydraulic treatment seem to entail redistribution of the effective charges on the atoms in the inulin molecule and the products of its hydrolysis resulting, in turn, in the shift of the equilibrium in the system either to production of hydrolysis products or to recombination of low-molecular products into oligomers with a higher polymerization degree.

CONCLUSIONS

1. The process of electrohydraulic treatment (EHT) of suspensions and solutions of inulin and inulin-containing chicory was studied to produce fructose-oligosaccharide mixtures.

2. An optimal EHT regime was found (35 kV and 20 pulses) for production of mixtures with the maximum content of fructose and inulo-oligosaccharides with a low polymerization degree.

3. The classical Muller method for the determination of the content of reducing substances and the method of laser-beam scattering were applied to prove that, during EHT, two oppositely directed processes evolve: hydrolysis of inulin and recombination of low-molecular inulides. The shift of the equilibrium in the inulin and low-molecular inulides depends on the specific EHT regime.

REFERENCES

1. *Mikrokhvil'ovi tekhnologii v narodnomu gospodartsvi: Vprovadzhennya. Problemy. Perspektyvy* (Microwave Technologies in National Economy: Introduction, Problems, and Perspectives), Kalinin, L.G., Ed., Odessa: OKFA, 1996.
2. Glazyrin, B.N., Litkov, B.K., and Kartov, A.V., *Pishch. Prom.*, 1992, no. 3, pp. 12–13.
3. Romaswamy, H. and van de Voort, F.R., *Can. Eust., Food. Sci. Am. Technol.*, 1990, vol. 23, no. 1, pp. 17–21.
4. Gulii, I.S., Pushanko, M.M., Orlov, L.O., Mironchik, V.G., and Ukrainets, A.I., *Obladnannya pidpriemst pererobnoi v kharchovoi promaslovosti* (Equipment of Enterprises of Processing and Food-Processing Industry), Vinnitsa: Nova Kniga, 2001.
5. Alekseeva, T.I., Barskaya, A.V., and Lobanova, G.L., On Dispersion of Peat with Electric Pulse Discharges, *Tez. dokl. VIII nauchn. shkoly "Fizika impul'snykh razryadov v konservirovannykh sredakh"* (Abstr. of Papers of VIII

Scient. School "Physics of Pulse Charges in Conserved Media"), Nikolaev, 1997.

6. Samokhin, I.I., Zablitseva, N.S., and Kompantsev, V.A., Russian Patent no. 218369, *Byull. Izobret.*, 2000, no. 43.
7. Minenko, V.I., Petrov, S.M., and Mits, M.N., *Magnitnaya obrabotka vody* (Magnetic Treatment of Water), Kharkov, 1962.
8. Rempel', S.I. et al., *Novaya Tekh. Zhil.-Komm. Khoz. Vodosnab. Kanaliz.*, 1964, issue 3, ser. IV, pp. 18–21.
9. Minenko, V.I., *Elektromagnitnaya obrabotka vody v teploenergetike (vorposy teorii i praktiki)* (Electromagnetic Treatment of Water in Heat Power Engineering (Theory and Practice)), Kharkov: Vishcha Shkola, 1981.
10. Presman, A.S., *Elektromagnitnye polya i zhivaya priroda* (Electromagnetic Field and the Live Nature), Moscow: Nauka, 1968.
11. Mogda, V.P., *Mekhaniz. Elektrif. Sots. Sel'sk. Khoz.*, 1970, no. 3, pp. 27–30.

ISSN 1068-3755, Surface Engineering and Applied Electrochemistry, 2007, Vol. 43, No. 2, pp. 131–135. © Allerton Press, Inc., 2007.
Original Russian Text © A.S. Lupashko, G.K. Dikusar, O.F. Lupu, 2007, published in Elektronnaya Obrabotka Materialov, 2007, No. 2, pp. 66–70.

ELECTRICAL TREATMENT
OF BIOLOGICAL OBJECTS AND FOODSTUFFS

Kinetics of Drying Kernels of Apricot Stones Using a High-Frequency Current

A. S. Lupashko, G. K. Dikusar, and O. F. Lupu

Technical University of Moldova, bul. Stefan Cel Mare 168, ÃD-2004, Chisinau, Republic of Moldova

Received November 8, 2006

Abstract—Application of a convective method and a combined method employing a high-frequency current alongside convection for drying kernels of apricot stones is experimentally studied. The drying rate, the drying rate constants, and the duration of the first and second periods are determined. The effect of a high-frequency electromagnetic field on the kinetics of the drying is analyzed.

DOI: 10.3103/S1068375507020123

The average quantity of secondary products (food wastes) at enterprises of the food-canning industry amounts about 21% of the mass of the processed primary product.

Fruits pits comprise a substantial share of the total volume of the primary product being processed. Their afterproducts possess good qualities and may be regarded as a rather valuable sort of secondary raw material.

Nowadays, air-and-sunshine drying of fruit stones on unequipped open sites is still widely used. For drying kernels of apricot stones, a convective method and a combined method where high-frequency currents (HFC) are used has been proposed. The aim is to intensify the drying process while retaining the biological value of the product, improve the cost effectiveness of the process, and make the process ecologically friendly.

The experimental setup described in [1] was employed for the investigations. Kernels of stones of the "Krasnoshchekii" variety of apricot with an initial moisture content of U_0 = 146% were dried.

A VNTz-200 mechanic balance was used to register the mass loss. The rate of the air supply to the drying chamber was automatically kept constant at 1.1 m/s. The air parameters were measured before the heat treatment (initial temperature t_0 and relative humidity φ_0) and after the process (t_1).

At the first stage of the work, the kinetics of the convective drying were studied at temperatures of the drying agent of 60, 70, 80, 90, and 100°C. The mass loss was measured over intervals of 5 min, and the drying continued to the equilibrium moisture content of 30% [2].

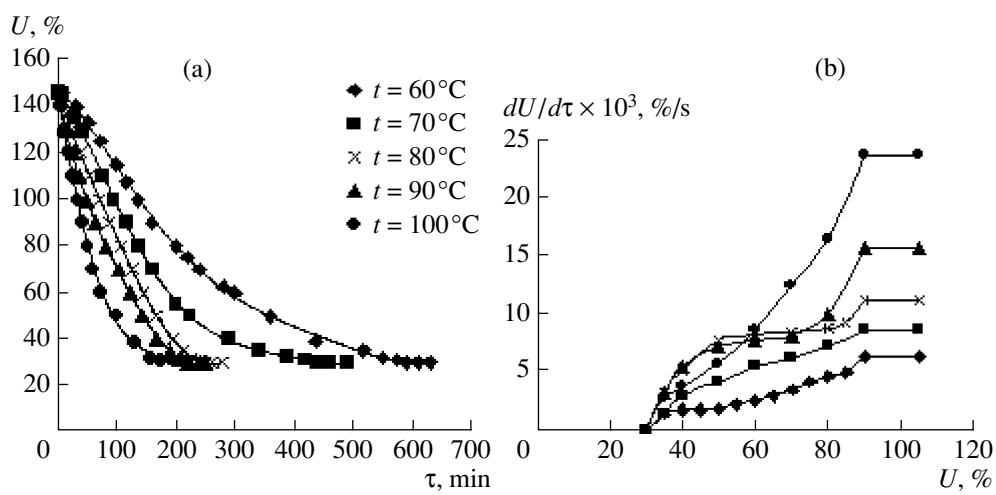

Fig. 1. Drying curve (a) and drying rate curve (b) for kernels of apricot stones using a convective energy supply.

Table 1. Experimental parameters of the kinetics of drying kernels of apricot stones by a convective method

no.	t_1, °C	U_{cr}, %	$\left(\frac{dU}{d\tau}\right)_1 \times 10^3$, %/s	K_1, %/(m^2 s)	$K_2 \times 10^6$, s^{-1}	$\tau_{preheat}$, min	τ_1, min	τ_2, min	τ_{gen}, min
1	60	90	6.46	58.6	1.6	100	240	280	620
2	70	90	8.62	63.5	3.2	89	184	232	505
3	80	95	11.18	65.9	4.0	78	158	169	415
4	90	95	15.74	84.35	4.98	59	122	137	318
5	100	95	23.61	107.1	5.6	35	91	94	220

Figure 1 shows the drying curves $U = f(\tau)$ and the drying rate curves $\left(\frac{dU}{d\tau}\right)_1 = f(U)$ for kernels of apricot stones. As can be seen from the drying curves, the process duration amounted 620 min and 220 min at the temperatures of 60°C and 100°C, respectively; that is, its decrease by a factor of 2.85 was observed.

The curves of the drying rate (Fig. 1b) are typical for colloidal and capillary bodies and involve the range of preheating as well as the first and the second periods of drying [3].

The drying rate was calculated using the experimental data for the first period of drying. Table 1 shows the drying temperature values t_1 (°C), the critical moisture content U_{cr} (%), the drying rate for the first period $\left(\frac{dU}{d\tau}\right)_1$ (10^3) (%/s), the constants of the drying rate for the first period K_1 and for the second period K_2, the preheating time $\tau_{preheat}$, and the drying duration for the first period τ_1 (min) and for the second period τ_2 (min).

At the second stage of the experiment, the effect of the combined action of high-frequency heating, together with the convective method of energy supply, upon the drying kinetics at various regimes of the electromagnetic field $E = 8.75 \times 10^3$ and 1.8×10^4 V/m was studied.

The experimental results are presented in Figs. 2 and 3 as the drying curves and the drying rate curves.

The time of the drying process decreases with the field strength increase for various temperatures. The time of drying to a moisture content of 30% amounted 410 min at a temperature of 60°C and an electromagnetic field strength of 8.75×10^3 V/m, and it was equal 370 min at a strength of 1.8×10^4 V/m; that is, it decreased by 40 min.

The data presented in Fig. 2 demonstrate that the combined action of the high-frequency electromagnetic field and the convective method substantially intensifies the drying process.

Comparison of the dewatering process at the minimal temperature and electromagnetic field strength values (t = 60°C and $E = 8.75 \times 10^3$ V/m) with that at the

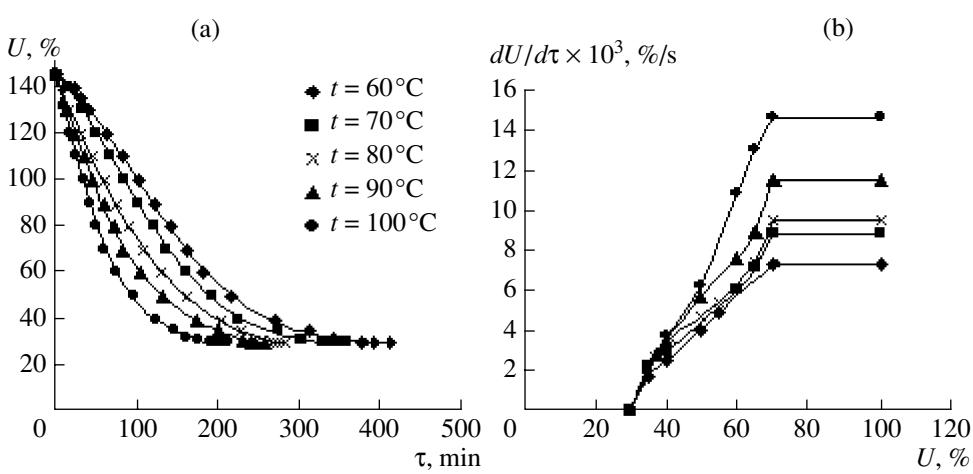

Fig. 2. Drying curve (a) and drying rate curve (b) for kernels of apricot stones using a combined method (convection + HFC); the electromagnetic field strength is E = 8750 V/m.

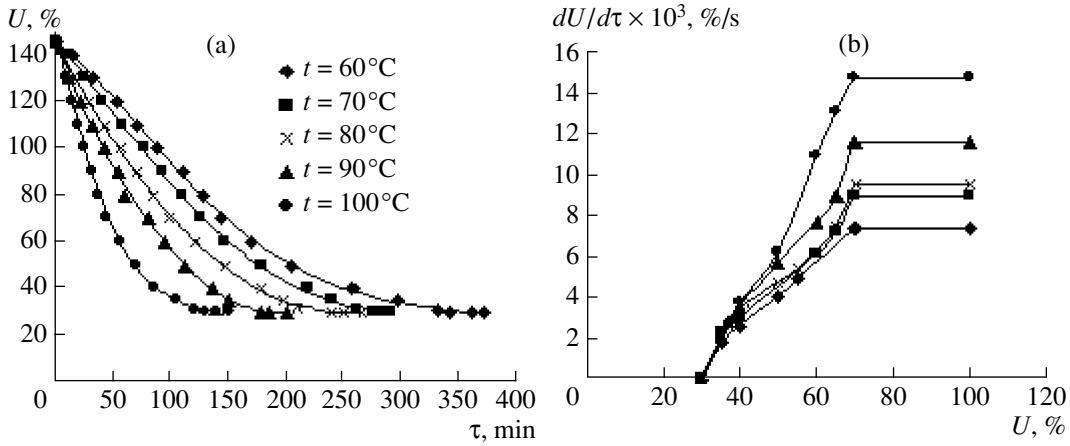

Fig. 3. Drying curve (a) and drying rate curve (b) for kernels of apricot stones using a combined method (convection + HFC); the electromagnetic field strength is $E = 1.8 \times 10^4$ V/m).

maximal temperature and electromagnetic field strength values (t = 100°C and $E = 1.8 \times 10^4$ V/m) shows that the time for drying from 146 to 30% decreases by a factor of 2.8.

The duration of the drying process of the kernels reduces due to the more intensive heat release in the unit volume of the kernels with the field strength increase; therefore, the drying process rate quickly increases to its maximal value when the high-frequency field is used.

At the temperature of the drying agent of 60°C (Fig. 2b) with the electromagnetic field strength $E = 8.75 \times 10^3$ V/m, the maximal rate value increases by 17.8%. The maximal rate of the drying process increases with the temperature increase. When the temperature increases from 60 to 100°C at the same field strength, the drying rate increases by a factor of 2.

The kinetic characteristics of the drying process were calculated both for the convective drying method and for the combined method (convection + HFC) for various values of the field strength and are presented in Table 2.

For the second period, the drying rate constant K_2 at the temperature of 60°C increased by 14.4% with the

Table 2. Experimental parameters of the kinetics of drying kernels of apricot stones by a combined method (convection + HFC)

no.	t_1, °C	U_{cr}, %	$\left(\frac{dU}{d\tau}\right)_1 \times 10^3$, %/s	K_1, %/(m^2 s)	$K_2 \times 10^6$, s^{-1}	$\tau_{preheat}$, min	τ_1, min	τ_2, min	τ_{gen}, min
Electric field strength $E = 8.75 \times 10^3$ V/m									
1	60	70	7.41	67.2	3.53	80	235	85	410
2	70	69	8.93	65.8	4.09	56	223	61	340
3	80	69	9.59	56.6	4.65	28	193	59	280
4	90	70	11.61	62.2	5.86	25	187	48	260
5	100	70	14.72	76.8	6.45	17	165	33	215
Electric field strength $E = 1.8 \times 10^4$ V/m									
1	60	68	8.73	79.2	4.04	45	273	47	365
2	70	72	9.44	69.6	4.37	33	235	31	300
3	80	69	9.61	56.5	4.56	30	185	29	245
4	90	66	11.01	59.0	5.90	17	158	23	198
5	100	72	20.63	93.6	9.55	13	112	20	145

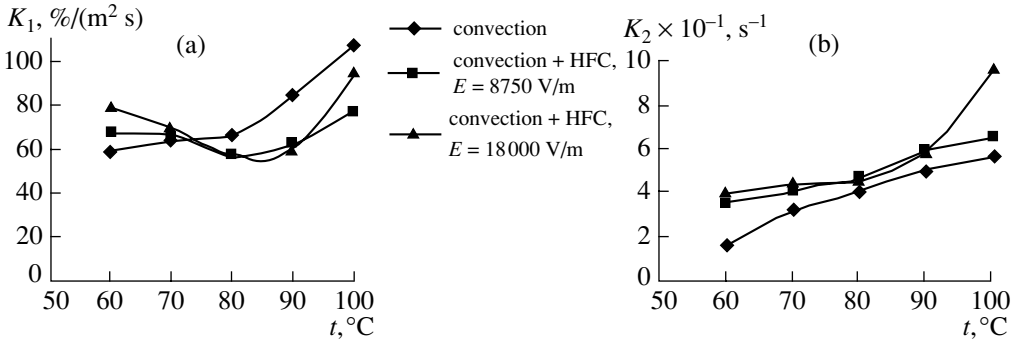

Fig. 4. Dependence of the drying rate constants vs. temperature for various types of energy supply: (a) first period, (b) second period.

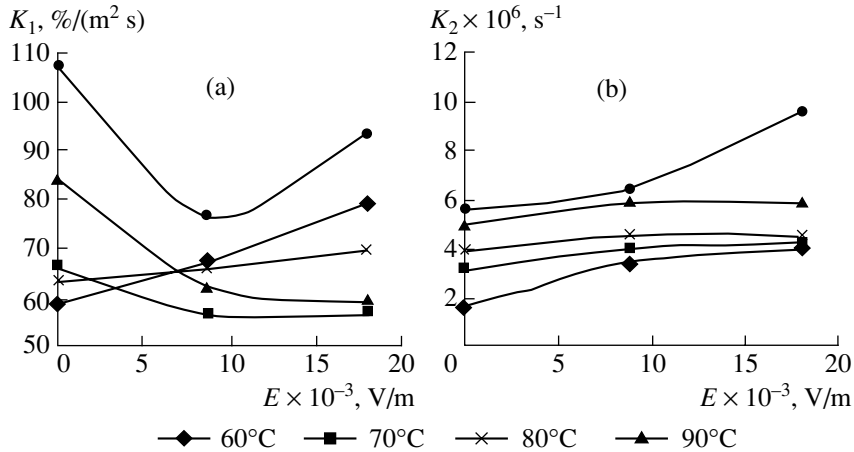

Fig. 5. Dependence of the drying rate constants vs. the electromagnetic field strength for various types of energy supply: (a) first period, (b) second period.

increase in the electromagnetic field strength. The temperature increase from 60 to 100°C and the field strength increase from $E = 8.75 \times 10^3$ to $E = 1.8 \times 10^4$ V/m resulted in an increase in the drying rate constant K_2 from 83 to 136%. These values demonstrate that the HFC exerts a substantial effect upon the drying process (especially in the second period) due to the effect of the HFC on the product structure and the rupture of bonds between the moisture and material. The variation of the drying rate constants is shown in Figs. 4 and 5.

The experimental results lead one to the conclusion that the combined action of HFC together with the convective method of energy supply alters the kinetics of the drying process: in comparison with pure convection, the heating duration of the material decreases from 100 to 13 min (which is more than by a factor of 7) and the duration of the second period of drying decreases by a factor of 14.

Analysis of the dependence of the drying rate constants vs. the temperature demonstrates that the combined action of the electromagnetic field HFC exerts the greater effect upon the internal heat and mass exchange; at that, in the second period, the drying coefficient increases by a factor of 1.83 for $E = 8.75 \times 10^3$ V/m and by a factor of 2.4 for $E = 1.8 \times 10^4$ V/m. This gives evidence of the reciprocal effect of the temperature and the electromagnetic field strength. The curve for $E = 1.8 \times 10^4$ V/m (Fig. 4b) explicitly shows the sinergetic effect of their action.

The results obtained in the experiments on the drying process of kernels of apricot stones with a convective heat supply (Fig. 1) and with the combined action of a convective heat supply and heating with a high-frequency electric field (Figs. 2 and 3) demonstrate that the kernels are a complex organic product. In the course of the heat treatment, the mass loss occurs in the kernels not only due to the moisture removal (typical for the majority of materials) but also due to the biochemical modifications taking place at the high temperatures. Therefore, the applicability of the drying method for such kinds of products as kernels should be justified taking into account these features.

The experiments have shown that the high-frequency heating combined with a convective energy

supply is more promising for its application in the dewatering process of kernels of apricot stones if compared with pure convection. The most intensive regime occurs when the drying is performed by the combined action at a temperature of the drying agent of 100°C and with an electromagnetic field strength of $E = 1.8 \times 10^3$ V/m. The drying process is best performed in two steps. At the first stage, a convective energy supply should be used (100°C) down to the critical moisture content in the kernels of 110%. At the second stage, a combined energy supply (convection + HFC) with an electromagnetic field strength of $E = 1.8 \times 10^4$ V/m should be used to obtain an equilibrium moisture content of 30%.

REFERENCES

1. Lupu, O.F., Theoretical and Experimental Study of the Drying of Apricots Using High-Frequency Current, *Extended Abstract of Doct. Sci. (Eng.) Dissertation*, Chisinau, 2005.

2. Ginzburg, A.S. and Savina, I.M., *Massovlagoobmennye kharakteristiki pishchevykh produktov. Spravochnik* (Mass and Moisture Transfer Parameters on Foodstuffs. Handbook), Moscow: Legkaya i Pishchevaya Promyshlennost', 1982.

3. Lykov, A.V., *Teoriya sushki* (Theory of Drying), Moscow: Energiya, 1968.

ISSN 1068-3755, Surface Engineering and Applied Electrochemistry, 2007, Vol. 43, No. 2, pp. 136–139. © Allerton Press, Inc., 2007.
Original Russian Text © P.G. Dumitrash, M.K. Bologa, 2007, published in Elektronnaya Obrabotka Materialov, 2007, No. 2, pp. 71–74.

OPERATING EXPERIENCE

Dispergation and Homogenization of Disperse Systems in an Acoustic Field

P. G. Dumitrash and M. K. Bologa

Institute of Applied Physics, Academy of Sciences of Moldova, ul. Akademiei 5, Chisinau, MD-2028 Moldova

Received October 20, 2006

DOI: 10.3103/S1068375507020135

INTRODUCTION

It is conventional that cavitation is a means of attack on heat- and mass-exchange processes, as well as on the structure and contact interaction of solids. This action is associated with nonlinear cavitation effects arising when a powerful ultrasound propagates in a medium or when hydrodynamic currents flow behind a barrier or in narrow channels. In this case, high temperatures and pressures are achieved, as well as relatively high velocities of their variation, in comparison with those implemented in natural processes and used in technological procedures. Cavitation actions lead to physical and chemical transitions in working media that can decisively affect the development of technological processes, which is especially genuine and promising during the development of investigations concerning nanodisperse-material production.

Emulsions and suspensions being dispersion media with a variety of compositions and properties are widely used in the food, chemical, textile, metallurgy, metal working, and building industries and in reprocessing technologies, and their preparation is a very important link in many industries. In addition, the qualitative composition of the final product and the expenditures associated with its fabrication, in many respects, depend on the choice of the technological procedures for performing these processes. For more or less extended time, we investigate the phenomena and applied effects of cavitation with the purpose of intensifying the emulsification and dispersion on the basis of application of two-frequency cavitation actions. In particular, it is established that it provides for the fabrication of juice with pulp with the maximum saving of the palatability and nutritious qualities, while providing considerable simplification of the technology and equipment. With reference to the wine-making industry, it is possible to produce a suspension of bentonite with submicronic particles whose contacting area with the wine stock is 2–3 orders of magnitude higher, which allows considerable intensification of the process of adsorption of pectinaceous substances and their flocculation. Taking this into account, in this work, we present the results of investigations of the dispersion process in bentonite (Moldova deposits) with initial particles from 200–300 μm to submicronic sizes.

EXPERIMENTAL PROCEDURE AND ANALYSIS

Experiments were carried out on an ultrasonic cavitation installation operating under excessive static pressure. The processing method is chosen on the basis of an analysis of theoretical and experimental data indicating the fact that the maximum effect of increasing the efficiency of the ultrasonic dispersion is exerted by acoustical Pa and static $P0$ pressures with the ratio $Pa/P0 \approx 0.5$ [1]. In a sonic bath with a volume of about one liter, we poured bentonite in distilled water with a ratio of 1 : 20 between the solid and liquid phases; the ultrasonic system was tuned to the resonance frequency and the necessary vibration amplitude and the cavitation processing was carried out. The particle-displace-

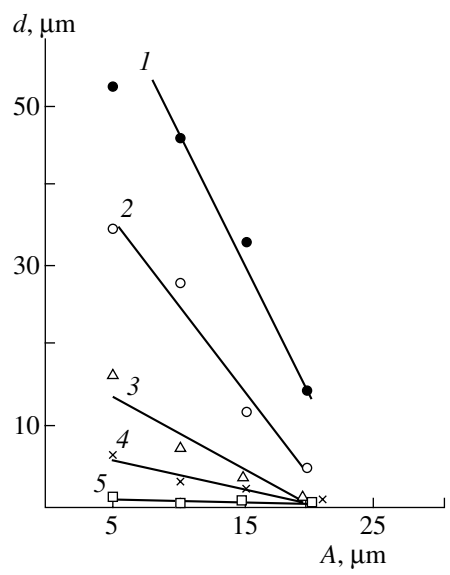

Fig. 1. Dependence of bentonite-particle sizes on the ultrasonic-vibration amplitude A, μm: (*1*) 4; (*2*) 8; (*3*) 12; (*4*) 16; (*5*) 20.

Table 1. Particle size d as a function of the vibration amplitude A and the time τ of the ultrasonic cavitation processing

Vibration amplitude A, μm	Duration τ of the cavitation processing, min					
	monitoring	4	8	12	16	20
	particles size d, μm					
5	100–200	52	35	17	7	3
10	″	46	18	7	2	0.5
15	″	31	11	4	1	0.4
20	″	14	4	1	0.5	0.4

ment amplitude was measured by an electrodynamic sensor, whose principle of operation is known [2]. The cavitation mode was detected using the signals received from a waveguide probe by an oscillograph; this fact was confirmed by the characteristic pattern of the cavitation-noise spectrum.

The process of the bentonite nanodispersion in distilled water under the action of ultrasonic cavitation was studied as a function of the sounding time and the vibration amplitude in the waveguide. We determined the particle sizes in the suspension and the degree of bentonite dispersion using electron microscopy.

RESULTS AND DISCUSSION

For the detection of the basic regularities describing the ultrasonic cavitation dispersion, the possibilities of control and simulation of the conditions of the process as applied to various solid materials, the kinetic features of the process, and their correlation with the properties of the bentonite suspension with nanometric particle sizes are of considerable interest.

The experimental conditions and the data characterizing the dependence of the bentonite-particle sizes on the time of the ultrasonic cavitation processing and vibration amplitude are listed in Table 1. The results indicate that the particle sizes decrease with increasing the vibration amplitude and the cavitation duration (Fig. 1).

With increasing the duration of the cavitation action, the angular coefficients $\Delta\alpha$ for the straight lines $d = f(A)$ increase and amount to the following: $\Delta\alpha = 2.5$, 2.1, 1.1, 0.4, and 0.2 for $\tau = 4$, 8, 12, 16, and 20 min.

The ultrasonic-action duration exerts the most important effect on the bentonite dispersion (Fig. 2).

The increase in the cavitation duration is accompanied by an intense decrease in the particle sizes; the tendency to reach a stationary value of the fine particle dispersion is observed when the processing lasts for more than 12 min. The degree of the effect of the processing time depends on the vibration amplitude, and, the larger the amplitude is, the more strongly it manifests itself.

The dispersibility was also investigated depending on the ultrasonic-vibration amplitude for various durations of the cavitation action (Table 2).

The results of the investigation of the effect of the ultrasonic-vibration amplitude and the processing duration on the degree of dispersion show (Fig. 3) that a

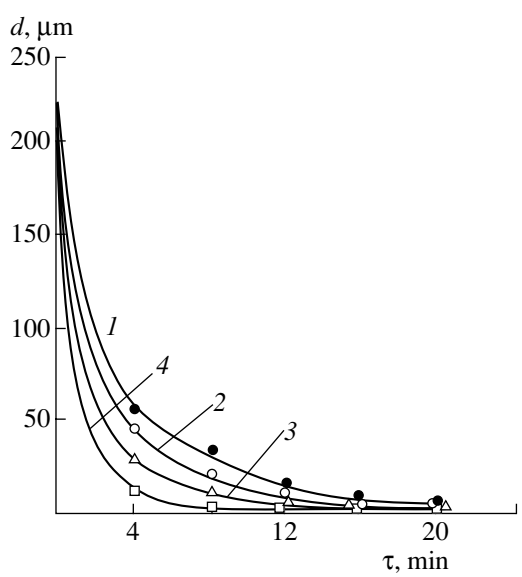

Fig. 2. Bentonite-particle sizes as functions of the duration τ of the ultrasonic-cavitation action, min: (*1*) 5; (*2*) 10; (*3*) 15; (*4*) 20.

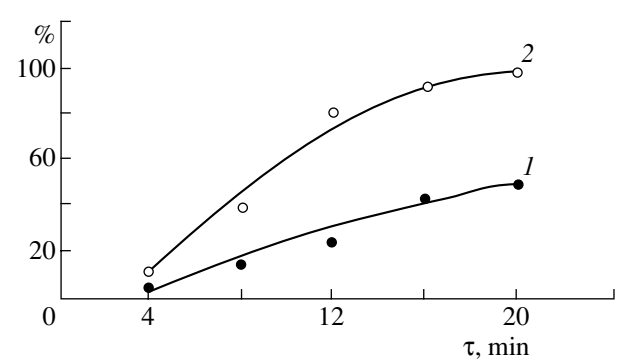

Fig. 3. Percentage of bentonite particles with sizes of 0.5–2 μm as a function of the duration τ of the ultrasonic cavitation processing, min: (*1*) 5; (*2*) 20.

Table 2. Percentage of bentonite particles with sizes of 0.5–2 μm prevailing in the suspension

Vibration amplitude A, μm	Cavitation-action duration τ, min				
	4	8	12	16	20
	Particle-size range, μm / Percentage of particles of 0.5–2 μm				
5	52–5 / 3	30–3 / 18	17–1 / 25	7–0.5 / 43	7–0.5 / 48
20	14–2 / 12	4–1 / 39	1–0.5 / 80	1–0.4 / 92	0.5–0.3 / 98

homogeneous suspension with bentonite-particle sizes of 0.5–2 μm is achieved for the vibration amplitudes above 20 μm and the action time exceeding 16 min.

The electron-microscopic analysis indicates that the suspension volume contains bentonite particles of different sizes. The average particle sizes (longitudinal and transverse) before the onset of the ultrasonic processing amount to 200–100 μm. The visual microscopic survey of the samples confirms the effect of the fine-grained homogenization of the suspension when processing by cavitation (Fig. 4).

From the analysis of the obtained results and the data [3–5], it is possible to conclude that the dispersion process influences all the major effects arising in powerful ultrasonic fields: the cavitation, the acoustical pressure, the acoustocapillary effect, and the acoustic flows. The cavitation effect is maximal. In the compression stage of the acoustic wave, the cavitation bubble and the gas in it are compressed to high pressures. In the rarefaction phase of the wave, there is an instantaneous expansion of the cavitation bubble (a microexplosion), which forms a shock wave with a powerful acoustical pressure.

On the bentonite-particle surface, where there are microcracks and surface irregularities, the cavitation-bubble "germs" are formed. Under the action of the acoustocapillary effect and the intense acoustic microflows, the fluid penetrates into pores and cracks and an acoustical shock wave arises as a result of the bubble collapse, thus, destroying bentonite particles.

The analysis of the results (Fig. 1–3) indicates that the ultrasonic dispersion proceeds in two phases. The first phase (processing time up to 5 min, Fig. 2) proceeds much faster than the second phase because of the presence of a large number of microdefects on the surface of the initial bentonite particles. Under these conditions, the friction and mutual collision of particles provides an increase in the grinding rate. Then, the second phase begins when the particles take on a spherical shape (Fig. 4c) and the grinding process decelerates (Fig. 2, processing time more than 5 min).

The bentonite dispersion proceeds intensely provided that the effort acting a particle during the cavity collapse (acoustical and static pressure) is higher than the actual strength of the crushed bentonite. When choosing the optimum processing duration (15–18 min), i.e., acoustical (2 W/cm^2) and static (~5 atm) pressures, high dispersibility can be achieved when using the cavitation method for virtually all the bentonite mass.

CONCLUSION

The ultrasonic-cavitation effect provides the dispersion of the bentonite to submicronic sizes. With increasing the cavitation-processing duration (more than 16 min) and vibration amplitudes (above 15–20 μm), the tendency of reaching a stationary value of the fine dispersibility of the particles is observed. A homogeneous

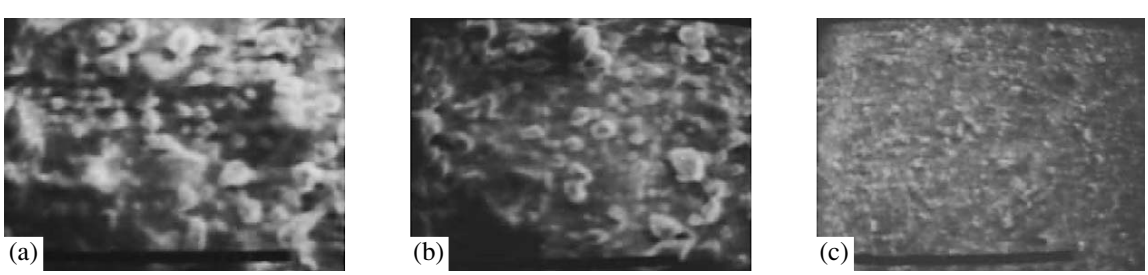

×500 ×5000 ×5000

Fig. 4. Electron-microscopic patterns of the bentonite-particle dispersion: (a) monitoring (200–100 μm); (b) A = 5 μm, τ = 4 min, d = 52 μm; (c) A = 20 μm, τ = 20 min, d = 0.4 μm.

suspension with particles 0.4–2.1 μm in size is achieved during the processing for more than 16 min for amplitudes above 20 μm, and provides an essential decrease in the initial bentonite mass.

REFERENCES

1. Agranat, B.A., Dubrovin, M.N., and Khavskii, N.N., *Osnovy fisiki i tekhniki ul'trazvuka* (Fundamentals of Physics and Technologies of Ultrasound), Moscow: Vysshaya Shkola, 1987.
2. Herbert, J., *Ultrasonic*, 1967, vol. 3, pp. 239–241.
3. Prokhorenko, P.P., Dezhkunov, N.V., and Konovalov, G.E., *Ul'trazvukovoi kavitatsionnyi effekt* (Ultrasonic Cavitation Effect), Minsk, 1981.
4. Dobatkin, V.I., Eskin, G.I., Abramov, O.V., et al. *Vozdeistvie ul'trazvuka na mezhfaznuyu poverkhnost' metallov i splavov* (Ultrasonic Action on Interface of Metals and Alloys), Moscow, 1986.
5. Vladimirskaya, M.A., Ermilov, A.C., and Agranat, B.A., Theoretical and Experimental Investigation of Dispersion Process in Materials with Stratified Structure in Ultrasonic Field, in *Problemy sozdaniya i ispytaniya vysokotemperaturnykh plastichnykh smazok* (Development and Testing of High-Temperature Plastic Lubricants), Moscow, 1970, pp. 33–36.

ISSN 1068-3755, Surface Engineering and Applied Electrochemistry, 2007, Vol. 43, No. 2, pp. 140–142. © Allerton Press, Inc., 2007.
Original Russian Text © B.E. Egamberdiev, B.Ch. Kholliev, A.S. Mallaev, 2007, published in Elektronnaya Obrabotka Materialov, 2007, No. 2, pp. 75–77.

OPERATING EXPERIENCE

Investigation of Profiles of the Distribution of Ion-Implanted Mn Atoms using the Rutherford Back Scattering Method and the Influence of Thermal Annealing on Them

B. E. Egamberdiev, B. Ch. Kholliev, and A. S. Mallaev

Tashkent State Technical University, ul. Universitetskaya 2, Tashkent, 700095 Uzbekistan

Received July 29, 2006

Abstract—This paper presents the results of the RBS method investigation of profiles of the distribution of Mn atoms implanted into Si depending on the irradiation dose and annealing temperature. The thermal annealing influence on the distribution of Mn and other impurities (in particular, oxygen) is studied. The possibility of applying the RBS method for analysis of both the distribution of doping impurities and their interaction is discussed.

DOI: 10.3103/S1068375507020147

Obtaining thin layers with set electrophysical properties and a certain thickness in the Si surface region is of great interest both from the viewpoint of technology and for the design of various highly sensitive sensors and devices.

In this aspect, the introduction of doping impurities of the transition group elements (in particular, manganese) is the most interesting. From the technological viewpoint, it is impossible to obtain thin layers with limited depth and sufficient concentration in silicon by the diffusion method due to the high value of the diffusion coefficient of these elements. Therefore, the ion-beam doping method is applied.

However, works on ion implantation and the investigation of profiles of the manganese depth distribution in silicon are practically absent in the literature.

Since Mn impurities in Si may be found both in sites and interstitial sites of the crystal lattice and may interact with the lattice defects, the Mn distribution at ion implantation and the Mn activation mechanism are of interest.

The aim of this research is to study profiles of the distribution of implanted manganese atoms in silicon depending on the irradiation dose and annealing temperature.

As is known, for studying profiles of the distribution of ion-implanted layers, the traditional methods of secondary ion mass- and Auger-spectroscopy with layer-by-layer removal are used. These methods do not give high accuracy of the quantitative characteristics, although accurate quantitative data on the concentration of doping impurities are necessary for obtaining thin layers with set electrophysical properties.

Therefore, in the present work, the profiles of the distribution of Mn doping impurities and the influence of the activation temperature on the distribution were investigated using the method of Rutherford back scattering (RBS).

Plates of KDB brand (Russian) single crystal silicon of at p= 10 Ohm cm were used. The Mn ions were implanted in silicon using a Russian ILU-3 installation at an ion energy of 40 keV along the crystallographic axis (111). The implantation dose N_0 was varied in the range of 10^{15}–10^{17} ion/cm^2. The sample resistivity was measured by the four-probe method.

Figure 1 shows profiles of the distribution of the manganese ions implanted in silicon with an energy of 40 keV at different implantation doses; irrespective of the implantation dose, the distribution is described by

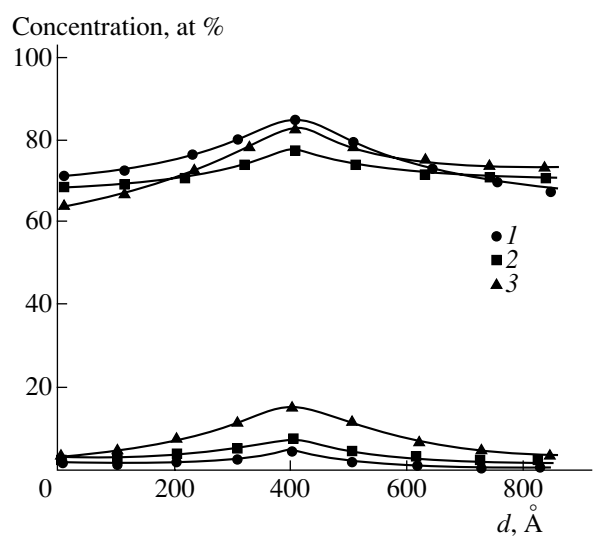

Fig. 1. Mn concentration depth distribution in Si at an irradiation dose of 10^{15}–10^{17} ion/cm^2. (*1*) at 1×10^{15} ion/cm^2, (*2*) at 1×10^{16} ion/cm^2, and (*3*) at 1×10^{17} ion/cm^2.

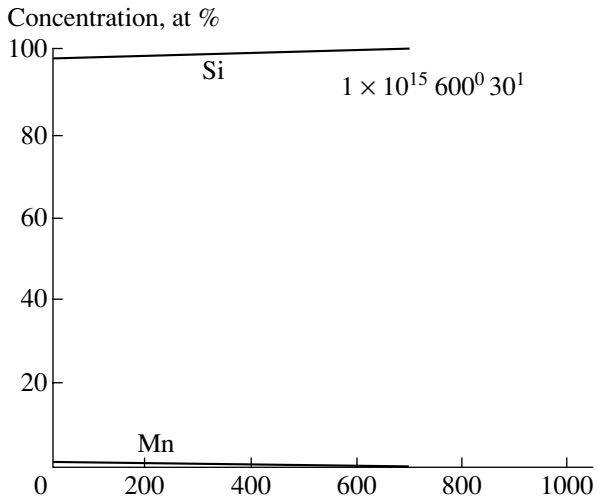

Fig. 2. Mn concentration depth distribution in Si at an irradiation dose of 10^{15} ion/cm^2 after annealing at a temperature of 600°C for 30 min.

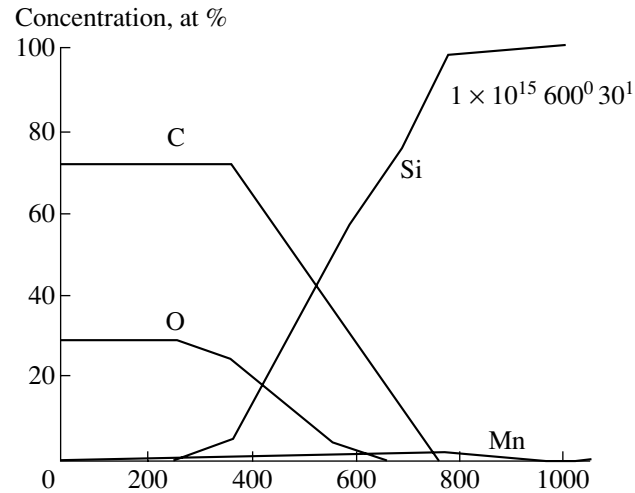

Fig. 3. Mn concentration depth distribution in Si at an irradiation dose of 10^{16} ion/cm^2 after annealing at a temperature of 900°C for 30 min.

the Gauss function. The depth of the projected path R_p depending on the irradiation dose is in the range of 398–410 Å. This coincides with the data of the investigation of these samples by other methods, e.g., SIMS [1].

Investigation of Si samples after Mn implantation at a dose of 10^{15} ion/cm^2 by the RBS method gave the following results on the sample surface: 83% Si, 15% O, and 2% Mn in atomic units. In the sensitivity range, manganese is observed up to a depth of ~600 Å and oxygen is observed up to ~900 Å. For the silicon plates after the Mn ion implantation at a dose of 10^{16} ion/cm^2, the percentage of silicon, oxygen, and manganese in atomic units on the surface is 76, 18, and 6%, respectively. A significant change of the percentage is observed at a depth of ~ –400 Å, where 82% Si, 3% O, and 15% Mn are found. Within the range of the method sensitivity, Mn is observed up to a depth of 650 Å. Beginning from this depth, a sharp change in the oxygen content is observed. At a depth of ~900 Å, oxygen is practically not found. At Mn implantation at a dose of 10^{17} ion/cm^2, the following picture is observed: 64% Si, 34% O, and 2%Mn on the surface; 82% Si, 3% O, and 15% Mn in atomic units at a depth of ~400 Å.

Analysis of the obtained data shows that, in the ion implantation process, both on the sample surface and at the depth of the Mn distribution maximum, the oxygen content is mainly changed. One may suppose that implanted Mn ions supplant oxygen everywhere. This guess will prove to be correct if the oxygen in the silicon crystal is in the free state [2, 3].

The influence of thermal annealing on the behavior of doping impurities (in particular, on the depth distribution) is of great scientific and practical interest. The results of the influence of a 30 min thermal annealing on the Mn depth distribution for Si samples are given below (Fig. 2).

As is seen, the temperature annealing at 600°C does not considerably influence the impurity depth distribution. Strong influence begins at a temperature of 900°C. For the samples doped with Mn at a dose of 10^{15} ion/cm^2, the distribution maximum shifts to a depth of ~800 Å and the Mn concentration to 2 at % (Fig. 3). On the surface, the Mn content is not found; the oxygen decreases down to 27 at %; and, at a depth of 800 Å, it is not registered.

For the samples doped at a dose of 10^{16} ion/cm^2, annealing for 30 min at a temperature of 600°C significantly influences the Mn distribution. The maximum break is observed. At an annealing temperature of 900°C, the distribution maximum shifts to a depth of 800 Å with the Mn maximum decreasing down to 5 at %. The impurity distribution for the samples doped with Mn at a dose of 10^{17} ion/cm^2 suffers considerable changes at thermal annealing. Temperature annealing at 600°C for 30 min leads to a shift of the distribution maximum to a depth of 380 Å and to a certain increasing of their content on the surface. Temperature annealing at 900°C for 30 min strongly influences the Mn distribution. The maximum shifts at a depth of 600 Å. The distribution shape becomes more gentle, and Mn is observed up to a depth of about 1200 Å in the range up to 5 at %.

The analysis of the data obtained allows us to state that application of the RBS method makes it possible to obtain data on both the impurity depth distribution and the quantitative characteristics.

In our opinion, the relation between the distribution of manganese and oxygen in silicon crystals is of interest. Comparison of these distributions shows that, at the Mn distribution maximum depth, the oxygen content is minimal, and, vice versa, in places of the maximum O

content, there is a minimum of the Mn concentration. For the nondoped initial Si samples, an oxygen distribution with an excess on the surface with its monotonous decreasing in the sample depth is observed; further, a uniform distribution takes place. After the ion implantation, this distribution undergoes a strong change. The concentration on the surface and in the near-surface regions increases, and, in the Mn distribution concentration maximum range, a sharp decrease of the oxygen concentration is observed. This change takes place for all the samples with different irradiation doses.

The ion implantation process influences the state of the oxygen and of the defects too. The defects formed both on the surface and at a depth of the Si open free radicals, which attract free particles (in particular, O).

On the basis of the obtained data, the following conclusions may be drawn:

—In all the investigated samples, the profiles of the doping impurity distribution had the Gauss form. The maximum depth of the distribution depended on the irradiation dose and ion energy. For example, at $N_0 = 10^{15}$ ion/cm^2 in the case of Mn, the Rp achieved 400 Å. A further increase of the concentration led to the Rp decreasing down to 290 Å.

—The experiments have shown that, by controlling the dose of implanted ions, one can form a sharp transition region near the surface of the silicon. Depending on the type and dose of the ions, this depth is in the range of 290–380 Å.

—The investigation of the influence of the annealing temperature on the profiles of the doping impurity distribution has shown that, in contrast to the elements of the third and fifth groups, after thermal annealing, the surface concentration of the elements of the transition groups does not increase; on the contrary, it decreases.

—Appreciable diffusion starts at temperatures above 600°C. The maxima shift to the sample depth occurs according to the diffusion laws.

—The investigation of the concentration ratios of the doping impurities and the silicon itself by the RBS method has given the following results: for manganese implanted at a dose of 10^{15} ion/cm^2 on the sample surface, 83% silicon, 15% oxygen, and 2% manganese in atomic units was found. Within the range of the method sensitivity, manganese is observed up to a depth of 600 Å. At an irradiation dose of 10^{16} ion/cm^2, the ratios of the elements on the surface are the following: 76% silicon, 18% oxygen, and 6% manganese in atomic units. At an irradiation dose of 10^{17} ion/cm^2, at a depth of 400 Å, the element ratios appeared to be the following: 82% Si, 3% O, and 15% Mn in atomic units. The percentage is significantly influenced by the annealing temperature. Thus, for the doped samples with an irradiation dose of 10^{16} ion/cm^2, the distribution maximum shifts at a depth of 800 Å with the content decreasing at the maximum down to 5%.

REFERENCES

1. Bakhodyrkhanov, M.K., Egamberdiev, B.E., Abdugabbarov, M.S., and Khaidarov, K., *Neorg. Mater.*, 1995, vol. 31, no. 3, pp. 301–303.
2. Bulle–Lienwma, C.W.T., Van Ommen, A.H., and Uzendorn, L.J. van., *Appl. Phys. Lett.*, 1989, vol. 54, p. 244.
3. Namavar, F., Kalkhoran, N.M., Manke, J.M., Luo, L., and McGinn, J.T., *Proc. MRS*, 1992, vol. 235, p. 285.

ISSN 1068-3755, Surface Engineering and Applied Electrochemistry, 2007, Vol. 43, No. 2, pp. 143–147. © Allerton Press, Inc., 2007.
Original Russian Text © K.Z. Nuriev, 2007, published in Elektronnaya Obrabotka Materialov, 2007, No. 2, pp. 78–83.

OPERATING EXPERIENCE

Angular and Energy Distribution of Ions Emitted from a Solid Surface under Laser Mass-Spectrometric Analysis

K. Z. Nuriev

Azerbaijani National Aerospace Agency, pr. Azadlyg 159, Baku, Republic of Azerbaijan

Received August 29, 2006

Abstract—The distribution of ions of tungsten and aluminum by angular and initial energy parameters at laser plasma spreading into a vacuum is studied in the present paper. It is shown that the angular distribution is isotropic at a density of the laser emission flux of 10^8 W/cm^2; an increase of the latter leads to the maxima appearance. The energy distribution at the determined angles exhibits a difference in the experimental and theoretical results caused by the additional acceleration of ions by two mechanisms.

DOI: 10.3103/S1068375507020159

INTRODUCTION

At present, a great number of mass-spectrometric devices with laser ionization of substances are being designed. In these devices, lasers in the switched Q mode allow obtaining pulses with a duration of 10^9 to 10^{-7} s and an emission flux intensity of 10^8–10^{12} W/cm^2. The influence of such a powerful emission results in the formation of plasma, which serves as a source of ions for mass-spectrometric analysis [1, 2].

Laser mass spectrometry made it possible to obtain basic results concerning the properties of the laser plasma, to characterize it as an emitter of ions, and to formulate the requirements for various types of laser sources of ions [3, 4]. All this allowed construction of devices characterized by high sensitivity, reliability, and reproducibility when analyzing solids by this method.

However, the good reproducibility and correctness of the results obtained by this method do not allow its application for analysis of a solid substance of complex composition without knowledge of the processes of formation, heating, and spread of dense high temperature laser plasma. First of all, this affects the treatment of experiment data under standard and free analysis to obtain accurate quantitative results. It is true that, in some works [5, 6], it is shown that, in essence, it is possible to carry out this analysis by assuming that the relative sensitivity coefficient (RSC) is equal to one [7, 8]; however, this is not confirmed by analytic practice [9, 10].

Therefore, it seems to us, for quantitative laser mass-spectrometric analysis, studying the basic physical processes taking place during the formation and spread of laser plasma in a vacuum may be of interest, because these processes determine the properties and composition of ion beams obtained at late stages of its spread. Solution of the urgent problem concerning the character of the quantitative relation of the ion parameters (energy, charge composition, direction, etc.) and the sample element composition will help to determine the RSC value for various elements of the probe under analysis.

On the other hand, since ions of laser plasma spread in vacuum at different angles and with different energies, information on their energy and angular distributions would favor the choice of better orientation of the sample surface normal with respect to the ion–optic system of the analyzer and registering system.

The present paper is dedicated to experimental investigation of the angular and energy distribution of ions at the laser plasma spread from a solid surface.

EXPERIMENT METHODS

The investigations were carried out by virtue of the installation shown in Fig. 1 using a time-of-flight mass spectrometer with an axially symmetric electrostatic field. The analyzer resolution was no less than 400 [11]. Plasma was obtained by the emission of an Nd laser working in the switched Q mode, which was placed outside the ion source chamber. The laser emission entered the ionization chamber through a glass window in the ion source chamber.

The duration (80 ns) and the energy of the pulse (E = 2 J) were maintained constant during the whole experiment. The angle of the emission incidence was adjusted from 45 to 10 angular degrees with respect to the sample surface normal. The samples were plates of tungsten and aluminum in the form of a disk with a diameter of 10 mm and a thickness of 1 mm fixed on a holder in special recess 4 of plunger 2; its edge was removed from the ion source through a high-vacuum quick-acting lock [12] and had the possibility to rotate about its z axis. The normal could rotate about the z axis on the xy plane. The laser was placed on a special apparatus,

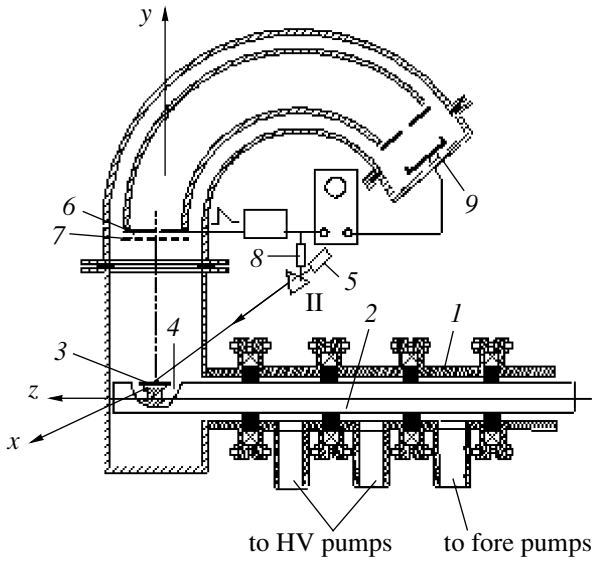

Fig. 1. Experimental installation. (*1*) the high vacuum lock, (*2*) the plunger, (*3*) the sample, (*4*) the recess, (*5*) the laser, (*6*) the diaphragm, (*7*) the net, (*8*) the PET, and (*9*) the ion detector.

which could rotate about the x axis on the yz plane by 10–45°.

Thus, irrespective of the angle of the laser emission incidence, which may be set in any position (10–45°), ions spreading at an angle from –90° to +90°o with respect to the target normal, depending on position of plunger 2, can enter the analyzer entrance slit.

For investigation of the ion energy distribution at a chosen angle of spread from the sample surface, a slit grid with 85% transparency was placed in front of the diaphragm entrance. Between the grid and the diaphragm, a pulse is applied ($\tau = 10^{-6}$ s) hindering the potential in a saw-toothed form changing from zero to 500 V. Synchronization of the triggering of the high-frequency generator (HFG) and the oscillograph scan was performed by virtue of the laser emission divider and an FEK[Russian]-9 photoelectron transducer with a repetition frequency of 10–25 Hz.

The energy distribution of the ions of the spreading plasma was studied using the formula

$$f(E) = \frac{1}{(Ze^2)S}\left[\frac{di}{dV_3}\right], \quad (1)$$

where Z is the charge order, e is the electron charge, S is the diaphragm slit area, and V_3 is the potential of the hindering field by graphic differentiation of the curve $i(V_3)$.

RESULTS AND DISCUSSION

Under the influence of a laser emission with a relatively high flux intensity on the target, the light quanta are absorbed by electrons of the target material. As a result of their interaction with other electrons and phonons of the lattice, the target material heats up. The emission may influence the substance by various mechanisms depending on the intensity of the incident emission flux [13, 14]. For analytic practice, it is important to find how the composition of the ion beam formed at the laser selection of the substance reflects the probe composition.

As shown in [14], at low intensities of the flux ($q \sim 10^6$–10^7 W/cm^2), the amount of the evaporated substance depends on the solid heat conductivity stronger than on the evaporation heat. In this case, the basic characteristics of the destruction may be determined from solution of the heat conductivity problem for the object under emission. The investigations show that, as the intensity of the incident laser emission grows, the heat emission becomes so rapid that it cannot be withdrawn due to the heat conductivity in time.

Figure 2 shows the energy distribution of ions W^+ at different values of the laser emission density q. As is seen from the figure, the W^+ energy spectra have one maximum each and their position practically does not depend on the emission flux density. At the same time, a tendency of the appearance of additional maxima with q increasing is observed. This particularity of the character of the energy distributions obtained at higher flux density confirms the mentioned tendency. The behavior of the dependence of the maximal energy of the registered ions on the emission flux density corresponded to $E_{max} \sim q^{1/2}$. Estimation of the ion temperature in the plasma formed has shown that $T \sim 10^4$ K (8.6 eV) at a flux density of 10^8 W/cm^2. This corresponds to their energy at a plasma spread of 60–80 eV. Respectively, $T = 6 \times 10^4$ K (12 eV) with $E_{max} \approx 100$–150 eV at $q = 4 \times 10^9$ W/cm^2, and $T = 10^5$ K (~15 eV) with $E_{max} \approx 150$–200 eV at $q \approx 10^{10}$ W/cm^2, and so on.

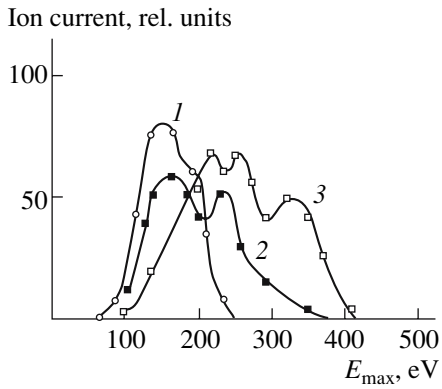

Fig. 2. The energy distribution of laser plasma ions. q, W/cm^2: (*1*) at 10^7; (*2*) at 10^8; (*3*) at 10^9.

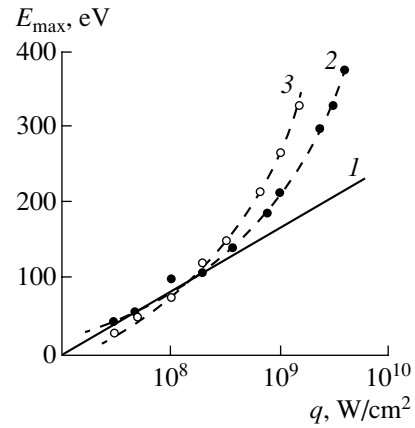

Fig. 3. Dependence of the maximal ion energy on the emission flux. (*1*) is the calculation curve; (*2*) is the experimental curve for the angle 0°; (*3*) is the curve for the angle 30°.

As one can see, these values of the energy somewhat differ from the measured ones.

The difference observed between the experimental and calculation results may apparently be explained by the fact that laser plasma ions may be additionally accelerated by the electrostatic field appearing at the plasmoid boundary. The field appearance is due to the following. The electrons possessing significantly higher velocities of heat movement tend to leave the plasma, and an electrostatic field favoring the acceleration of ions is obtained. The neutrality violation occurs on the plasmoid periphery, where the plasma density is lower and the forming layer thickness is equal in order to the Debye radius r_0 of the screening. The ions moving in the field are accelerated up to velocities considerably exceeding the thermal one. The calculations show that, for carbon plasma at $q = 10^{10}$ W/cm^2 and $r_0 =$ 60 μm, the field intensity in this electric field on the plasma boundary at a distance of 5 mm from the target is above 2000 V/cm [13].

According to the electrostatic acceleration mechanism, the maximal kinetic energy of the ions E_{max} must depend on the ion charge and must not change with the ion mass M. However, the results [16] show that, for the elements with atomic mass <20 amu, an increase of E_{max} with the increasing of the emission flux intensity is observed. In [1], this discrepancy of the maximal energy of the ions at the late stages of the plasma spread is explained by the gas-dynamic spread of the plasmoid in vacuum under the pressure gradient influence.

Let us note that the laser plasma spread in vacuum occurs in the time τ_p, which is less than the laser pulse duration; that is, at the time when the plasma is still absorbing the laser emission. Indeed, since the velocity of the plasma spreading near the target surface is $\upsilon =$ 10^5 m/s and the plasma radius initial moment is $r_0 \approx$ 10^{-1} mm (the laser emission radius), the characteristic time of the spreading is $\tau_p = r_0/\upsilon = 10^{-9}$ s, while $\tau_n \approx 2$–5×10^{-8} s; i.e., $\tau_p \ll \tau_n$.

The dependence of E_{max} on the laser emission flux density is shown in Fig. 3. As is seen from the figure, the experimental and calculation curves slightly differ. This means that, at the plasma spread, the ions are additionally accelerated; this acceleration may take place, probably, due to both the gas-dynamic pressure and electrostatic field on the plasmoid boundary. For example, in [15], the maximal ion energy with account for the electrostatic acceleration is given by the expression

$$E_{max} \sim T_e Z^2 [A(\xi_i) ln\delta]^2, \quad (2)$$

where T_c is the electron temperature, $A(\xi)$ is the factor taking into account the plasma charge composition, and δ is the plasma dimension in Debye radii.

As for the acceleration due to the pressure gradient, the authors suppose that, as a result, the Cd^+, TE^+, and Al^+ ions acquire the energy $E_0 = 40 \pm 5$ eV; for the O^+ and C^+ ions, it is 60 ± 3 eV.

The space distribution of the ions of the plasma at the late stages of its spread is a very important characteristic of the ion component of the laser plasma.

For determination of the angular distributions of the ions, a chamber of their source was used. In it, at a change of the target plane normal angle (tungsten or aluminum) with respect to the ion–optic axis of the mass analyzer, the laser emission incidence angle is not changed. In order to avoid the influence of craters on the angular ion distributions, the sample was shifted along the z axis in the proper plane by virtue of the vacuum lock plunger (Fig. 1).

The angular distributions of the W^+ and Al^+ ions were studied at different ion energies at $q = 10^7$ W/cm^2 (Fig. 4a). The angular distributions of the ions with an energy of $E \leq 300$ eV at different flux densities were stu died as well (Fig. 4b).

As is seen from Fig. 4a, the angular distributions of the ions with energy from 100 to 300 eV are isotropic within the range of the angles where ions are registered

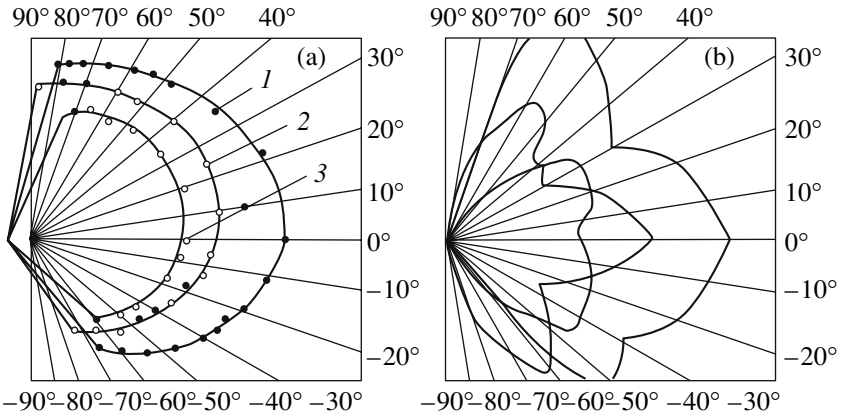

Fig. 4. Angular distribution of the ions W^+ (a) at different energies of the ions, eV: (*1*) at ≤300, (*2*) at ≤200, (*3*) at ≤100; (b) at different densities of the emission flux, W/cm^2: (*1*) at 10^9, (*2*) at 10^8, (*3*) at 10^7.

at all the values of the laser emission flux density. At a flux density of 10^9 W/cm^2, the ions with energy higher than 250–300 eV (Fig. 4b) have an anisotropic angular distribution; for the ions with an energy above 300 eV, characteristic ejections in directions differing from the normal are observed. The angular distribution of the ions with the maximal energy has the form of a petal elongated along the normal. As the energy increases, the solid angle where the spread occurs decreases.

Investigation of the material ejection under the laser emission influence shows that it takes place chiefly in the direction perpendicular to the target irrespective of the laser beam direction. The angular distribution of the ejected material is approximately described by the dependence cosθ, where θ is the angle calculated from the irradiated surface normal [16]. At measurement of the angular distribution of ions from the tungsten target, under irradiation of a ruby laser working in the switched Q mode, a distribution law close to $\cos^2\theta$ was obtained [13].

Let us note that, in many experiments carried out for different values of the emission flux density, the charge value, and the energy of the ions (at a constant angle of emission incidence on the target), symmetry of the angular ion distribution with respect to the sample plane normal is observed.

On the energy distributions obtained at an angle of 0°, 30°, and 60° to the normal, the presence of several maxima is found. The maximal energy decreases with increasing of the registration angle.

It is possible to interpret the observed angular distributions of the ion energy using models of the ion acceleration in the electric field appearing on the boundary of the spreading plasma and recombination. In addition, it is necessary to take into account that the ion spread occurs in a certain solid angle decreasing with increasing energy. This means that recombination of the ions with of energy E_{max} makes a contribution to the angular distributions of the ions with less energy than the ions with higher energy.

On the other hand, the role of recombination is also shown by the following. At almost any angle, slow ions are not registered and the energy spectrum starts from a certain minimal value $E_{min}(z)$. Recombination of the accelerated ions leads to the appearance of several minima in the energy spectra.

We also investigated the angular and energy distributions of ions with different charges. The experiments have shown that the ion spread occurs in the solid angle decreasing with increasing of the charge value. The results are preliminary; therefore, they are not given in the present paper. Let us note here that, in our opinion, the anisotropy observed in Fig. 4b is also caused by the spreading of ions of higher charge value in the direction of the target normal.

CONCLUSIONS

The experiments have given the following results. The angular distributions of the ions with energy from 100 to 400 eV are isotropic within the ranges registered irrespective of the laser emission intensity. At flux densities of 10^8–10^9 W/cm^2, in the angular distribution anisotropy, two minima determined by the ion recombination at the spreading are observed. At all the flux densities and angles of the laser emission, the distribution symmetry with respect to the surface normal is observed.

The energy distribution obtained at different angles E_{max} decreases with increasing of the angle. The character of the energy distribution of the laser plasma ions is explained by the processes of ion acceleration in both the matched field and gas-dynamic broadening.

REFERENCES

1. Bykovskii, Yu.A. and Nevolin, V.N., *Lazernaya mass–spektrometriya* (Laser Mass–Spectrometry), Moscow: Energoatomizdat, 1994.

2. Belousov, V.I., *Zh. Analit. Khimii*, 1984, vol. 39, no. 5, pp. 909–927.
3. Ramendik, G.I., *Zh. Analit. Khimii*, 1991, vol. 46, issue 9, pp. 1681–1685.
4. Oksenoid, K.G., Ramendik, G.I., Sil'nov, S.M., et al., *Zh. Analit. Khimii*, 1996, vol. 51, issue 6, pp. 1197–1204.
5. Bykovskii, Yu.A., Basov, T.D., and Belousov, V.I., *Zh. Analit. Khimii*, 1995, vol. 50, no. 11, p. 2090.
6. Boriskin, A.I., Bryukhanov, A.S., Bykovskii, Yu.A., et al., On Possibility of Standard–Free Analysis of Solids by Laser Mass–Spectrometric Method, *Pribory Sistemy Upravleniya*, 1983, no. 1, p. 26.
7. Nuriev, K.Z., *Elektronnaya Obrabotka Materialov*, 2006, no. 1, pp. 80–83.
8. Fainberg, V.S. and Ramendik, G.I., *Zh. Analit. Khimii*, 1991, vol. 46, issue 2, p. 241.
9. Libikh, F., Ramendik, G.I., Blokhin, A.G., et al., *Zh. Analit. Khimii*, 1987, no. 10, p. 1783.
10. Ramendik, G.I., Kryuchkova, O.I., and Kaviladze, M.Sh., *Zh. Analit. Khimii*, 1983, vol. 38, no. 10, p. 1749.
11. Nurubeili, Z.K., Nuriev, K.Z., and Nurubeili, T.K., *Problemy Energetiki*, 2005, no. 2, pp. 60–65.
12. Nuriev, Z.K., *Izv. NAN Azerbaijana, Ser. Fiz.–Mat. i Tekh. Nauk*, 2004, vol. 24, no. 5, pp. 138–144.
13. Mendel, C.W. and Olsen, J.N., *Rev. Lett.*, 1985, vol. 44, pp. 859–866.
14. Anisimov, S.I., Imans, Ya.A., Khod'ko, Yu.V., et al., *Deistvie izlucheniya bol'shoi moshchnosti na metally* (Influence of High Intensity Emission on Metal), Moscow: Nauka, 1990.
15. Bykovskii, Yu.A. et al., *Zh. Tekh. Fiz.*, 1973, vol. 434, pp. 2540–2547.
16. Gilmour, A.S. and Giozi, F.A., The Use of the Quadropolo Mass–Spectrometer for Laser Surface Studies, *23th Annual Conference on Mass–Spectrometry and Allied Topics*, S. Louis (MO), 1985, pp. 153–161.

ISSN 1068-3755, Surface Engineering and Applied Electrochemistry, 2007, Vol. 43, No. 2, pp. 148–151. © Allerton Press, Inc., 2007.
Original Russian Text © E.M. Godzhaev, A.M. Magerramov, S.S. Osmanova, M.A. Nuriev, E.A. Allakhyarov, 2007, published in Elektronnaya Obrabotka Materialov, 2007, No. 2, pp. 84–88.

OPERATING EXPERIENCE

Charge State of Composites Based on Polyethylene with Semiconductor Filler $TlInSe_2$

E. M. Godzhaev, A. M. Magerramov[1], S. S. Osmanova, M. A. Nuriev[1], and E. A. Allakhyarov

Azerbaijani Technical University, pr. G. Dzhavida 25, AZ1000, Baku, Republic of Azerbaijan

[1] Institute of Radiation Problems, ul. F. Agaeva 9, AZ1143, Baku, Republic of Azerbaijan

Received October 2, 2006

Abstract—In the present work, the spectra of currents of thermostimulated depolarization for composite corona electret LDPE + φ vol % $TlInSe_2$ are obtained by the thermoactivation spectroscopy method [11] and their electret properties and change conditions are investigated.

DOI: 10.3103/S1068375507020160

INTRODUCTION

Obtaining of polymer composites with specific electrophysical, electret, sensor, tensor sensitive, etc., properties significantly depends on the nature of the filler and on the form, dimension, and character of the particle distribution, as well as on the degree of interaction between the components. The character of the aggregation of the filler particles, the crystallization conditions, and a number of other factors change the polymeric matrix morphology; as a result, the composite materials obtained on their basis acquire unique properties. This leads to widening of the possibilities of their practical application. Electroactive (electret; piezo–, pyro–, and ferroelectric; photovoltaic; etc.) polymer composite materials of the following types are of special interest [1–3]: polymer–metalliferous, polymer–metallooxidic, polymer–polymer, polymer–ferroceramic, polymer–nanoparticles, polymer–fullerenes C60 and C70, and polymer–semiconductor fillers.

Depending on the polymer matrix nature and filler type, various methods for obtaining the electroactive state are applied. For investigation of the charge stabilization particularities, various dielectric and electrophysical methods are used.

Numerous experimental data convincingly show that the electroactive properties of the heterogeneous polymer–filler system are mainly determined by the phase charge state and by the particularities of the structure and interphase interaction and the polarization distribution in the composite [5, 6]. Control of the charge accumulation and relaxation processes in polymer composites under corona discharge in air is of great practical and scientific interest for finding the relation between the polarization parameters and the particularities of the structure and interphase interaction.

Polyethylene (PE) of high density was taken as a binder because it is well studied and because, in the oriented state, PE exhibits stability of the electret effect with the effective surface charge density equal to 10^{-5} to 10^{-4} C/m^2. $TlInSe_2$ was chosen as a filler for two reasons: on the one hand, for studying its interactions with polymers as a nucleating agent and, on the other hand, for the possibility to create flexible electroactive elements of arbitrary configuration. It should be noted that $TlInSe_2$ is characterized by high photo and tensor sensitivity, switching properties with memory, etc. [7–10]. In addition, the following are insufficiently explored in these systems: the contact phenomena, the change of the electrophysical and electroactive properties of the heterogeneous polymer–semiconductor systems, the particularities of the interphase phenomena, the presence of percolation effects, and the formation of space charges at polarization processes.

EXPERIMENTAL

The components of the powders of the PE and $TlInSe_2$ semiconductor are mechanically intermixed to obtain a homogeneous mixture. Then, films with a thickness of 100–150 μm are prepared from it using the hot pressing method. The sample polarization in the needle–plane system was performed by a corona discharge action at a voltage of 6 kV for 5 min. The distance between the polarizing electrodes (needle–plane) was U_k ~10 mm. The electret potential difference was measured using the noncontact compensation method [4]. The surface charge density σ was determined by the formula

$$\sigma = \frac{\varepsilon\varepsilon_0 U_k}{d},$$

where ε_0 is the dielectric constant, ε is the dielectric permeability of the composite, and d is the film thickness.

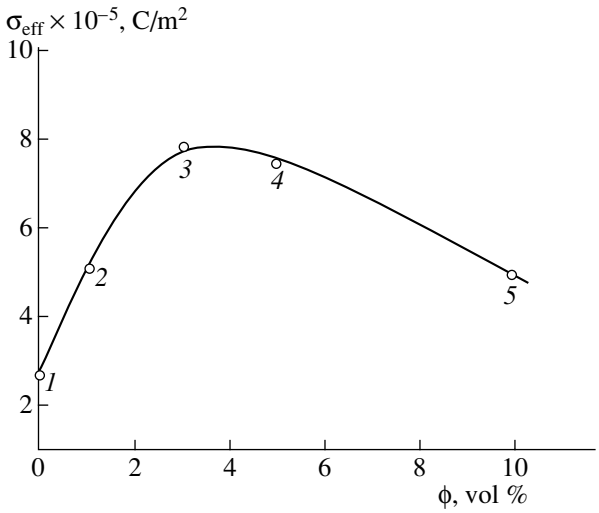

Fig. 1. Dependence of the surface charge density of the corona electrets of polymer composite LDPE + *x* vol % $TlInSe_2$ (where *x* is equal to (*1*) 0, (*2*) 1, (*3*) 3, (*4*) 5, and (*5*) 10) on the filler volume content.

The spectra of the currents of the thermostimulated depolarization (TSD) were measured using a standard method [5, 11]. The composite samples were placed between two electrodes short circuited through a U[Russian]5–11 electrometric amplifier into a heated measuring cell [5]. A TSD in a temperature range of 293–543 K was recorded at the linear growth of the sample temperature with a velocity of ≈2.5 K/min.

RESULTS AND DISCUSSION

Figure 1 shows the dependence of the surface charge density σ on the content of the filler ϕ for the composites PE + $TlInSe_2$. As one can see, the dependence has an extreme character. When the content of the filler φ increases up to 3–5 vol %, the σ value grows, and a further increase of the former leads to a decrease of the latter.

Such a dependence was observed in a number of works on studying the influence of various fillers on the electret properties of composites based on PE [6, 7]; it is a common regularity for polymer composites [1, 6]. The character of the electret state formation in these composites is determined, in the opinion of some authors [1, 5, 6], by polarization phenomena and by the electrophysical processes taking place at the interface of the polymer matrix and the filler. When the filler quantity grows, the effective surface of the interface increases, new centers for charge stabilization are formed, and the interlayer polarization increases leading to an increase of the surface density of the electret charges. At certain values of the filler content, its particles form agglomerates and the integral surface of the interface decreases, being accompanied by a decrease of the surface charge density value.

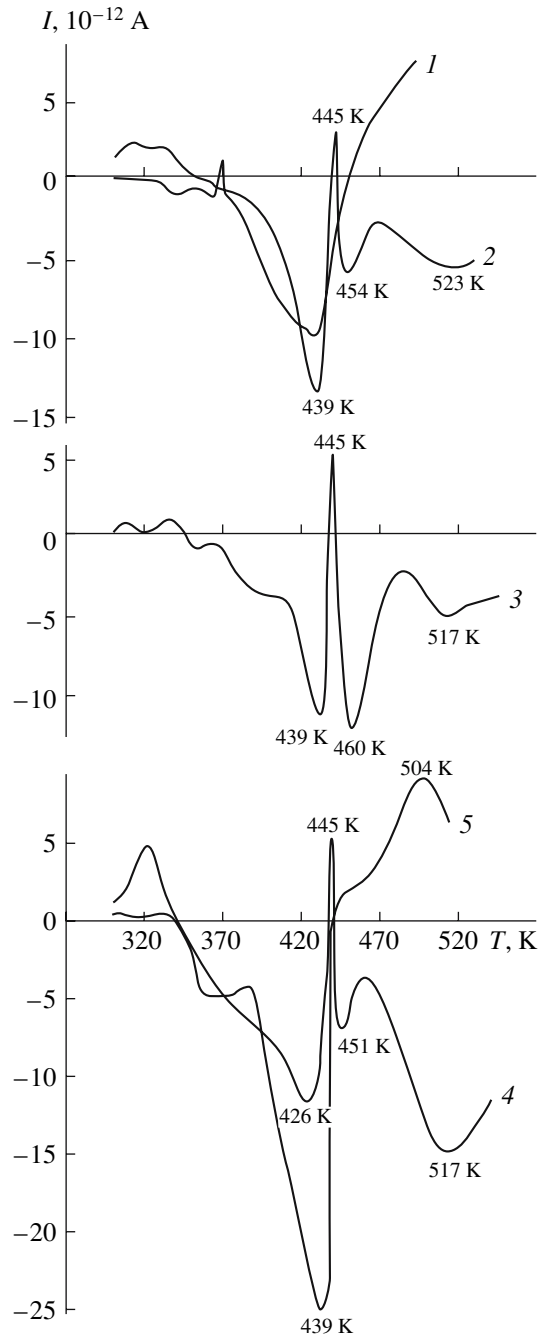

Fig. 2. Spectra of thermostimulated depolarization of the composites LDPE + *x* vol % $TlInSe_2$ (where *x* is equal to (*1*) 0, (*2*) 1, (*3*) 3, (*4*) 5, and (*5*) 10).

Figure 2 shows the TSD spectra for PE (curve *1*) and for the samples of PE + $TlInSe_2$ with different contents of the filler (curves *2*, *3*, *4*, and *5*). These spectra are characterized by the observation of an obvious narrow peak inversion on the TSD curves of the composite samples with filler contents of 1, 3, and 5 vol % at a temperature of 445 K. In addition, a high temperature broad peak within the temperature range of 500–520 K is observed. These compounds have three identical

maxima. The temperature position of the first maximum corresponds to 432–439 K, the second to 450–460 K, and the third to 517–523 K. The composite samples containing 10 vol % $TlInSe_2$ have two maxima with opposite signs of the accumulated charge (homocharge and heterocharge). The first maximum at 426 K corresponds in temperature to the first maximum of the other composites and initial polymer, and the second maximum is close in temperature to the third maximum of the composites.

Analyzing the TSD spectra, one can note that introduction of 1–5 vol % of the filler into the polymer leads to the appearance of deeper centers of the carrier capture. The number of traps of injected charges at the corona (increase of the intensity and area of the corresponding maximum) and the depth of their occurrence (the temperature position shifts to the high temperature range) increase.

The nature of the inversion peak appearance at 445 K against the background of the large base peak within the range of 432–455 K can be explained as follows. At electretization, in the process of the corona discharge action, a space charge is formed, and, in the field of the space charges (SC), at the interface of particles of the $TlInSe_2$ and the polymer, the interphase polarization (IP) appears [12]. The direction of this polarization is opposite to the space charge field. In this case, at depolarization in the TSD spectra, the inversion currents determined by the IP are observed. Our explanation of the inversion peak formation agrees, in a sense, with the Maxwell–Wagner effect, according to which the charge accumulation on inhomogeneous materials (composites in our case) is due to the conduction difference in the amorphous and crystal phases. At electrification of such a material, carriers will either agglomerate near the given interface or, vice versa, will leave it, depending on which of the two conduction currents is greater. The difference in the local conduction currents also leads to the charge dissipation at measurement of the TSD currents, because, in this case, the currents flow in the opposite direction. It should be noted that the given maximum is, to a higher degree, due to the charge relaxation on the $TlInSe_2$ particle surfaces, because, with increasing of the filler content in the composites, the peak value increases.

The effects of sign inversion in the TSD current were also observed for other electroactive dielectrics, electrets, and polymer composites [13]. However, interpretation of these phenomena is still controversial. Depending on the temperature position of the inversion peak, the surface state, the nature of the polymer matrix and filler, the polarization character, and other factors, the observed currents with the opposite sign on the TSD curves are also related to reorientation of dipoles existing in the polymer.

In our opinion, the maxima at the temperatures of 432–439 K and 450–460 K are of the same character; that is, they are a part of one and the same maximum connected with the α relaxation in the PE. The observed inversion in a narrow temperature range is, to our thinking, a result of the $TlInSe_2$ conduction decrease at repolarization of the space charges in the IP in the SC field. Let us assume that the temperature position of the α-relaxation process may be influenced by the volume content of $TlInSe_2$ in the composite.

The third high temperature maximum at 517–523 K is probably due to the increasing of the filler intrinsic conductivity, because the peak value grows with increasing of the filler content in the composite.

For the quantitative estimation of the interphase layer thickness in heterogeneous polymer composites, in a number of cases, the notion of a double layer formation is used (this viewpoint is widely maintained in impurity semiconductors, where the conduction difference leads to the double layer formation).

In polymer mixtures and composites, the interphase layer thickness may be estimated by the formula

$$d_i^2 = \frac{2\varepsilon_1\varepsilon_2\varepsilon_0 kT}{ne^2},$$

where ε_1 and ε_2 are the dielectric permeabilities of each phase, ε_0 is the dielectric constant, n is the charge carrier concentration (for polymer dielectrics, $n = 10^{21}$ m^{-3}), e is the electron charge, k is the Botzmann constant, and T is the absolute temperature. Calculations of the d_i values by the given formula show that it is about 0.4–1.2 μm.

CONCLUSIONS

Thus, the results of the investigation of the particularities of currents of TSD of electret films based on samples of LDPE + $TlInSe_2$ composites crystallized under hardening conditions at 273 K show that, on the TSD curves, rows of depolarization peaks are observed in the temperature ranges relating to the charge release out of traps bound by both separate components (PE and $TlInSe_2$) and the appearance of interphase polarization in the space charge field. At a temperature of 445 K, on the TSD curves of the composite samples, an inversion peak with a half-width of 3–5 K is found. In the TSD spectra in electret composites with $TlInSe_2$ at temperatures of 515–520 K, a depolarization peak determined by a new center (of traps) of the electret charge stabilization is observed.

$TlInSe_2$ fillers of p conductivity and dispersion of 50–63 μm in composites with polyethylene play the role of a structure former in the crystallinity degree increase and in the change of the supermolecular structure of the polymer.

REFERENCES

1. Galikhanov, M.F., Eremeev, D.A., and Deberdeev, R.Y., *Russian J. Appl. Chem.*, 2003, vol. 76, no. 10, pp. 1651–1654.

2. Trakhtenberg, L.I., Gerasimov, G.N., Potapov, V.K., et al., *Vest. Moskov. Univ.*, 2001, vol. 42, no. 5, pp. 325–331.

3. Sessler, G.M. and Gros, B. *Braz. J. Physics*, 1999, vol. 29, no. 2, pp. 220–225.

4. *Elektrety* (Electrets), Sesler, G., Ed., Moscow: Mir, 1983.

5. Lushcheikin, G.A., *Polimernye elektrety* (Polymer Electrets), Moscow: Khimiya, 1984.

6. Magerramov, A.M., *Strukturnoe i radiatsionnoe modifitsirovanie elektretnykh, p'ezoelektricheskikh svoistv polimernykh kompozitov* (Structural and Radiation Modification of Electret, Piezoelectric Properties of Polymer Composites), Baku: Elm, 2001.

7. Guseinov, G.D. and Abdullaev, G.B., *DAN SSSR, Ser. Fizika*, 1973, vol. 208, no. 5, pp. 1052–1054.

8. Godzhaev, E.M. and Gyul'mamedov, K.D., *Izv. RAN "Neorganicheskie materialy,"* 2002, vol. 38, no. 12, pp. 416–421.

9. Godzhaev, E.M., Khalilov, Kh.S., Khalilova, Kh.S., Guseinov, M.A., and Suleimanova, A.M., *Inzh.–Fiz. Zh.*, 2003, vol. 76, no. 2, pp. 76–79.

10. Godzhaev, E.M., Ragimov, R.S., and Rustamov, V.D., Optic Switchers Based on $TlInSe_2$ Single Crystals, *XVIII Mezhdunarodnaya nauchno–tekhnicheskaya konferentsiya po fotoelektricheskim priboram nochnogo videniya* (XVIII International Scientific–Technical Conference on Photoelectric Night Viewing Devices), Moscow, 2004, pp. 110–111.

11. Gorokhovatskii, Yu.A. and Bordovskii, G.A., *Termoaktivatsionnaya tokovaya spektroskopiya vysokoomnykh poluprovodnikov i dielektrikov* (Thermoactive Current Spectroscopy of High–Ohmic Semiconductors and Dielectrics), Moscow: Nauka, 1991.

12. Oshmyak, V.G., Timak, S.G., and Shamaev, M.Yu., *Vysokomol. Soed., Ser. A*, 2003, vol. 45, no. 10, pp. 1689–1698.

13. Magerramov, A.M., Sherman, M.Y., Lesnykh, O.D., Kovchagin, A.G., and Turyshev, B.I., *Polymer Science, Ser. A*, 1998, vol. 40, no. 6, pp. 590–595.

ISSN 1068-3755, Surface Engineering and Applied Electrochemistry, 2007, Vol. 43, No. 2, p. 152. © Allerton Press, Inc., 2007.
Original Russian Text © by the Editorial Board, 2007, published in Elektronnaya Obrabotka Materialov, 2007, No. 2, p. 89.

INFORMATION

DOI: 10.3103/S1068375507020172

FIFTH INTERNATIONAL CONFERENCE HYDROGENOUS ECONOMY AND HYDROGENOUS TREATMENT OF MATERIALS (HTM–2007)

Donetsk, May 21–25, 2007

ORGANIZERS

INTERNATIONAL ASSOCIATION OF HYDROGEN ENERGY TECHNOLOGIES

JOINT SCIENTIFIC AND COORDINATION COUNCIL

on the prospects of transition to hydrogenous economy

PERMANENT INTERNATIONAL COMMITEE
on hydrogenous treatment of materials

*

UN AGENCY FOR INDUSTRIAL DEVELOPMENT

INTERNATIONAL CENTER OF HYDROGEN ENERGY TECHNOLOGIES

(UNIDO–ICHET)

*

DONETSK NATIONAL TECHNICAL UNIVERSITY

*

The general topics of the HTM conferences are hydrogenous economy and materials, the efficiency and safety of modern hydrogen-intensive works, and the problems of transition to the hydrogenous civilization of the future.

The specific target of the HTM conferences is the organization of wide information exchange and personal communication for representatives of the hydrogen community from countries of the CIS and of the world hydrogenous movement, thus, initiating new insight into the following:

- the problems of transition to hydrogenous economy and the long-term goals of revealing bifurcation points on the path to hydrogenous civilization;
- the goals and methods for solution of modern industrial problems connected with hydrogenous degradation of materials being accentuated due to the expiration of the design service life of the constructions, communications, and devices of many hydrogen-intensive and hydrogen-hazardous works in countries of the CIS; and
- the prospective goals of the nearest future in the field of physics, chemistry, and physical chemistry of hydrogen–condensed matter systems in the field of hydrogenous, thermal, and plastic treatment of construction and functional materials for ensuring the safety and efficiency of their use in industry, transport, and everyday life in the period of commercialization of hydrogenous economy.

Find more information on the HTM conferences by visiting the Hydrogen Community portal on the Internet (its address is **http://donntu.edu.ua/hydrogen-community/**)

or in special issues of *The International Journal of Hydrogen Energy* (1997, vol. 22, no. 2/3; 1999, vol. 24, no. 9; 2002, vol. 27, no. 7–8; 2006, vol. 31, no. 2).

The address for correspondence is the following:

Gol'tsov Victor Alekseevich (Chairman of the Organizing Committee of HTM-2007)

Kotel'va Raisa Vasil'evna (Chief Scientific Secretary of the Organizing Committee)

Donetsk National Technical University, ul. Artema 58, Donetsk, 83000 Ukraine

E-mail: goltsov@physics.dgtu.donetsk.ua

ISSN 1068-3755, Surface Engineering and Applied Electrochemistry, 2007, Vol. 43, No. 2, p. 153. © Allerton Press, Inc., 2007.
Original Russian Text © by the Editorial Board, 2007, published in Elektronnaya Obrabotka Materialov, 2007, No. 2, p. 90.

INFORMATION

DOI: 10.3103/S1068375507020184

VII International Scientific School–Seminar

"Pulse Processes in Mechanics of Continua"

XIII International Scientific School–Seminar

"Physics of Pulse Discharges in Condensed Media"

In the third week of August 2007, the Institute of Pulse Processes and Technologies of the National Academy of Sciences of Ukraine, together with other institutes from Ukraine and Russia, will hold the VII International Scientific School–Seminar "Pulse Processes in Mechanics of Continua" and the XIII International Scientific School–Seminar "Physics of Pulse Discharges in Condensed Media." The school–seminars will be held on the premises of one of the holiday hotels located on the shore of the Black Sea (in the village of Koblevo in the Nikolaev region).

Scientific topics of the school–seminars

VII School–Seminar:

1. Physical and mathematical models of continuous and multiphase media.
2. Nonsteady wave processes in continuous and multiphase media.
3. Interaction of hydrodynamic perturbations with space deformed bodies.
4. Physical–mechanical properties and structures of media under pulse hydrodynamic influence.
5. Pulse sources and technologies.

XIII School–Seminar:

1. Physics of electric and optic discharges in condensed media.
2. Physics of electric explosion of semiconductors.
3. Physical properties of dense imperfect low temperature plasma.
4. Physical properties of condensed media under the influence of electromagnetic pulse fields.
5. Diagnostics of the influence of intensive energy fluxes on substances.
6. Prospective sources and means of generation of high energy densities.

We invite all interested scientists and specialists to take part in the mentioned events and to make reports.

Theses of reports (up to 3 pages and formatted according to the requirements of the organizing committee) should be submitted no later than April 15, 2007. The publication cost for the thesis of one report is equivalent to $10. The materials of the schools–seminars will be published by the date of their beginning. The working language of the schools–seminars is Russian.

More information on the schools–seminars, including the requirements for formatting and submission of theses of reports and bank information may be found on the website of the IPPT NAS of Ukraine (www.iipt.com.ua).

Address of the organizing committee:

**Institute of Pulse Processes and Technologies of the National Academy of Sciences of Ukraine,
pr. Oktyabr'skii 43a, Nikolaev, 54018 Ukraine**

Telephone numbers: (0512) 22–41–19; (0512) 49–62–09; (0512) 49–62–26

Email: iipt@iipt.com.ua

Working Organizing Committee

ISSN 1068-3755, Surface Engineering and Applied Electrochemistry, 2007, Vol. 43, No. 2, pp. 154. © Allerton Press, Inc., 2007.
Original Russian Text © by the Editorial Board, 2007, published in Elektronnaya Obrabotka Materialov, 2007, No. 2, p. 91.

INFORMATION

DOI: 10.3103/S1068375507020196

Demidov State University, Yaroslavl'
Institute of Applied Physics of the Academy of Sciences of the Republic of Moldova
Moscow Physical Society
Joint Physical Society of the Russian Federation, Vladimir Regional Branch

Bulletin

From June 29 to July 2, 2007, at Demidov State University in Yaroslavl, the regular conference Long-Living Plasma Formations and Insufficiently Explored Forms of Natural Electric Discharges in the Atmosphere will be held

Applications for reports on the following topics are being received:

1. Ball lightning: statistical treatment of descriptions of observations of the natural state; experimental and theoretical modeling.
2. Descriptions of experiments on obtaining long-living plasma formations under laboratory conditions.
3. Experimental and theoretical research of plasma erosion properties.
4. Insufficiently explored forms of natural electric discharges in the atmosphere (St. Elmo's fire, beaded lightning, flat lightning, etc.).

Theses will not be published. Reports selected by the organizing committee will be published in the journal *Elektronnaya Obrabotka Materialov.*

Applications with the titles of the reports, short (10–15 lines) annotations, and the names of the authors should be sent by E-mail to grig@uniyar.ac.ru and shir@uniyar.ac.ru or by mail to the following address: Grigor'ev Aleksandr Ivanovich, Demidov State University, ul. Sovetskaya 14, Yaroslavl', 150000 Russia

Accommodation in hotel rooms is for two or three people. Prepayment of booking is obligatory.

More information may be found at the following web site:
http://www.uniyar.ac.ru/~grig/Bl_conference